Université d'Ottawa · University of Ottawa

Université d'Ottawa · University of Ottawa

FACULTÉ DE ÉTUDES SUPÉRIEURES ET POSTDOCTORALES

FACULTY OF GRADUATE AND POSTDOCTORAL STUDIES

Jean-François MERCIER

AUTEUR DE LA THÈSE - AUTHOR OF THESIS

Ph.D (Physics)

GRADE - DEGREE

Department of Physics

FACULTÉ, ÉCOLE, DÉPARTEMENT - FACULTY, SCHOOL, DEPARTMENT

TITRE DE LA THÈSE - TITLE OF THE THESIS

New Modelling Tools for the Human Genome Project :
1. A Study of the Ogston Regime for Small Analytes and
2. Models for Solid Phase DNA Amplification

G. Slater

DIRECTEUR DE LA THÈSE - THESIS SUPERVISOR

CO-DIRECTEUR DE LA THÈSE - THESIS CO-SUPERVISOR

EXAMINATEURS DE LA THÈSE - THESIS EXAMINERS

B. Amsden

B. Joós

I. L'Heureux

P. Watson

J.-M. De Koninck, Ph.D

LE DOYEN DE LA FACULTÉ DES ÉTUDES SUPÉRIEURES ET POSTDOCTORALES

DEAN OF THE FACULTY OF GRADUATE AND POSTDOCTORAL STUDIES

New modelling tools for the human genome project:

1. A study of the Ogston regime for small analytes and 2. Models for solid phase DNA amplification

by

Jean-François Mercier

A thesis presented to the University of Ottawa
in fulfilment of the thesis requirement for the degree of
Doctor of philosophy in Physics

Ottawa, Ontario
October 22, 2004

Your file Votre référence
ISBN: 0-494-01737-6
Our file Notre référence
ISBN: 0-494-01737-6

"... as we know, there are known knowns; there are things we know we know. We also know there are known unknowns; that is to say we know there are some things we do not know. But there are also unknown unknowns – the ones we don't know we don't know."

Donald H. Rumsfeld, February 12, 2002

Summary

Now that the human genome project has been completed, the race is on to improve the existing sequencing techniques, or develop new ones, to allow affordable and reasonably quick personal DNA testing. This would help predict personal response to drugs and disease predisposition. The standard sequencing method is based on electrophoresis, which allows a sorting of molecules according to their size. In the first part of this thesis, I develop a new numerical method to rapidly obtain the continuum limit mobility of a migrating molecule, using results obtained on a lattice. I then use this technique to re-examine the theoretical foundation of the current model (the Ogston-Morris-Rodbard-Chrambach or OMRC model) used to describe the molecular size dependence of the electrophoretic mobility of small molecules during gel electrophoresis. I consider three-dimensional gels and electric field lines similar to the ones used in electrophoresis and show that the OMRC model could not reliably predict the mobility of a molecule in a gel. In the second part of this thesis, I present a computational study of a new technique that could be used to provide alternatives to electrophoresis-based sequencing. This technique, named solid phase DNA amplification, allows for the parallelization of DNA amplification (and ultimately, a new sequencing method). I use Monte Carlo and Brownian Dynamics simulations to model this new experimental technique. I show that it leads to a geometrical amplification of DNA molecules and sharp population size distributions.

Sommaire

Le projet du génome humain étant maintenant complété, une course, potentiellement très lucrative, vient d'être lancée pour le développement de nouvelles techniques de séquençage (ou l'amélioration des techniques existantes) qui permettraient d'obtenir des tests d'ADN personnels à des coûts et en des temps raisonnables. Ces tests pourraient être utilisés pour connaître les prédispositions à certaines maladies et prévoir la réponse individuelle aux médicaments. Présentement, la méthode de séquençage la plus répandue est basée sur l'électrophorèse, une technique qui permet de trier les molécules en fonction de leur taille. Dans la première partie de cette thèse, je développe une nouvelle méthode numérique pour obtenir rapidement la limite du continuum de la mobilité d'une molécule en utilisant des résultats obtenus sur un réseau. J'utilise ensuite cette technique pour examiner la base théorique du modèle Ogston-Morris-Rodbard-Chrambach (OMRC). Ce modèle est fréquemment utilisé pour prédire l'effet de la taille moléculaire sur la mobilité électrophorétique de petits analytes pendant l'électrophorèse sur gel. Pour tester le modèle OMRC, je considère des gels et des lignes de champ électrique similaires à ceux utilisés pendant l'électrophorèse sur gel. Mes résultats démontrent que le modèle OMRC est inadéquat pour prédire la mobilité d'un analyte dans un gel. Dans la deuxième partie de cette thèse, je présente une étude numérique d'une nouvelle technique qui pourrait devenir une alternative aux techniques de séquençage basées sur l'électrophorèse. Cette technique, nommée amplification de l'ADN sur phase solide, permet la parallélisation de l'amplification de l'ADN. J'utilise des simulations de type Monte Carlo et de type Dynamique Brownienne pour modéliser cette nouvelle technique expérimentale. Je démontre que ce phénomène d'amplification mène à une croissance géométrique des populations de molécules d'ADN et à une distribution de tailles caractérisée par un petit écart-type.

Remerciements

merci à ...

Gary; pour être le scientifique et superviseur qu'il est; pour m'avoir fait confiance; pour être une source inépuisable d'enthousiasme; pour le *flat panel.*

Fred; pour les *viewers*; pour le support technique.

Michel, Tatek et St-Hilaire; pour les dîners.

Fred, Martin et Michel; pour le débogage.

Laurette, Fred, Michel, Simona, Gary, Martin, Tatek, Yanick et Katarina; pour m'avoir enduré; pour le milieu de travail.

Ma famille; pour le support.

Pascale; pour beaucoup de choses.

Ma fille; pour la motivation de finir.

CRSNG, FCAR, OGS, OGSST, Manteia et l'Université; pour l'$.

List of Publications

This is a paper-format thesis. It is based on work reported in the following papers, referred to by roman numbers in the text:

I. J. F. Mercier and G. W. Slater.
Random walk and diffusion of hard spherical particles in quenched systems: Reaching the continuum limit on a lattice.
Journal of Chemical Physics, 113: 9109–9112, 2000.

II. J. F. Mercier and G. W. Slater.
An exactly solvable Ogston model of gel electrophoresis. 7. Diffusion and mobility of hard spherical particles in three-dimensional gels.
Macromolecules, 34: 3437–3445, 2001.

III. J. F. Mercier, F. Tessier and G. W. Slater.
An exactly solvable Ogston model of gel electrophoresis: VIII. Nonconducting gel fibers, curved field lines, and the Nernst-Einstein relation.
Electrophoresis, 22: 2631–2638, 2001.

IV. J. F. Mercier, G. W. Slater and P. Mayer.
Solid phase DNA amplification: a simple Monte Carlo lattice model.
Biophysical Journal, 85: 2075–2086, 2003.

V. J. F. Mercier and G. W. Slater.
Solid phase DNA amplification: A Brownian Dynamics study.
Submitted to *Biophysical Journal*.

Contents

Introduction

The Human Genome Project. Over the last 15 years, this gigantic undertaking has gained a mystic status. Its goal was to determine the deoxyribonucleic acid (DNA) sequence of the entire human genome: a 3 billion base pair long sequence. It began formally in 1990, as an international collaboration of government agencies, academia and industry. It was originally planned to last 15 years. However, the technological advances and the pressure coming from the private sector (a private company, Celera Genomics, actually archived the sequencing of the genome at the same time as the publicly-funded Human Genome Project) have allowed its completion in a little more than eleven years. When it was completed, in February 2001, both *Nature* [1] and *Science* [2], the leading scientific journals in the world, devoted a full issue to this achievement.

The reason why so many resources have been invested in this project, and why so much interest has been drawn and hope has been raised by the sequencing of the human genome, is that most of the human diseases have a genetic component (either inherited or resulting from the response to the environment). The hope is to use this information to develop new ways to treat and prevent diseases. In that regard, the complete sequencing of the human genome represents more of a starting point (a necessary one for sure) than an end point. Before any treatment can be developed, the role of the human genes in healthy and abnormal cells has to be better understood. This is an extremely difficult and important problem. For example, one of the most spectacular findings of the human genome project is that a normal human being has 30 000 genes (genes are specific sequences of our genome and contain the instructions on how to make proteins, which, in turn, perform most life functions and make up most of the cellular structures [2]). This number seems large, but it is far less than what was expected. Far from simplifying the researchers' life, it is now believed that this low number of genes actually means that each gene directs the synthesis of many proteins. Understanding how these mechanisms work promises to be a huge challenge.

The DNA of all human beings is 99.9 percent alike [2]. It is the 0.1 percent differences that lead to the great diversity of humankind. Most of these differences (90% of all human genetic variations) are actually a single nucleotide in a sequence (a single nucleotide alteration of the DNA common to at least 1% of the population is called a *single nucleotide polymorphism* or SNP). A DNA alteration can occur in both coding (gene) and non-coding regions of the genome. When it occurs in a gene, the encoded proteins could be unable to carry out their normal functions and genetic disorders can result.

Therefore, it is crucial to improve the sequencing (or SNP analysis) techniques, or develop new ones, to allow "personal" sequencing; that is to sequence the DNA of a given individual in reasonable time and cost. This information could be used to predict an individual's response to a given drug, make medical interventions more specific and predict disease predisposition, allowing one to adapt one's lifestyle to reduce the risk of developing those diseases. Of course, this knowledge comes with important ethical questions, but the possible improvements of both duration and quality of life are enormous.

The genome project and its ramifications have lead, directly or indirectly, to the development of many new technologies. Among the most important ones are: 1. *Gel and capillary electrophoresis.* This is probably the most important genomic technique, the workhorse of the genome project. The basic idea behind this technique is to use a polymer gel or entangled polymer solution (or even a dilute solution of polymers) to act as a sieving device to sort molecules (DNA or other charged molecules) according to their size. Section 0.3 will explain in more detail the mechanisms of electrophoresis. 2. *Polymerase chain reaction (PCR).* This technique allows the easy duplication and amplification of DNA molecules. It uses polymerase, a natural enzyme present in every living organism, and temperature cycles to make copies of a DNA molecule or of a part of it. Section 0.2 will provide more details on PCR. 3. *Bio-chemical tools.* The genome project has allowed an impressive array of tools to manipulate DNA to be developed. Most of them are natural enzymes, that are "domesticated" to serve certain useful chemical purposes. They include the polymerase, which copies DNA, restrictive enzymes, which can cut DNA molecules at a specific location, enzymes that can link two DNA fragments together, and various fluorophores, which can be attached to a nucleotide and allow a DNA molecule to be seen.

This thesis consists of four published articles and one submitted manuscript related to the sequencing of DNA. The first three articles [I, II and III] are part of a series that re-examines the theoretical foundation of the current model used to describe the molecular size dependence of the electrophoretic mobility of small analytes during gel or capillary electrophoresis (the so-called Ogston regime). This empirical model, developed over many years, assumes that the normalized mobility is equal to the fractional gel volume available to the analyte. In our articles, we used a new computational method to test the basic assumptions of the theory under various conditions. The last two papers [IV and V] of the thesis present a computational study of a new technique that allows the parallelization of DNA amplification (and ultimately, a new sequencing method): solid phase amplification (SPA). We used Monte Carlo and Brownian Dynamics simulations to model this new experimental technique.

This introduction is organized as follows. Section 0.1 describes the main characteristics of the DNA molecule while Section 0.2 describes the traditional experimental method used to amplify (make copies

of) DNA: the Polymerase Chain Reaction. Section 0.3 explains the main technique used to sequence (read) a DNA molecule: electrophoresis. Section 0.4 presents the current theory of one of the main regimes of gel electrophoresis: the Ogston model. Section 0.6 describes Solid Phase Amplification, and introduces my last two articles. The last few sections explain our collaboration with Manteia Predictive Medecine (Section 0.8), present the five papers of this thesis (Section 0.9) and my other contributions (Section 0.10) and finally I make a statement of originality in section 0.11.

0.1 DNA Characteristics

Deoxyribonucleic acid (DNA) is the most important molecule of life. Each cell of every living organism has a copy of its DNA. DNA contains the genetic information of the organism, that is, the master plan of that organism along with all the information necessary for its operation. Astonishingly, DNA uses only four "units" or bases to store all this information, the four nucleotides: adenine (A), thymine (T), guanine (G) and cytosine (C). James Watson and Francis Crick were the first to determine the detailed structure of DNA in 1953 (they received a Nobel prize for it). That structure, a "double helix" that can "unzip" to make copies of itself, confirmed that DNA carries life's hereditary information. Figure 1 shows both a chemical and a physical representation of a DNA molecule. A DNA molecule is made of a double series of nucleotides (A, T, C, and G) linked together by a polymer consisting of an alternating sugar-phosphate sequence (the backbone of the DNA molecule). Note that a DNA "molecule" consists in fact of two distinct molecules linked together by hydrogen bonds between the nucleotides. Each of these molecules is called a single stranded DNA (or ssDNA) and a molecule containing the two branches is called a double stranded DNA (dsDNA). The key to DNA duplication is that an adenine (A) nucleotide is always linked to a thymine (T) (with two hydrogen bonds), a cytosine (C) is always linked to a guanine (G) (with three hydrogen bonds) and vice versa. Therefore when a dsDNA molecule is separated ("unzipped"), the two branches of ssDNA can be used individually as a template to produce an exact replica of the initial molecule.

Physically, a dsDNA molecule forms a very rigid and charged polymer. Its persistence length (the length over which thermal energy is sufficiently strong to bend the molecule) depends on many factors (e.g. buffer, salt concentration, etc.) but is of the order of ~ 50 nm at room temperature [3]. Since the average distance between two nucleotides is only 0.34 nm for dsDNA, the persistence length corresponds to ~ 150 base pairs (an A=T or C≡G group in the double helix) [3]. In a DNA molecule, each phosphate group is negatively charged. Therefore the total charge of a DNA molecule is directly proportional to

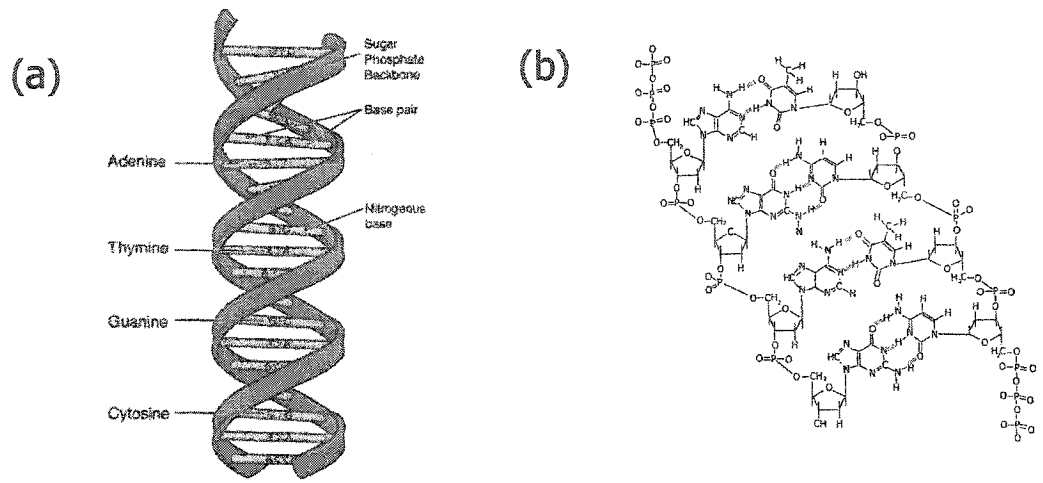

Figure 1: Physical (a) and chemical (b) representations of a DNA molecule. A dsDNA molecule is made of a double series of nucleotides (A, T, C, and G) linked together by a polymer consisting of an alternating sugar-phosphate sequence (the backbone of the DNA molecule). In a dsDNA molecule, an adenine (A) nucleotide is always linked to a thymine (T) (with two hydrogen bonds), a cytosine (C) is always linked to a guanine (G) (with three hydrogen bonds). Therefore, when a dsDNA molecule is separated ("unzipped"), the two ssDNA branches can be used individually as a template to produce an exact replica of the initial molecule. The image (a) is taken from www.genome.gov and is used with permission.

its length.

Since the two strands of a dsDNA molecule are linked only by hydrogen bonds, it is fairly easy to break such a molecule into its two ssDNA components. This can be accomplished either by physical, chemical or even thermal (heating the molecule) means. The breaking of a dsDNA molecule simply results in two ssDNA molecules. Each ssDNA molecule is still charged proportionally to its length. However, there are some fundamental differences between ssDNA and dsDNA. A ssDNA doesn't have the characteristic helix structure of the dsDNA and the average distance between two nucleotides is increased to 0.43 nm [4]. Furthermore the persistence length of a ssDNA is less than one tenth that of dsDNA, i.e. $\sim$ 4 nm or 10 bases [4].

0.2 Polymerase Chain Reaction

One of the most important molecular tools developed in connection with the genome project is Polymerase Chain Reaction (PCR). It was invented in the early 1980s by Kary Mullis of the Cetus Corporation. In fact, PCR is now so important in molecular biology that the prestigious Science magazine

named the polymerase (the molecule on which PCR is based) its first "Molecule of the Year" in 1989. Also, its inventer, Kary Mullis, won the Nobel prize for chemistry in 1993. This elegant method allows one to make unlimited copies of a single DNA fragment in a matter of hours. Note that PCR is actually explained (and modelled) in one of the articles of this thesis [IV]. Part of this introduction is essentially identical to the one of this article.

PCR is based on the proprieties of polymerase, a naturally occurring enzyme that catalyzes the formation and repair of DNA. Polymerase acts on a ssDNA molecule and generates the complementary strand. Therefore, if a dsDNA fragment is "unzipped" (by heating for example), a replica of the initial DNA can be obtained simply by letting the polymerase work, using each strand as a template (see figure 2). Nature uses polymerase to repair and copy DNA. In fact, the accurate replication of all living matter depends on this activity. Therefore, every living creature has its own form of polymerase.

PCR generally uses the Taq polymerase to make multiple copies of a piece of DNA. Taq polymerase is a thermostable polymerase coming from a bacteria (*Thermus aquaticus*) which lives at very high temperatures (which explains why this polymerase works at high temperature). Two characteristics of the polymerase make PCR possible. First, polymerase cannot copy a DNA chain without a short sequence of nucleotides to "prime" the process, i.e. to get the process started. This initial stretch of DNA is called a primer. In nature, the cell has another enzyme called a primase that actually fabricates the primer. In the lab, the primer has to be generated synthetically and should be designed to complement a specific sequence at one end of the target sequence (the section of the DNA fragment that needs to be amplified). The other characteristic of polymerase essential for PCR is that DNA polymerase can only act on one end (the 3'-end) of the primer. This comes from the structure of the sugar molecules present in the DNA double helix. The other end (the 5'-end) cannot be used by the polymerase. In a PCR experiment two primers are required (one for each strand). By carefully choosing these two primers, it is possible to multiply only a section of the total DNA fragment. Only the segment contained between the two primers (the target sequence) is amplified (figure 2).

In a typical PCR experiment, the four necessary components - a piece of DNA, large quantities of the four nucleotides (adenine A, cytosine C, guanine G, and thymine T), large quantities of the primers, and DNA polymerase - are mixed in an aqueous solution (the buffer, which is also used to maintain proper pH and salt concentrations). The PCR process itself consists of three distinct steps: denaturation, annealing and extension. During denaturation, the solution is heated to denature ("unzip") the complementary strands of a dsDNA fragments (figure 2b). During annealing, the solution is cooled down to allow the primers to bind (hybridize) to their complementary sequence on the ssDNA

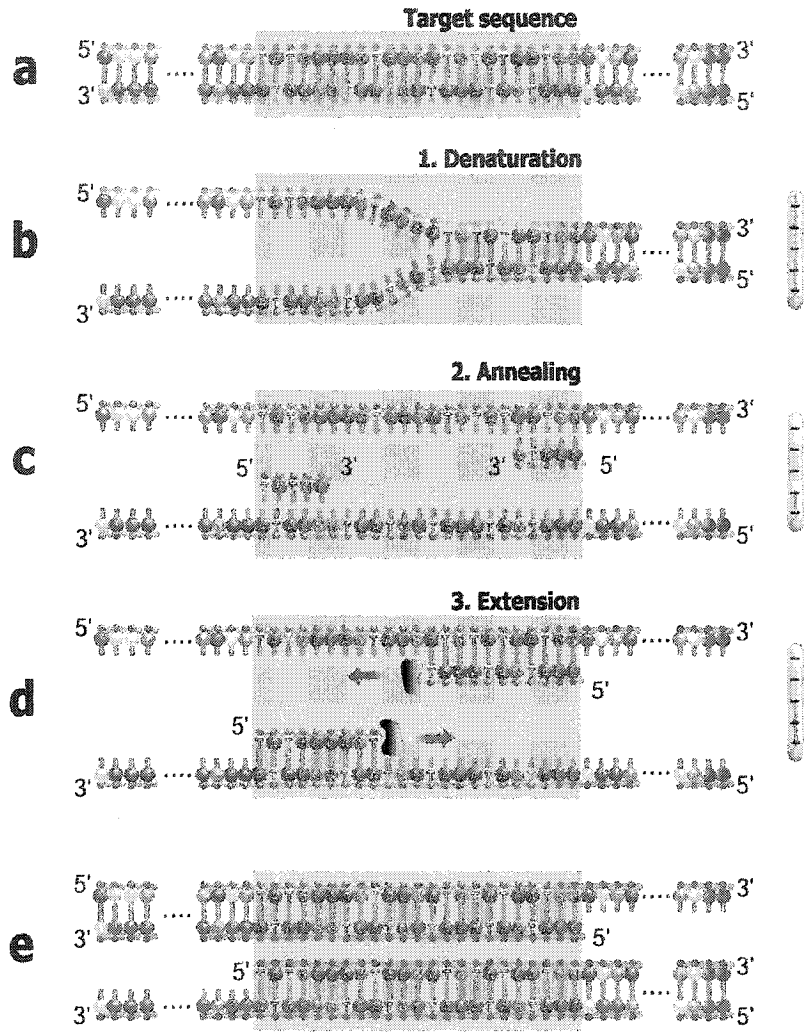

Figure 2: Representation of the PCR process. A dsDNA fragment (a) is first heated to break the molecule into its two complementary fragments (b). The solution is then cooled down to allow the primers to bind to their complementary sequences along the DNA fragments (c). Finally the solution is reheated to allow the polymerase to add nucleotides at the end of the primers and eventually make a complementary copy of the template (d). Because the polymerase can only act on one end of the DNA (the 3' end), the solution quickly consists almost exclusively of DNA fragments corresponding to the target sequence located between the two selected primers. This figure was taken from [IV].

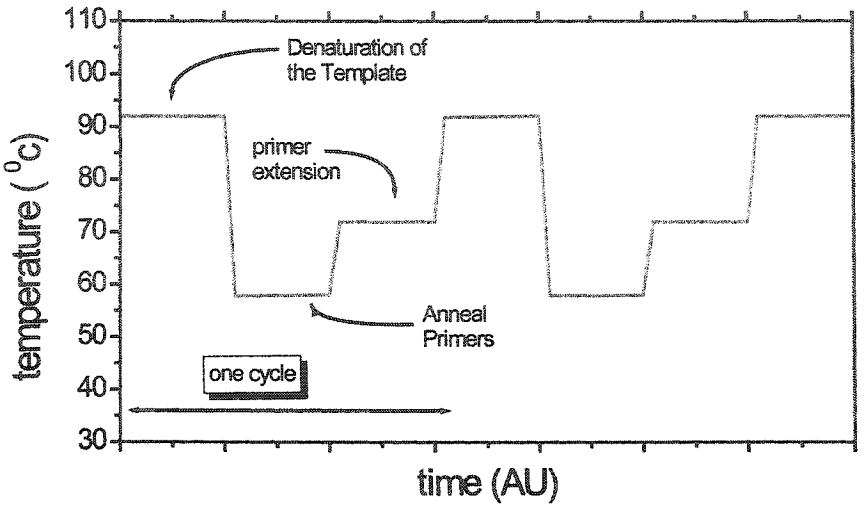

Figure 3: Temperature cycle corresponding to the three PCR steps: denaturation (95^0C), annealing (45^0C) and extension (72^0C) (see figure 2). A complete cycle can be achieved in a matter of minutes. The temperature values shown in the figure are typical values but can vary [5].

fragments (figure 2c). Note that re-attachment of the original strands to each other is highly improbable because of the high primer concentration. Finally, during extension, the solution is reheated a little to allow the (Taq) polymerase to add nucleotides to the primer and eventually make a complementary copy of the template (figure 2c).

The key is that this procedure can be used iteratively. Figure 3 shows an example of the first three cycles of a typical PCR experiment. After a few cycles, exact replicas of the target sequence have been produced. In the subsequent cycles, dsDNA of both the original molecules and the copies are used as templates. Solution PCR is thus characterized, at least initially (after a while, a lack of nucleotide and/or primer and/or enzyme can affect the growth rate), by an exponential growth. After several cycles, the pool is greatly enriched in pieces of DNA containing the target sequence (between the two primers). In about an hour, as many as 25 cycles can be completed, giving up to $2^{25} \simeq 67$ million-fold increase in the amount of the target sequence.

0.3 Sequencing DNA

The most common method to sequence ssDNA molecules uses (slab gel or capillary) electrophoresis and can be separated in three different steps. The first step is to produce fluorescent samples of all possible lengths of the molecule (the template). Figure 4 explains how this procedure is usually carried out. It

can be considered a variation of the PCR process discussed in the previous section. The first few bases (typically 20 bases) of the template have to be known in order to produce the primer for the reaction. To produce all possible lengths, a given proportion of the nucleotides are modified by attaching to them a fluorophore and by modifying their chemical structure in order to stop the elongation process by the polymerase. As a result, the polymerase is not able to work on them. Since the modified nucleotides are introduced at a random location in an elongation process, all possible lengths, finishing with a modified nucleotide, are produced after many PCR cycles. Two strategies can then be used. Only one experiment can be carried, in which the modified nucleotide types (A, T ,C and G) are marked with different fluorophores. The other option is to run four different experiments in which only one of the four nucleotides has part of its population modified (see figure 4). In this case the same fluorophore can be used for the four nucleotides (or the fluorophore can be directly attached to the primer). This is an advantage because the fluorophores affect the mobility of the fragment. If the four bases are modified with the same type of fluorophore, the mobility of all fragments are affected in a similar manner, and no mobility correction is necessary. On the other hand if four different nucleotides are used, the mobilities have to be adjusted accordingly. The reason is that in such a case band inversion is possible (i.e. a larger fragment can be faster than a smaller one because its fluorophore is smaller and has less effect on the net mobility of the molecule).

The next step is to sort the fragments according to their length. This is usually done by electrophoresis. The idea is to use the charge of the DNA (by applying an electric field E) to make the molecule migrate through a sieving matrix (gel or entangled polymer solution). After a given time period during which the different molecules are left free to migrate in the presence of the electric field, molecules of different sizes will have travelled different distances, allowing to easily separate them. The sieving matrix is formed of (cross-linked if it is a gel, entangled if it is a polymer solution) uncharged fibers, which can be considered immobile for the migrating analyte. The reason the sieving matrix is necessary is that the free flow (without a sieving matrix) electrophoresis mobility

$$\mu_0 = \frac{v}{E}, \tag{1}$$

where v is the speed of a molecule, is usually independent of the DNA size M because both the force and the friction increase linearly with M. The sieving matrix will introduce a size dependence on the mobility of the analyte.

The migration of a ssDNA molecule through a typical sieving matrix can be separated in five distinct regimes. Figure 5 schematically represents a mobility-size "phase" diagram (μ vs. M) showing these

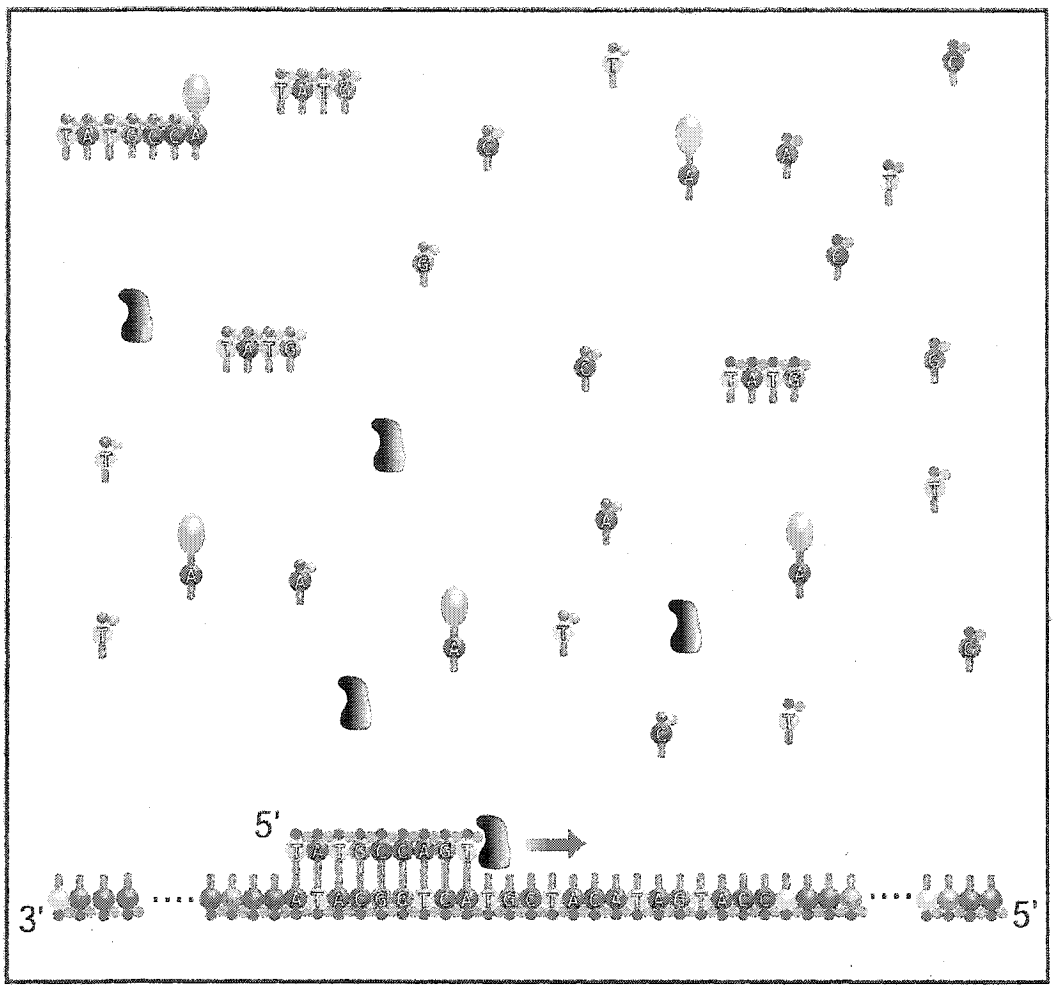

Figure 4: Sample preparation for DNA sequencing. The template ssDNA molecule is introduced in a solution containing DNA polymerase, large quantities of the primers, and large quantities of the four nucleotides (adenine A, cytosine C, guanine G, and thymine T). Part of the population of one of the nucleotides (here A) is modified by attaching to them a fluorophore and modifying their chemical structure in order to stop the elongation process by the polymerase. Many PCR cycles are then produced. Since the modified nucleotides are introduced at a random moment in the elongation process, all possible lengths of DNA (finishing by A) will be produced. An alternative to this procedure is to modify part of all types of nucleotides (A, T ,C and G) with different fluorophores [5].

regimes: I) *The Free-flow regime.* For very small ssDNA molecules, the contour length of the molecule is comparable to its persistence length. The molecule is thus a stiff rod and generally migrates as in free-flow (it doesn't feel the obstacles). In this regime, the mobility can actually increase with the size of the molecule. II) *The Ogston regime.* In this regime, the analyte is long enough to produce a random (self-avoiding) walk, but its size remains smaller than the average pore size (roughly the mean distance between two gel fibers) of the sieving matrix. The relevant size of the molecule then corresponds to its radius of gyration:

$$R_g(N) \propto N^{\nu}, \tag{2}$$

where N is the number of nucleotides of the ssDNA molecule, and $\nu = 0.59$ the Flory exponent. In this regime, the mobility decreases with the size of the analyte, presumably because of the collisions with the fiber. III) *Reptation without alignment regime.* Large DNA molecules must "reptate" head first, like a snake, because their radius of gyration is larger than the gel pore size. In this regime, the mobility also decreases with the size of the analyte. IV) *The transition regime.* The molecule gets trapped in U-shaped conformations and a minimum appears in the mobility vs size diagram. V) *Reptation with alignment regime.* Very large DNA molecules orient themselves in the direction of the field and the mobility is independent of the molecular size.

Separation is only possible when the mobility has a strong dependence on the molecule size. That usually means the Ogston (II) and the reptation without alignment (III) regimes. In ssDNA sequencing, this limits the range of molecule sizes which can be sequenced. Note however that the lower range limit is usually irrelevant for sequencing because the primer's length is always long enough for the molecule to be in the Ogston regime. Note that to sequence a molecule too large to be sequenced in one experiment, such as a whole chromosome, two approaches can be taken. The molecule can be split into small fragments with the position of each fragment carefully recorded. This is called the mapping of a molecule, and researchers usually use dsDNA molecules and agarose gel electrophoresis to do so. Once the proper mapping of the large molecule is completed, each fragment can be sequenced and the complete sequence can be obtained. This approach was used by the publicly-funded Human Genome Project. The other approach is to randomly break a large number of copies of the large molecule into fragments that can be sequenced. Once all the fragments are sequenced, the overlap in the different sequences can be used to compute the complete sequence. This method is called *shot gun* sequencing and was used by the private company Celera Genomics.

The final step of DNA sequencing, after the fragments have been separated using electrophoresis,

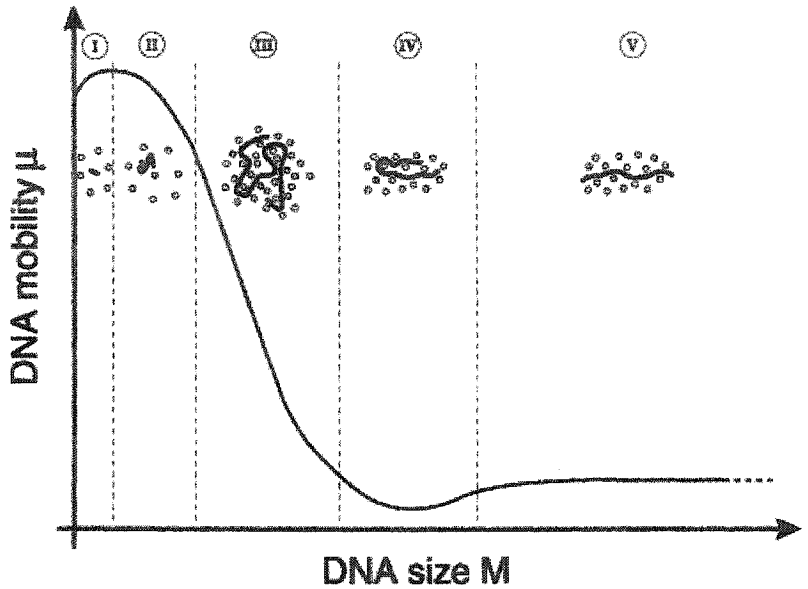

Figure 5: A schematic "phase" diagram showing a generic mobility μ versus size (M) relationship for DNA separation in a sieving matrix. The five distinct regimes are shown along with small cartoon pictures describing the relevant mechanisms. I) *The Free-flow regime.* Very small ssDNA molecules migrate as in free-flow. No separation is possible. II) *The Ogston regime.* Short random coil ssDNA molecules are well sieved by the seiving matrix. III) *Reptation without alignment regime.* Large DNA molecules must "reptate" head first, like a snake, through the gel. The mobility is a strong function of the DNA size and separation is possible. IV) *The transition regime.* The molecule gets trapped in U-shaped conformations and a minimum appears in the mobility vs size diagram. V) *Reptation with alignment regime.* Very large DNA molecules orient themselves in the direction of the field and the mobility is independent of the molecular size. This graph, was directly taken from a review article published by our group [6]. I was not an author of this paper.

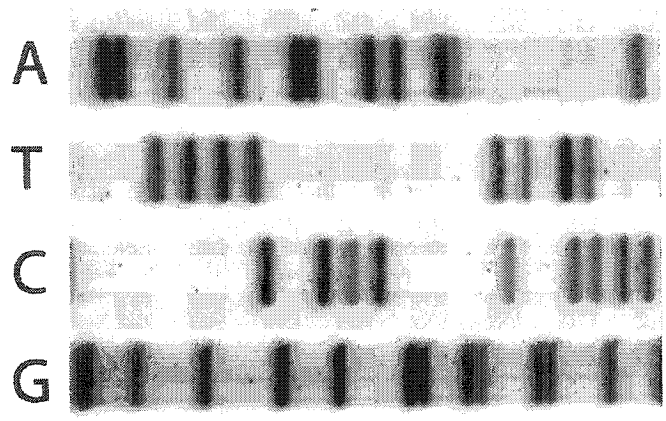

Figure 6: Typical gel electrophoresis result. Here four different samples are sequenced. In line A, part of the population A has been modified to stop the elongation process by the polymerase and by attaching them to a fluorophore. Similarly, in T, C and G, part of the T, C and G populations have respectively been modified. Since all possible length finishing by the modified nucleotide, have been produced in their respective columns, and since we know that the smaller the molecule, the further it will have migrated in a given time, the sequence can be read directly off the gel picture. The DNA sequence is thus (the fastest molecules are at the right): G A A G T A T G T A T C G A A C G C A C A G G A A G G T C T G G T C T C G C A C G . The image was graciously provided by Dr. Guy Drouin.

is the reading. Traditionally (that is, more than 10 years ago), polymer gels (usually polyacrylamide) were used as the sieving matrix and four experiments were run in parallel. In each of these experiments, only one type of nucleotide had a part of its population modified. After electrophoresis, bands corresponding to each of the different lengths appear in the gel and the sequence can be read directly (see figure 6). Today, capillary electrophoresis has almost completely replaced gel electrophoresis. Capillary electrophoresis is usually performed using an entangled polymer solution instead of a gel, and the reading is made by CCD cameras via laser induced fluorescence as the different bands pass through a detector. Only one experiment is carried out as the four nucleotide types (A-T-C-G) use different fluorophores.

0.4 The Ogston Regime

As mentioned in the previous section, the Ogston regime deals with the electrophoretic migration of a small analyte in a porous media. This could refer to a small hard particle such as a protein, or to a DNA molecule with a radius of gyration smaller than the mean pore size of the sieving matrix. Historically, the Ogston-Morris-Rodbard-Chrambach (OMRC) [7–10] model of gel electrophoresis has

been the central paradigm in this regime. The basic assumption of this model is that the scaled mobility μ^*, i.e. the ratio between the mobility μ in the separation media and the free-flow mobility μ_0, is equal to the fraction f of the gel volume available to the particle (without violating the steric constraints imposed by the medium):

$$\mu^* = \frac{\mu}{\mu_0} = f(C, M) = 1 - \phi \tag{3}$$

where C is the gel concentration, M is the molecular size of the particle and $\phi(C)$ is the (fractional) excluded volume. This is actually a semi-empirical formula that has never been properly tested experimentally. It seems to originate from a Morris paper [9] published in 1967. In this paper, Morris studied the sieving effect of gel electrophoresis using a model developed by Giddings and Boyack [11], and predicted that the scaled electrophoretic mobility of a specific system (namely, proteins in polyacrylamide gels) should be given by:

$$\mu^* \approx 1.1 f(C). \tag{4}$$

The appealing simplicity of Eq. 4 has led researchers to change the $\approx$ for an $=$ and to forget the 1.1 factor and the other assumptions of Morris and of Giddings and Boyack. The first authors to do so were Rodbard and Chramback [10] in 1970. To estimate the available volume $f(C)$, they used an early result of Ogston [7]. Using geometrical and statistical arguments, Ogston showed that the fractional volume available to a spherical particle in a random array of infinitely long (but not cross-linked) fibers is given by:

$$f(C, M) = e^{-KC}, \tag{5}$$

where $K = K(M)$ is the retardation coefficient of the analytes. Combining Eqs. 3 and 5 leads to:

$$\mu^* \approx e^{-KC}, \tag{6}$$

which we will call the Ogston-Morris-Rodbard-Chrambach model. This model is widely used and leads directly to the Ferguson plot ($\ln(\mu^*)$ vs C) as the standard data analysis method in electrophoresis of small analytes (including small DNA molecules) [8]. Note that the OMRC model implicitly assumed a low electric field since the field does not enter the model. This assumption might be true for gel electrophoresis, but it is likely to be invalid for capillary electrophoresis. However, people have used the model regardless of the field strength or the structure of the analyte or of the sieving matrix.

Over the years, a lot of effort has been spent computing the available volume $f(C)$ for a variety of media in order to achieve a better fit to experimental data. Surprisingly, very few attempts, if any, have focused on verifying the validity of Eq. 3. To verify such a model, we must rely on either very accurate experimental measurements, precise theoretical calculation or computer simulations. However, direct measurements have failed to validate the OMRC model because μ^* and $f(C)$ cannot generally be measured independently. Theoretical calculations of similar systems have been carried out based on a variational principle [12, 13], multistage analysis, the [14] volume averaging approach [15–18] and the method of moments [19, 20]. However, to the best of my knowledge, those more macroscopic methods only provide a mean field approximation and would not be enough to test conclusively the OMRC model. We must therefore rely on computer simulations. Although strategies can be used, many simulation algorithms, such as Molecular Dynamics or Brownian Dynamics, are so computer intensive that a general study of the OMRC model would be (or at least was at the time) impractical. Monte-Carlo (MC) techniques offer a fast and well documented alternative. However, intrinsic uncertainties associated with MC simulations (or any other stochastic simulation technique) can prevent one from observing subtle geometric effects that the gel might have on the electrophoretic mobility.

In 1995, Slater and Guo proposed a lattice model in order to explain the contribution of obstruction to gel electrophoretic sieving at the microscopic level. They showed that MC simulations where not necessary for such systems and that the exact mobility, in the zero-field limit, can be obtained for any lattice system using periodic boundary conditions. The idea was to calculate the probability for the presence of the analyte on each lattice site (in the steady-state), and multiply these probabilities by the local mobilities. This method reduces the problem to the solution of a large system of linear equations. For very small systems, they used the numerical capabilities of Mathematica, to solve the linear system exactly and to obtain exact results in the form of rational fractions. For larger systems, they used a very small value such as $\varepsilon = 10^{-y}$ to solve the equations numerically (using, e.g., an iterative procedure) to obtain the mobility with a precision of about y decimal places.

In a series of papers [21–23], they used this approach to test the predictions of the OMRC model (both μ^* and f can be calculated exactly and independently providing a straightforward way to test Eq. 3) for a large variety of sieving systems. They found that the OMRC model was actually equivalent to a mean-field model. The big advantage of the novel approach is that the exact mobility allows them to discover some subtle effects of the sieving matrix on the mobility of the analyte. However, the very computer-intensive algorithm that they used limited their efforts to small and somewhat unrealistic two-dimensional systems.

My master's degree [24] was the continuation of the early work of Slater and Guo. In particular, I found a powerful algebraic simplification for this algorithm. I also showed that the problem could be further simplified by using special index storage methods developed for sparse matrices and iterative solving algorithms. Together, these two improvements have allowed us to tackle problems two orders of magnitude larger than previously possible and have lead to three articles. The first one summarizes the numerical approach we developed to obtain exact mobilities [25] (this articles is include in this thesis as an appendix), while the last two articles apply the method to the study of various systems including fractal obstacles [26] and three dimensional periodic gels [27]. Again, we found that the OMRC model could not reliably predict the mobility of an analyte in a gel. Not surprisingly, we found μ to be a function of the geometry of the gel and not only of the free volume fraction f.

One drawback of our model was that the results obtained generally depend on the type of lattice used. During the first part of my Ph.D., I developed a new numerical method to reach the continuum limit, i.e. the limit where the size of the lattice mesh is infinity small in comparison with the size of both the analyte and the obstacles. In this limit the results are independent of the lattice type and are identical to the ones obtained with off-lattice simulations. The first article of this thesis [I] describes the new technique and compares the results we obtain with others found in the literature. In the second article [II], we use this new approach to investigate both periodic and random three-dimensional gels. Again, we find μ^* to be a function of the geometry of the gel.

Another aspect that was neglected in our original model was the non-trivial electric field lines present in a real gel. We always considered uniform (straight) electric field lines, unaffected by the presence of the obstacles. In reality, non-conducting obstacles, like gel fibers, should affect (or "curve") the field lines. Since we always considered the low-field limit, where the Nernst-Einstein relation has to be valid for both straight and curved field lines, we decided to work exclusively with the uniform field lines, which are easier to implement in our numerical scheme. However, in 1999, Locke and Trinh published a paper in which they directly challenged our work and argued that the assumption of the uniform field lines was the reason why our results disagreed with the OMRC hypothesis [28]. We immediately tested this idea by extending our model to take into account the curvature of the field lines around non-conducting gel fibers. Our results showed that the dependence of the mobility of a point-like particle upon the concentration of the gel is not affected by the field line distortions in the low-field limit. Therefore, Locke and Trinh's claim was incorrect and the OMRC hypothesis is invalid for both straight and curved field lines in this limit. The third article of this thesis shows these results [III]. In a following article [29], Locke seems to retract his claim that the field lines have an impact

on the electrophoretic mobility in the zero field limit: "In the case where the obstacles, or beta-phase, have low permeability to the solute of interest, the conductivity of the beta-phase has no effect on the effective electrophoretic mobility.". However he still claims that the OMRC is valid in the case of nonconductive obstacles: "The assumption of Morris that the mobility ratio equals the volume fraction is only satisfied for the case of nonconductive obstacles". In their work, Locke and Trinh used the theoretical volume averaging method [15–18]. The reason why the two approaches don't agree on such a simple and well defined problem are unclear. We fell strongly that our approach provides reliable results: indeed, we have shown many times that our results agree very well with MC simulations, when similar systems are considered [26, 30]. Furthermore, in a recent series of articles Dorfman [31, 32] has developed an independent technique which allows the exact calculations of both the mobility and the diffusion coefficient of a lattice system for arbitrary electric fields. In the low field limit, his results are in perfect agrement with our work for all cases studied. He also found that the volume averaging method fails to correctly predict the low field mobility for at least one system [31].

Other members of Dr. Slater's group have continued to expand our study of the Ogston regime. Josée Labrie has considered attractive gel-analyte interactions and their effects on the Ferguson plot [33]. Justin Boileau has modified our numerical approach to study oligomers (short polymers) [34]. More recently, Michel Gauthier has found a clever mathematical method to expand our approach to treat high electric fields [35, 36].

0.5 Diffusion and obstruction effects

Another motivation for developing an expression or a calculation technique for the scaled mobility μ^* is the fact that, in the limit where the external field, ε, goes to zero, the scaled mobility is directly related to the scaled diffusion coefficient D^* using the modified Nernst-Einstein relation:

$$\frac{D}{D_0} = \lim_{\varepsilon \to 0} \frac{\mu}{\mu_0}, \tag{7}$$

where D and D_0 are the diffusion coefficients of the analyte in free solution and in the gel, respectively. Therefore, all the results obtained for the mobility in the zero-field limit can be re-interpreted as thermal diffusion data and vice versa. The problem of obstructed diffusion in a quenched system of obstacles is of great interest in a large number of physical, biological and chemical problems. A non-exhaustive list of examples includes solid-solid composite dispersion [37], migration of proteins in biological membranes [38], diffusion in sediment-water mixtures [39] and of course analyte diffusion in hydrogels [40]. Given

its importance, it is no surprise that obstructed diffusion problems have been widely studied, and that an impressive number of, not always compatible, theories have been developed. It should also be noted that many excellent review articles and books have been written on that subject [37, 39, 40]. In particular in the field of analyte diffusion in hydrogels, Amsden [40] offers an extensive review of the different models currently used in that field.

Another twist to this great problem is that a non-trivial mathematical analogy exists among physically different transport problems. This allows the direct comparison of results obtained in different fields, when the transport properties are expressed in a reduced form [37, 41–43]. For example, the reduced diffusion coefficient of a random walker among fixed obstacles can not only be related to the zero-field limit mobility but also to the thermal conductivity [44, 45], the electrical conductivity [46] (sometimes referred to as the formation factor), the dielectric constant [47], the magnetic permeability [41] and even to the effective optical [48] and elastic coefficients [49] of similar systems. The issue of electrical conductivity in particular offers useful insights. First, the experimental simplicity of electric conductivity problems could lead to direct and precise measurements of both the conductivity and the available volume providing a direct verification of theories [50]. Second, this mature field offers well established solutions for simple problems. For instance Lord Rayleigh [51] derived the expression for the two-dimensional isolated periodic circles in 1892. This is the case that I used in article [III] to test our numerical approach with curved field lines.

Finally it should be noted that although, as I just discussed, the low field electrical mobility of an analyte migrating in a gel can be related to many other problems in a broad part of the scientific spectrum, no one, outside the electrophoresis community, claims that a single formula (such as the OMRC relation $\mu^* = f(C)$) could predict the transport properties of a sample regardless of the geometry of the system.

0.6 Solid Phase DNA Amplification

Given the importance of DNA sequencing, it is not surprising that there are tremendous efforts aimed at developing faster and cheaper sequencing methods. Many new, and sometimes very imaginative ideas have been proposed. For example some groups are developing artificial gels made of nano-fabricated solid-state structures [52–55]. Other groups try to sequence a DNA molecule by measuring the change in electric current observed when a DNA molecule passes through a nanopore [56, 57]. Others have suggested to measure the force required to unzip a dsDNA molecule [58]. Since the A=T pairs are

linked by fewer hydrogen bonds (2) than the C≡G ones (3), the force required to break them is smaller. Another very promising method has been proposed by Manteia Predictive Medicine and is called Solid Phase DNA Amplification [59]. The modelling of this new method has lead to the last two articles of my thesis [IV and V]. Part of what follows and some figures have been taken directly from these articles.

Solid Phase DNA amplification (SPA) is a variation on the classic PCR process. The central idea of this novel method is to attach the 5'-end of the primers to a surface instead of letting the primers freely diffuse in the solution (see figure 7). Using thermal cycles, similar to the ones used in PCR, it is then possible to amplify a DNA sample. Since the amplification is spatially limited to a two-dimensional surface, it is possible to amplify, and ultimately sequence, a large number of different DNA strands in the same experiment. Furthermore, SPA could provide an alternate route to DNA target implantation on DNA chips for genomic studies (see next section).

Because the primers are attached to the surface, two types of amplification are possible in SPA. First, if freely diffusing DNA targets are present in the solution, they can be grabbed by a surface-bound primer and then be copied in a manner similar to solution PCR (see figure 7 a-b-c-d). Note that the molecules have to be modified so that their free ends match the grafted primers. This is called *interfacial amplification*. In this type of amplification, the copy stays attached to the surface while the initial DNA molecule returns to the solution after the annealing step. If some DNA copies are attached to the surface, a second type of amplification called *surface amplification* is possible. In this case, the free end of the attached copy hybridizes to the primer complementary to its own sequence, and the PCR process can start (see figure7 e-f-g-h and i-j-k-l). The grafted molecule thus needs to bend to find a matching primer in order for *surface amplification* to be possible. It is important to note that this *surface amplification* process leaves both molecules attached to the surface, hence its name.

Like PCR, the SPA amplification can also be divided in three distinct steps - annealing, extension and denaturation - which are repeated in an iterative way. In the first cycle, interfacial amplification is the only type of amplification possible (this is the implantation phase). To ensure that only *surface amplification* occurs in following cycles the initial solution is washed away and replaced with a solution free of DNA targets. The net result of a surface amplification is a new ssDNA molecule attached to the surface in the immediate proximity of the initial strand (figure 7 h and i). Surface amplification thus results in an area covered with copies of both strands of the original DNA target. This area can be seen as a DNA colony. The number of colonies depends on the amount of DNA targets absorbed (via interfacial amplification) before the initial solution is washed. If different DNA targets are absorbed,

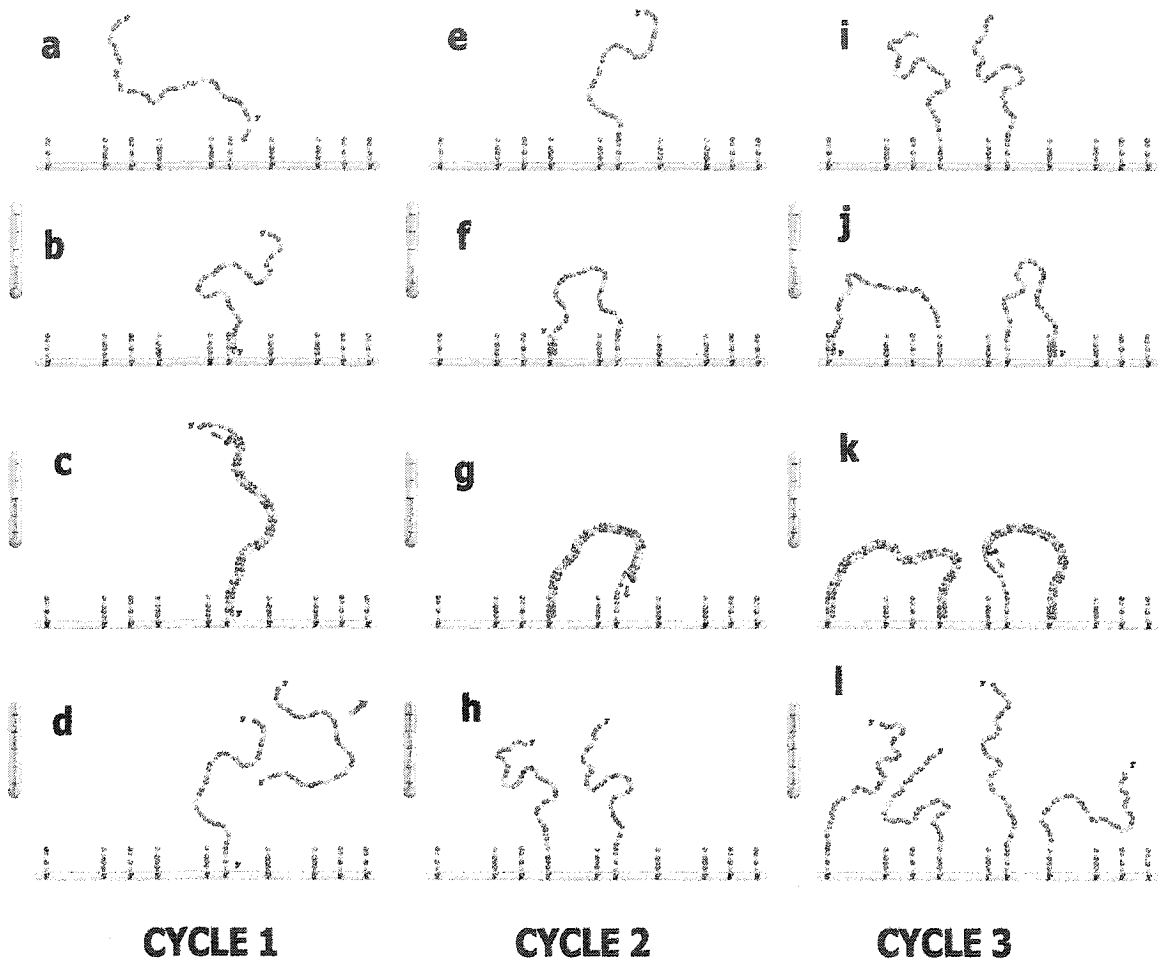

Figure 7: Representation of the solid phase amplification process. In the first cycle (a-b-c-d) the DNA is replicated by interfacial amplification. The net result is that one ssDNA is now attached to the surface via the primer. The solution is then replaced with a new one free of DNA targets. In the following cycles (e-f-g-h and i-j-k-l), only surface amplification is possible. This results in a spatially located DNA colony. Note that since a molecule always generates its complementary sequence in a thermal cycle, the two complementary branches will be present in the colony and two different types of primers have to be attached to the surface. This picture was taken from [IV].

many types of colonies will exist on the surface. If the colonies are far enough from each other (a situation that is favored by using a small concentration of DNA targets in the initial solution), each colony is amplified by PCR but remains isolated from the others.

SPA thus allows the parallelization of the DNA amplification process without any direct human intervention. One possible application is to directly and simultaneously sequence all the colonies using fluorescent nucleotides and image analysis algorithms. The idea is the following. After SPA amplification is completed, the $2D$ surface is populated with thousands, possibly millions, of isolated DNA colonies, each made of identical ssDNA molecules. A new solution with large numbers of the primer matching one of the two ssDNA strands is introduced. The temperature is set so the primers will hybridize with the DNA template. The solution is then again changed with a new one containing large quantities of one of the nucleotides (A for example). Part of these nucleotides are marked with a fluorofore. ssDNA molecules for which the first nucleotide corresponds to the incorporated nucleotide become fluorescent and so is the corresponding colony (ATTGAAC ... for example). By alternating solutions containing the four nucleotide bases, it is then possible to sequence each colony simultaneously. One of the major challenges of this sequencing technique is that the image processing algorithm shall make the difference between a colony that integrated one base (ATTGAAC ...), two bases (AATTGAAC) or even more bases (AAAAATCT). However, if these challenges can be resolved, SPA could offer a very promising sequencing technique.

In 2001 we started a collaboration with Manteia Predictive Medicine. Our role was to model the growth of a DNA colony. The details of the collaboration are given in section 0.8

0.7 DNA Chips

As previously mentioned, genome sequencing is only one step in the quest for new drugs and treatments. Another important one is to understand the role of genes in healthy and abnormal cells. This is a complex task and many strategies can be used. One of the most promising technology in this field is certainly DNA chips (also known as gene micro-arrays or gene-chips).

The idea behind DNA chips is very simple. A DNA chip consists of a two-dimensional surface (usually a few cm^2) dotted with thousands of DNA snippets (figure 8 a). Each of these snippets hosts a colony of a known ssDNA fragment (the targets). An unknown DNA sequence (the probe) is then exposed to this surface, and allowed to hybridize with its complementary strand (if present on the chip) (figure 8 b). Fluorescent labels, which can be directly attached to the probes (one can also

add intercalating dyes specific to dsDNA after the hybridization step), then indicate which one of the snippets has been the site of the hybridization process, thus revealing immediately the probe sequence.

DNA chips can be used for many applications. For example if the snippets host all of the 2^{19} possible combinations of a 20 base pairs ssDNA sequence (this has been done), one can easily sequence any 20 base DNA molecule in a manner of seconds. If the snippets correspond to the coding regions of genes, then it is possible to see which genes have been expressed in a cell offering clues to what makes a neuron a neuron, or a breast cancer cell divide. DNA chips could also allow easy comparisons of the gene expression of two different cells. The idea is to use two different fluorescent labels for the two cells (e.g. blue and yellow). When a gene is expressed in the two cells, the corresponding snippets are a mix of the two colors (e.g. green) but in the case where only one cell expresses a gene, the corresponding snippets are of the color attributed to that cell (e.g. blue or yellow). DNA chips can also be used as diagnostic tools, by populating the snippets with viral DNA (e.g. HIV), or with a gene mutation which corresponds to a given cancer or genetic disease. Ultimately, DNA chips can then test thousands of known diseases.

As often, the key to the future success of a new technology is cost-related. DNA chips must become cheaper than other diagnostic/sequencing methods in order to be mass-produced. Presently, DNA chips are relatively expensive and their use is limited to research applications. However, the possible market (and profit) is huge and many companies are investing massive amounts of money in this approach. One of the main difficulties, and this is where SPA could play a role, is to generate the snippets with a high density of DNA targets. Many strategies are presently used, from photolithographic to robot deposition and droplet sprays. SPA could in principle be used to generate the snippets. The idea would then be to hybridize one probe in each snippet and then generate the rest of the colony using solid phase DNA amplification. This technique could represent a cheap alternate route to DNA target implantation on the chips and could produce extremely dense self-assembled snippets.

0.8 The Manteia - University of Ottawa Collaboration

In 2001 we started a three year contract with Manteia Predictive Medicine (which, unfortunately, had to close at the end of 2003) which has led to the last two publications of this thesis. Manteia Predictive Medicine, a small company located in Nyon near Geneva in Switzerland, was exclusively focussing on the development of the SPA technology. One of the main researchers of the company (and the inventor of the SPA technique), Pascal Mayer, is a physicist who spent two years as a post-doctoral fellow in

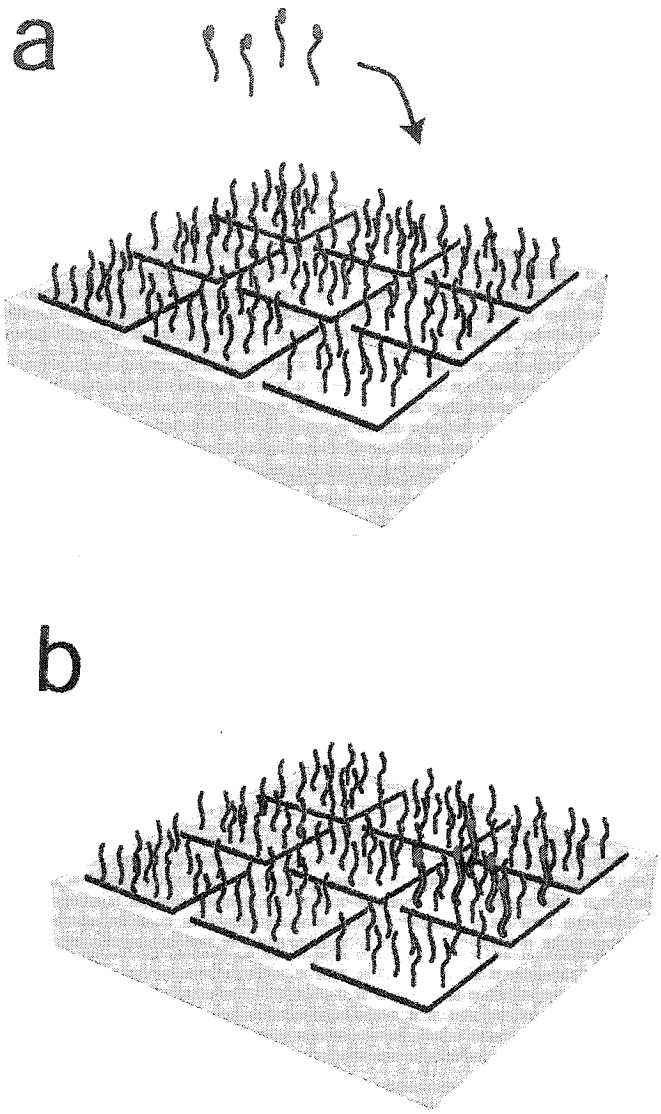

Figure 8: Representation of a DNA chip. Each section of the chip contains a colony of DNA fragments with a known sequence. The unknown sample (which has a fluorescent tag) is then introduced (a) and it soon binds to its complementary strand (b). Detection of the fluorescence indicates the location of the sample, and hence its identity.

Dr. Slater's group at the University of Ottawa in 1992-1994. Most of the research at Manteia focused on the biology and technical aspects of SPA. Dr. Mayer contacted us to look at the problem in a more fundamental way and to undertake the modelling of the growth of the DNA colonies. The aim was to develop a better understanding of the kinetics of colony growth.

Along with the modelling and theoretical work done for my thesis, I also performed experimental work at the Manteia Predictive Medicine facilities. Over two trips, I spent close to three months at the company facilities, most of it in the summer of 2002. During these visits, I performed SPA related experiments under various conditions. Unfortunately, technical problems and some legal aspects, have prevented us to use any of these results for publication or for this thesis. Note that in the framework of the collaboration, I also wrote two confidential reports (some non-sensitive parts of these reports are used in [IV] and [V]).

0.9 Presentation of the Thesis

The core of this thesis in made of four published and one submitted articles.

[I] J. F. Mercier and G. W. Slater. Random walk and diffusion of hard spherical particles in quenched systems: Reaching the continuum limit on a lattice. *Journal of Chemical Physics*, 113: 9109–9112, 2000.

In the first article, we explain our new numerical method to rapidly reach the continuum limit using results obtained on a lattice. We show that, used in combination with the exact mobility calculation method (developed in my master's degree), this new numerical method allows one to rapidly obtain lattice-independent diffusion coefficients (or alternatively, low-field mobilities) for particles migrating through systems of quenched impenetrable obstacles. To test the method, we consider the simple case of periodic spherical obstacles; a general relation between the diffusion coefficient, the total obstructed volume ϕ and the dimensionality of the problem is proposed.

[II] J. F. Mercier and G. W. Slater. An exactly solvable Ogston model of gel electrophoresis. 7. Diffusion and mobility of hard spherical particles in three-dimensional gels. *Macromolecules*, 34: 3437-3445, 2001.

In the second article, we use the continuum limit method developed in the first article, to test the main assumption of the OMRC model ($\mu^* = f(C) = 1 = \phi(C)$). We consider both periodic and random three-dimensional gels in the continuum limit and show that the mobility μ is not only affected by the

obstructed volume $\phi(C)$ but also by the geometry of the gel. However, we find that a modified relation $\mu^* \simeq 1 - \frac{2}{3}\phi(C) = \frac{1}{3} + \frac{2}{3}f(C)$ seems to be a good approximation for three-dimensional gels made of long stiff fibers.

[III] J. F. Mercier, F. Tessier and G. W. Slater. An exactly solvable Ogston model of gel electrophoresis: VIII. Nonconducting gel fibers, curved field lines, and the Nernst-Einstein relation. *Electrophoresis*, 22: 2631–2638, 2001.

The third article of this thesis is an answer to the critiques made by Locke and Trinh, who argued that the assumption of the uniform field lines was the reason why our results disagree with the OMRC hypothesis. We test this suggestion by extending our model to take into account the curvature of the field lines around non-conducting gel fibers. Our results showed that the dependence of the mobility of a point-like particle upon the concentration of the gel is not affected by the field line distortions in the low-field limit. Therefore, Locke and Trinh's claim is incorrect and the OMRC hypothesis is invalid for both straight and curved field lines.

[IV] J. F. Mercier, G. W. Slater and P. Mayer. Solid phase DNA amplification: a simple Monte Carlo lattice model. *Biophysical Journal*, 85: 2075–2086, 2003.

The fourth article of the thesis presents our first attempt at modelling Solid Phase DNA Amplification (SPA). We use a simple lattice Monte Carlo (MC) system, where a given lattice site can be either occupied by one DNA molecule or left empty (we later refined our model to let many particles occupy the same site). Using this model, we study the growth, stability and morphology of isolated DNA colonies under various conditions. Several non-ideal effects are also studied, and we demonstrate that such effects do not generally change the nature of the process, except in extreme cases. Our results indicate that, in most cases, SPA is characterized by a geometric growth and a rather sharp size distribution (in comparison with an exponential growth and a very broad distribution for solution PCR).

[V] J. F. Mercier and G. W. Slater. Solid phase DNA amplification: A Brownian Dynamics study. Submitted to *Biophysical Journal*.

The last article of the thesis will be submitted for publication as soon as some legal matters are resolved. In this manuscript, we develop a molecular approach to model the kinetics of a SPA experiment. To do so we use Brownian Dynamics simulations with a united atom model. The simulations mimic the temperature cycles and the molecule duplication process found in SPA; in particular, each

molecule whose free end comes very close to the surface during a given cycle duplicates at the location of the contact. Our results indicate that the finite size of the molecular colonies is an important factor because the molecules on the perimeter tend to lean outward. Furthermore, the growth of the colony as a function of the number of thermal cycles is found to be similar to the one obtained with our simple Monte Carlo simulations.

[Appendix 1] J. F. Mercier, G. W. Slater and Hong L. Guo. Numerically exact diffusion coefficients for lattice systems with periodic boundary conditions. I. Theory. *Journal of Chemical Physics*, 110: 6050–6056, 1999.

This paper was published during my master's thesis, and is included as supplementary information only. It explains in detail the numerical approach we used to obtain exact mobilities (section III) and compares this approach with a more complex one based on first passage times (section II).

0.10 Other Contributions

During my PhD, I contributed to other publications beyond the five articles that constitute the core of this thesis. I also presented my work at many conferences and wrote two confidential reports for Manteia Predictive Medicine. Here is a summary of these activities:

Articles

- G. W. Slater, S. Guillouzic, M. G. Gauthier, **J. F. Mercier**, M. Kenward, L. C. McCormick and F. Tessier. Theory of DNA electrophoresis 1999 $\sim$ 2002$\frac{1}{2}$, *Electrophoresis*, 23: 3791–3816, 2002.
- G. W. Slater, C. Desruisseaux, S. J. Hubert, **J. F. Mercier**, J. Labrie, J. Boileau, F. Tessier and M. P. Pépin. Theory of DNA electrophoresis: A look at some current challenges, *Electrophoresis*, 21: 3873–3887, 2000.
- J. Labrie , **J. F. Mercier** and G. W. Slater. An exactly solvable Ogston model of gel electrophoresis V. Attractive gel-analyte interactions and their effects on the Ferguson plot, *Electrophoresis*, 21: 823–833, 2000.

Graduate Student Physics Meeting

- Oral Presentation: 2003 (Merida, Mexico). "Solid Phase DNA Amplification: A Simple Monte Carlo Lattice Model". Jean-François Mercier, Gary W. Slater, Pascal Mayer.

American Physical Society Annual Meeting

- Poster Presentation: 2004 (Montréal). "A Brownian Dynamics study of dense DNA brushes". Jean-François Mercier, Gary W. Slater, Pascal Mayer.
- Poster Presentation: 2003 (Austin). "Solid Phase DNA Amplification: A Simple Monte Carlo Lattice Model". Jean-François Mercier, Gary W. Slater, Pascal Mayer.
- Poster Presentation: 2001 (Seattle). " On the validity of the Ogston Obstruction model for diffusion and electrophoresis in gels". Jean-François Mercier, Gary W. Slater.
- Poster Presentation: 2000 (Minneapolis)."Diffusion of hard spherical particles in gel-like systems: Reaching the continuum limit on a lattice". Jean-François Mercier, Gary W. Slater.

Confidential Reports

- Jean-François Mercier, Gary W. Slater, Pascal Mayer Modelling Surface Amplification Polymerase Chain Reaction, 2002.
- Jean-François Mercier, Gary W. Slater, Pascal Mayer. First Annual Report for the Manteia S.A, Predictive Medicine- University of Ottawa collaboration, 2003.

0.11 Statement of Originality

The work presented in this thesis is, to the best of my knowledge, new and original. I developed all the original ideas, with crucial input from my supervisor Gary W. Slater. I wrote all the papers, with again some critical proof reading by Dr. Slater. In the third paper [III], Frederic Tessier provided the lattice electric field intensity. He used the successive over-relaxation technique to solve the Laplace equation for the system considered in the article. He did not participate in the writing of the article. For the last two papers [IV and V] Dr. Pascal Mayer, then at Manteia Predictive Medicine, has provided useful suggestions.

ARTICLE I

J. F. Mercier and G. W. Slater.

Random walk and diffusion of hard spherical particles in quenched systems:

Reaching the continuum limit on a lattice.

Journal of Chemical Physics, 113: 9109–9112, 2000.

Corrections

1. In FIG. 4, the formula at the top of the figure should read:

$$D^* = 1.7(\pi/4 - f)^{0.5}$$

2. It should have been pointed out that Lord Rayleigh [51] has actually derived the expression for the two dimensional isolated periodic circles (Equation 4) in 1892.

JOURNAL OF CHEMICAL PHYSICS VOLUME 113, NUMBER 20 22 NOVEMBER 2000

Random walk and diffusion of hard spherical particles in quenched systems: Reaching the continuum limit on a lattice

Jean-François Mercier and Gary W. Slater[a)]
University of Ottawa, 150 Louis-Pasteur, Ottawa, Ontario K1N 6N5, Canada

(Received 19 July 2000; accepted 30 August 2000)

Lattice Monte Carlo methods are widely used to study diffusion problems such as the random walk of a probe particle among fixed obstacles. However, the diffusion coefficient D found with such methods generally depends on the type of lattice used. In order to obtain experimentally relevant results, one often needs to consider the continuum limit, i.e., the limit where the size of the lattice parameter is infinitely small compared to the size of both the probe particle and the obstacles. A numerical procedure to reach this limit for a single particle diffusing between quenched impenetrable obstacles is presented. As an example, the case of a system of periodic spherical obstacles is treated and a general relation between the diffusion coefficient D, the total obstructed volume f, and the dimensionality d of the problem is proposed. © *2000 American Institute of Physics.* [S0021-9606(00)50444-9]

I. INTRODUCTION

The problem of obstructed diffusion in a quenched system of obstacles is of great interest in a large number of physical, biological, and chemical problems.[1] Numerous groups have studied this problem and an impressive number of analytical and empirical theories, often contradicting one another, have been developed. In several cases, the experimental or simulation uncertainties are so large that many theories can claim success in describing data far from the percolation limit. One of the main conceptual difficulties is to isolate the contributions of the hydrodynamic and obstruction interactions between the particle and the fixed obstacles. Amsden recently reviewed many theories with and without hydrodynamic interactions and concluded that the obstruction interaction was the predominant effect in the case of the diffusion of hard particles in gels.[2] But even when the hydrodynamic interactions are neglected, many competing theories still remain. Computer simulations cannot yet discriminate between them.

Computational methods such as molecular dynamics and Brownian dynamics simulations are very CPU intensive and the steady-state regime (described by the diffusion coefficient D) is sometimes hard to reach because one has to wait for the transient regime(s) to decay. To obtain better statistics faster, lattice Monte Carlo (MC) models can be used. However, the diffusion coefficient D found with such models generally depends on the type of lattice used. In order to obtain experimentally relevant results, one actually needs to consider the continuum limit, i.e., the limit where the size of the lattice parameter is (infinitely) small compared to the size of both the probe particle and the fixed obstacles. In this limit, the results should be identical to the ones obtained with off-lattice (MC) simulations (i.e., a simulation where the positions of the particle and obstacles are continuous variables).

[a)]Author to whom correspondence should be addressed; electronic mail: gslater@physics.uottawa.ca

In this paper, a novel high-precision numerical (non-MC) procedure to reach this limit for a probe particle diffusing through quenched impenetrable obstacles is described. As an example, we apply our procedure to the case of spherical periodic obstacles. Our goal is to show that such an approach can be used efficiently and that it can provide extremely accurate information. In fact, we believe that it represents a very powerful alternative to MC and off-lattice simulation methods and that it can be used to discriminate between different obstruction models of diffusion.

II. METHOD

In lattice MC models, the migration of the probe particle is represented by a random walk on a finite-size lattice (usually with periodic boundary conditions) with certain sites being forbidden. However, we recently demonstrated[3,4] that MC simulations are not necessary if one is interested in the asymptotic (steady-state) behavior. When the obstacles are fixed, the Monte Carlo algorithm can in fact be solved exactly and one can obtain the exact reduced diffusion coefficient:

$$D^* = \frac{D}{D_0} = \frac{1}{D_0} \lim_{t\to\infty} \frac{\langle x^2(t)\rangle}{2dt}, \tag{1}$$

where D_0 is the free (no obstacle) diffusion coefficient, $\langle x^2(t)\rangle$ the mean square displacement, t the time, and d the dimensionality. Our exact numerical approach uses the following modified Nernst–Einstein relation:[3]

$$D^* = \lim_{\epsilon\to 0} \frac{\mu(\epsilon)}{\mu_0}, \tag{2}$$

where μ and μ_0 are, respectively, the mobility of the migrating particle with and without obstacles, and ϵ is an external field. This equation relates the unbiased diffusion coefficient of a particle in a system of obstacles to its zero-field ($\epsilon \to 0$) mobility in the same system. It turns out that the prob-

9110 J. Chem. Phys., Vol. 113, No. 20, 22 November 2000 J.-F. Mercier and G. W. Slater

lem of the related field-driven migration is much easier to treat than the original diffusion process. With this approach, computing the diffusion coefficient D^* of the probe particle on the chosen lattice is reduced to the solution of a (large) system of linear equations. This approach only provides information about the steady-state regime (the diffusion coefficient D^*) and does not allow one to investigate short time dynamics. However, it gives exact diffusion coefficients and is usually faster than MC methods, making it possible to study more complex and more interesting systems with greater precision. The reader can consult Refs. 3 and 4 for detailed explanations of this numerical procedure. In the following, we will demonstrate that it can be adapted to yield diffusion coefficients for off-lattice systems.

A. Modeling spheres on a cubic lattice

To build a pseudospherical probe particle or obstacle of diameter $2r$ on a lattice with a mesh size ξ, we first center the object (at the center of a unit cube for odd diameters, and on a lattice site for even diameters) and we add the unit cubes whose centers are within a distance r of the starting position. The resulting objects become perfect spheres in the $r/\xi\to\infty$ limit. Figure 1(a) shows the shape of our "spherical" objects [on a three-dimensional (3D) cubic lattice] for $\xi\leqslant 2r\leqslant 10\xi$, while Fig. 1(b) shows a two-dimensional (2D) example.

The problem of a spherical probe particle of radius R diffusing in a system made of spherical obstacles of radius r is equivalent to the problem of a spherical particle with an effective size $r+R$ diffusing in a system of pointlike obstacles (or vice versa). In fact, the relevant parameter is the obstructed volume $f(R,r,C)$, i.e., the fraction of the volume not accessible to the probe particle when the latter is reduced to a pointlike object. Note that f is meaningful even when the particle and/or obstacles have irregular forms. When calculating diffusion coefficients, we use the simple procedure of replacing a given system by a pointlike probe and obstacles of effective size $r'=r+R$. To obtain the results in term of experimental values (R, r, and C), one would simply need to establish the relation between the obstructed volume f, the particle size R, the obstacle size r, and the concentration C.

B. The continuum limit

The diffusion coefficient generally depends on the type of lattice used because the lattice amplifies the effect of the particle and obstacle shapes and modifies the correlation between consecutive particle–obstacle collisions. Of course, those differences are usually unphysical and in order to obtain experimentally relevant results, one generally needs to consider the continuum limit where the lattice parameter is infinitely small in comparison with all other lengths. In this limit, the result should be independent of the type of lattice and should also correspond to the one obtained with off-lattice simulations.

One straightforward way to approach the continuum limit is to progressively decrease the mesh size ξ of a given problem, i.e., to decrease the relative size of the lattice parameter while keeping R and r constant [see Fig. 1(b) for an example], and to estimate the asymptotic continuum diffusion coefficient $D^*(f)\equiv D^*(f,\xi\to 0)$. To obtain the dependence of the asymptotic diffusion coefficient $D^*(f)$ upon the obstructed volume f, one then needs to repeat the procedure for different obstructed volumes f, and finally fit the $\xi\to 0$ extrapolated data using, e.g., a polynomial form:

$$D^*(f)=1+\sum_{i=1} a_i f^i. \tag{3}$$

Another approach consists in finding the dependence (also in a polynomial form) of the diffusion coefficient $D^*(f,\xi)$ upon the obstructed volume f for a large number of mesh sizes ξ, and then extrapolate the corresponding coefficients $a_i(\xi)$ in the $\xi\to 0$ limit. While less intuitive, this approach is more efficient when f is small, i.e., the asymptotic coefficients $a_i\equiv a_i(\xi\to 0)$ can be found with greater precision. As an example, Sec. III studies the dependence of D^* upon the obstructed volume f for a system made of periodic spherical obstacles in d dimensions. This system has been widely studied[5–11] and thus represents a good test for our approach.

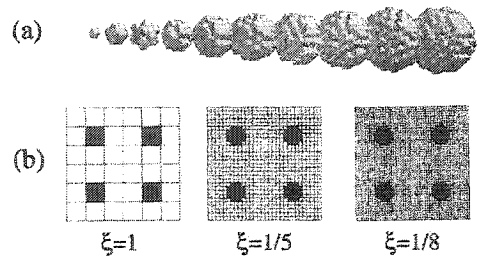

FIG. 1. (a) Our 3D "spherical" objects on a cubic lattice for diameters $1\xi\leqslant 2r\leqslant 10\xi$. (b) Lattice representation, for mesh sizes $\xi=1,\frac{1}{5}$, and $\frac{1}{8}$, of a two-dimensional system made of periodic circular obstacles of effective diameter $2(R+r)=1$. Periodic boundary conditions are applied in both directions.

III. ISOLATED OBSTACLES

A. In two dimensions

Figure 1(b) shows the lattice representations of a two-dimensional system made of periodic circular obstacles of effective diameter $2(r+R)=1$. Note that the obstacles become perfect circles in the $\xi\to 0$ limit. The procedure is thus to calculate the exact values of $D^*(f,\xi)$ and then fit the data using Eq. (3) to find the coefficients $a_i(\xi)$. The last step is to extrapolate these coefficients toward the $\xi\to 0$ limit. Figure 2 shows the first coefficient a_1 for square and triangular lattices as a function of the mesh size ξ. As expected, the results for the first coefficient converge toward the same value in the continuum limit [$a_1(0)=-1.002(8)$]. Similarly we obtain $a_2=+1.01(5)$ for the square lattice (although less precise, the results for the triangular lattice agree with this value; not shown). In fact, the extrapolated value for coefficient a_3 (not shown) converges toward a value of -1 (however, the uncertainties are much larger). These results seem to indicate that an excellent description of the dependence of the diffusion coefficient upon the obstructed volume (for small values of f) is provided by the following simple formula:

J. Chem. Phys., Vol. 113, No. 20, 22 November 2000

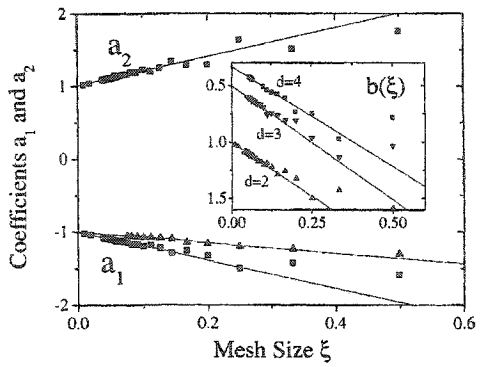

FIG. 2. Coefficients $a_1(\xi)$ and $a_2(\xi)$ of the polynomial fit of $D^*(f)$ [see Eq. (3)] vs the mesh size ξ. The extrapolated values are: $a_1(0) = -1.003(6)$ and $a_2(0) = +1.01(5)$ for the square lattice and $a_1(0) = -1.00(1)$ for the triangular lattice. Inset: Coefficient $b(\xi)$ in Eq. (5) for periodic spherical obstacles in two, three, and four dimensions. The asymptotic values are, respectively, $b_{d=2}(0) = 1.003(6)$, $b_{d=3}(0) = 0.50(1)$, and $b_{d=4}(0) = 0.33(2)$. The results have been obtained using hypercubic lattices.

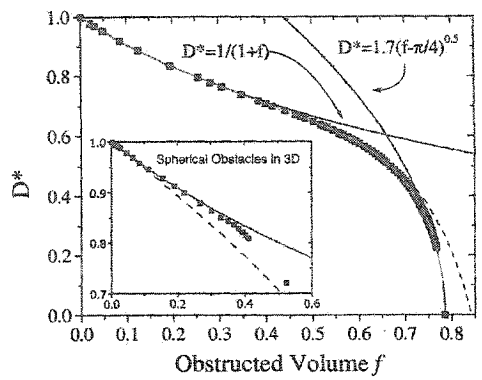

FIG. 4. Asymptotic diffusion coefficient D^* vs the total obstructed volume f for a pointlike probe particle ($d=2$). The dashed line is the Keller and Sachs function (8) while the solid lines represent Eqs. (4) and (6) for small and large f, respectively, and the interpolation function (7). There is an inflection point at $f=0.38(3)$. The inset is a similar plot for the three-dimensional case. The solid and dashed lines represent Eqs. (9) and (10), respectively.

$$D^*(f) \simeq \frac{1}{1+f} = 1 - f + f^2 - f^3 + \cdots . \tag{4}$$

This can be verified in Fig. 3 where $1/D^*(f)$ is plotted as a function of the obstructed volume f for various mesh sizes ξ. The simple linear relation:

$$1/D^*(f) = 1 + bf, \tag{5}$$

is in superb agreement with the data. For small values of ξ, the data are indeed linear for obstructed volumes as large as $f=30\%$. Furthermore, the data get closer to the suggested relation (4) as the mesh size ξ decreases (i.e., $b \to 1$ when $\xi \to 0$; see the inset of Fig. 2). This result has been predicted theoretically in Ref. 6 using variational principles. Of course, this formula cannot be valid for very large values of f since it does not predict a percolation threshold. As shown in Fig. 4, Eq. (4) gives essentially a perfect fit for small f. However, when the separation between obstacles becomes comparable to their radius ($f=\pi/9 \simeq 0.35$), D^* starts decreasing much faster and $D^*=0$ when the obstructed volume is larger than the percolation threshold ($f^*=\pi/4$). Close to f^*, our data agree with the following power-law decay:

$$D^*(f) = 1.7(2)(f^* - f)^{0.50(3)}. \tag{6}$$

This is in perfect agreement with previous works[8] where a one half exponent was reported. Note that a similar power law decay, with an exponent of 1.3, has been reported for randomly distributed overlapping circular obstacles.[8] A very good interpolation formula is provided by the simple function (Fig. 4)

$$D^*(f) = \frac{[(1-(f/f^*)^5)\times(1+0.57(f/f^*)^5)]^{1/2}}{1+f}. \tag{7}$$

In particular, it reproduces both Eqs. (5) and (6) in the appropriate limits and predicts an inflexion point at $f=0.40$. In a similar study, Schlicht and Ilgenfritz[11] found that the Keller and Sachs function[10]

$$D^*(f) = \frac{1 - f - 0.305\,84f^4 - 0.013\,363f^8}{(1-f)(1+f-0.305\,84f^4-0.013\,363f^8)} \tag{8}$$

was in excellent agreement with their simulation data. As shown in Fig. 4, Eq. (7) is clearly more accurate for $f \gtrsim 0.7$. For smaller values of f, the two functions are almost indistinguishable. Note that numerous other interpolation formulas have been proposed for this problem; see, e.g., Ref. 7.

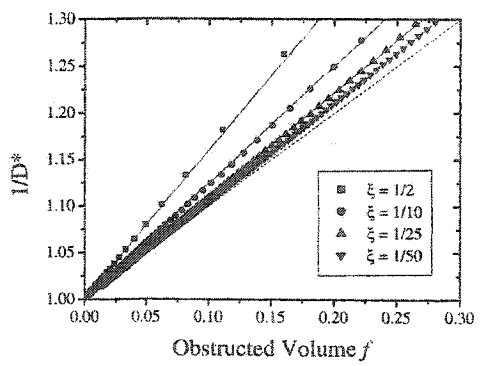

FIG. 3. Inverse diffusion coefficient $1/D^*$ vs the obstructed volume f for various mesh sizes ξ. The solid lines are linear fits and the dashed line is $1/D^* = 1+f$, the suggested asymptotic result for the $\xi \to 0$ continuum limit.

B. In higher dimensions

We also studied periodic spherical obstacles in $d=3$ and $d=4$ dimensions in order to check whether Eq. (5) would still apply when f is small. The inset of Fig. 2 shows the corresponding coefficients $b(\xi)$ as a function of the mesh size ξ. Remarkably, the values appear to converge exactly to $\frac{1}{2}$ and $\frac{1}{3}$ for three and four dimensions, respectively. These results suggest the following general relation for all similar systems in d dimensions:

$$D^*(f)=\frac{1}{1+\frac{1}{d-1}f}. \tag{9}$$

For $2\leq d\leq 4$, this simple linear relation provides superb agreement with the small f data. For $d=3$, Eq. (9) is essentially a perfect fit for $f\lesssim 0.2$ and is clearly more accurate than the "unsymmetrical Bruggeman equation":

$$D^*(f)=(1-f)^{1/2}, \tag{10}$$

proposed by Ilgenfritz and Runge in a similar study[11] (inset of Fig. 4). In fact, Eq. (10) wrongly predicts a negative curvature near the origin, while Eq. (9) qualitatively and quantitatively predicts the correct positive curvature. Also, Eq. (9) predicts the expected results for the trivial $d=1$ and $d\to\infty$ cases.

IV. CONCLUSION

In this article, we described a novel numerical procedure to rapidly compute lattice-independent high-precision diffusion coefficients for a probe particle diffusing through quenched impenetrable obstacles. We showed how such a procedure can be applied efficiently to the case of simple periodic systems to generate extremely accurate results. For example, we have been able to obtain a general relation (in the low obstruction limit) between the diffusion coefficient D^*, the total obstructed volume f, and the dimensionality d of the problem in the case of spherical periodic obstacles. Also, we investigated the highly obstructed limit for the two-dimensional case. Our data agree with a power law decay near the percolation threshold. For this case we also found a simple interpolation formula which is in excellent agreement with our data for all values of f. In principle, this procedure could be used to study any periodic system in any dimension using any type of lattice. We could also easily modify the geometry of the obstacles (or the probe particles) or add interactions between the obstacles and the probe particle.[12] Also of great interest are problems with penetrable obstacles (domains) as models for biomembranes.[1,13–15] The case of random systems could also be treated using this approach but this generalization is not trivial.[3,4] The main issue is that the lattice size has to be much larger than the correlation length of the system. Thus, one needs to treat much larger lattice systems in order to obtain relevant results, especially near the percolation threshold and at very low concentration. Nevertheless, we believe that this procedure provides a powerful alternative to off-lattice simulation methods and, in particular, that it could be used very efficiently to discriminate between different obstruction models of diffusion in a wide variety of problems. More complex systems, such as the cage problem,[16] are currently being studied, and a detailed analysis will be published elsewhere.

ACKNOWLEDGMENTS

We want to thank Professor Hyuk Yu for calling our attention to Ref. 9 and Professor A. R. Day for useful discussions. This work was supported by a Research Grant to G.W.S. and a scholarship to J.F.M. from the Natural Science and Engineering Research Council (NSERC) of Canada, and by scholarships from the University of Ottawa (Excellence and SAD Awards) to J.F.M.

[1] M. J. Saxton, Curr. Top. Membranes **48**, 229 (1999).
[2] B. Amsden, Macromolecules **21**, 8382 (1998).
[3] J.-F. Mercier, G. W. Slater, and H. L. Guo, J. Chem. Phys. **110**, 6050 (1999).
[4] J. F. Mercier and G. W. Slater, J. Chem. Phys. **110**, 6057 (1999).
[5] D. A. Hadden, R. L. Rill, L. McFaddan, and B. R. Locke, Macromolecules **33**, 4235 (2000).
[6] D. S. Tsai and W. Strieder, Chem. Eng. Commun. **40**, 207 (1986).
[7] A. R. Day, K. A. Snyder, E. J. Garboczi, and M. F. Thorpe, J. Mech. Phys. Solids **40**, 1031 (1992).
[8] S. Feng, B. I. Halperin, and P. N. Sen, Phys. Rev. B **35**, 197 (1987).
[9] L. Schicht and G. Ilgenfritz, Physica A **227**, 239 (1995).
[10] H. Keller and D. Sachs, J. Appl. Phys. **35**, 537 (1964).
[11] G. Ilgenfritz and F. Runge, Physica A **181**, 69 (1995).
[12] J. Labrie, J.-F. Mercier, and G. W. Slater, Electrophoresis **21**, 823 (2000).
[13] P. F. F. Almeida and W. L. C. Vaz, *Handbook of Biological Physics* edited by R. Lipowsky and E. Sackmann (North-Holland, Amsterdam, 1995), Vol. 1, p. 305.
[14] K. Tamada, S. Kim, and H. Yu, Langmuir **9**, 1545 (1993).
[15] K. Tanaka, P. A. Manning, V. K. Lau, and H. Yu, Langmuir **15**, 600 (1999).
[16] P. A. Netz and T. J. Dorfmuller, J. Chem. Phys. **107**, 9221 (1997).

ARTICLE II

J. F. Mercier and G. W. Slater.

An exactly solvable Ogston model of gel electrophoresis. 7.

Diffusion and mobility of hard spherical particles in three-dimensional gels.

Macromolecules, 34: 3437-3445, 2001.

Corrections

1. Prior to Equation 3, it should have been mentioned that the gel concentration C is expressed in terms of volume fractions.

2. The wrong set of data was used in Figure 3. The data should converge to $\mu^* = 0.882(1)$. Likewise, the end of the fourth paragraph of page 36 should read:

   " ... The mobility converges toward $\mu = 0.882(1)$ in the $\xi \to 0$ (continuum) limit."

3. On page 37, last paragraph of the first column. "Figure 7 shows an example of such a fit for a system with a lattice ..." should read "Figure 6 shows an example of such a fit for a system with a lattice ..."

4. Equation 17 should read:

$$\mu^* = \frac{1}{1 + \frac{1}{d-1}\phi}$$

Macromolecules **2001**, *34*, 3437−3445 **3437**

An Exactly Solvable Ogston Model of Gel Electrophoresis. 7. Diffusion and Mobility of Hard Spherical Particles in Three-Dimensional Gels

Jean-François Mercier and Gary W. Slater*

University of Ottawa, 150 Louis-Pasteur, Ottawa, Ontario K1N 6N5, Canada

Received September 6, 2000; Revised Manuscript Received January 19, 2001

ABSTRACT: We extend our lattice model of gel electrophoresis (and diffusion) to the study of the continuum limit (no lattice effect) for hard spherical particles migrating in periodic and random three-dimensional gels. To reach the continuum limit, the mesh size of the system is progressively decreased until a clear extrapolation to the continuum limit (where the size of the lattice parameter is infinitely small in comparison to the size of the gel fibers) can be done. Various types of gel are studied, starting from simple periodic parallel and straight fibers to a representation of a more realistic gel formed of irregular, cross-linked fibers placed along random directions. Our mobility data for pseudospherical particles in the continuum limit are interpreted in terms of the obstruction model of diffusion.

I. Introduction

Over the past few years we have developed a new microscopic model to study the gel electrophoresis (or, equivalently, the thermal diffusion) of hard particles. Our lattice model allows us to compute exact reduced mobilities μ^* (or exact reduced diffusion coefficients D^*) as well as exact free available volumes, f, for arbitrary gel structures and particle shapes in any dimension $d \geq 2$.[1−6] Because of the large computer resources needed to obtain exact results, we were first forced to study relatively simple and somewhat unrealistic particles and gels (e.g., two-dimensional systems, square particles, etc.). However, we recently proposed a much more efficient numerical approach[7,8] that makes it possible to tackle much larger (hence more realistic) analyte−gel systems. This article is the first one in which we study pseudospherical analytes migrating in realistic three-dimensional gels. Such systems closely correspond to the main reason why Ogston models are used to interpret electrophoretic data.[1−13]

Originally, the main goal of our investigation was to verify the standard Ogston−Morris−Rodbard−Chrambach (OMRC) model,[9−11] as well as a data analysis method based mostly on the so-called Ferguson plot.[12,13] In the framework of the OMRC model, the low-field reduced mobility $\mu^*(C)$ of an analyte is assumed to be equal to its free available volume $f(C)$:

$$\mu^*(C) = \frac{\mu(C)}{\mu_0} = f(C) = 1 - \phi(C) \tag{1}$$

where μ_0 is the free (no obstacle) mobility, $\phi(C)$ the excluded volume, and C the obstacle concentration. While never proven (experimentally or theoretically),[14] this assumption is the starting point the OMRC model, which is widely used within the electrophoresis community.

For a specific system, namely a spherical particle in a random array of infinitely long (but un-cross-linked) fibers, Ogston[9] showed that the fractional volume available to the analyte was given by

$$f(C) = e^{-\pi(R+r)^2/4a^2} \tag{2}$$

where R, r, and $a(C)$ are the radii of the analyte, gel fiber, and gel pore, respectively. For the Ogston ideal "gel", the mean pore size $a(C)$ is given by (this formula was derived for infinitely thin fibers)

$$a(C) = \frac{1}{\sqrt{4\nu l}} \propto \frac{1}{\sqrt{C}} \tag{3}$$

where ν is the concentration of fibers per unit volume and l the average fiber length. This leads to

$$\mu^*(C) = f(C) = e^{-KC} \tag{4}$$

where $K \propto (R + r)^2$ is the so-called retardation coefficient. This implies that the Ferguson plot ($\ln \mu$ vs C or $\ln \mu^*$ vs C) should be linear. In such cases, one can easily extract the retardation coefficient from the slope. Furthermore, when the square root of the retardation coefficient is plotted as a function of the particle radius R, the value of R where $K(R) = 0$ (found by extrapolating $K^{1/2}$ to negative values of R) gives $-r_K$, which is an estimate of the fiber radius r.

An effective mean pore size a_K can also be estimated when using the OMRC model to analyze experimental data. For example, the plot of the root of the log of the mobility as a function of the particle size ($\sqrt{-\ln\mu}$ vs R) should yield a straight line with a slope given by the inverse of the pore size. More frequently, one assumes that $R \gg r$ to obtain a value from the data using the fact that we then have $\mu^*(R=a) = e^{-\pi/4} \simeq 1/2$.[15]

In the previous parts of this series, we studied square or cubic particles diffusing in two-dimensional periodic, random, and fuzzy gels (parts I, II, III, and V[1−3,5]) and three types of three-dimensional periodic gels (parts IV and V[4,5]). For all these sieving gels, the basic assumption of the OMRC model, namely, that the low-field gel electrophoresis mobility μ of a (rigid) particle is proportional to the fractional gel volume $f = 1 - \phi$ available to the particle, was found to be inaccurate, except for the nonrealistic case where the gel constraints (the obstacles) were reset randomly at each time step (corresponding to a mean-field approximation or an annealed gel).[1] We also showed that, for two-dimensional

* To whom correspondence should be sent. E-mail: gslater@science.uottawa.ca.

10.1021/ma001544o CCC: $20.00
Published on Web 04/06/2001

gels, the curvature of the so-called Ferguson plot was related to the degree of disorder in the gel[1] and that certain gel architectures can have nontrivial sieving properties.[3] We further demonstrated that a modified Ferguson plot can nevertheless provide useful semiquantitative information about the gel properties (such as a reliable estimate of the mean pore size)[1-3] and that the occasional presence of inflection points in the Ferguson plot may be explained by the effect of obstacle–analyte attractive interactions.[5] Finally, we studied the mobility of small oligomers and found the Ogston model to be insufficient to describe the movement of these molecules.[6]

In this article, we present a detailed study of pseudospherical analytes migrating in three-dimensional gels, clearly a very Ogston-like system.[9] Our aim is to study the continuum limit and to draw fundamental conclusions about realistic systems without hydrodynamic interactions. The paper is organized as follows. After a short overview of our model and numerical techniques (section II), the mobility of the analyte is calculated for infinite periodic straight fibers placed perpendicularly to the net motion of the particle (section III). In section IV, the mobility is calculated for four types of three-dimensional gels. The first two are periodic and are made of straight infinite fibers placed along the three orthogonal axes with and without cross-links (section IV). The last two are random: one is made of straight orthogonal fibers places randomly, while the last one is made of irregular cross-linked fibers placed along random directions. Our conclusions are presented in section V.

II. The Model

Many computational methods can be used to study the diffusion (random or biased, with or without constraints) of a particle. However, most of them, like molecular dynamics and Brownian dynamics simulations, are very CPU intensive, and the steady-state regime is sometimes hard to reach. To obtain better statistics faster, lattice models can be used. In such models the migration of the particle is represented by a random walk on a finite-size lattice (usually with periodic boundary conditions) where certain sites are forbidden (this may represent, e.g., gel fibers). These investigations often involve Monte Carlo methods and, with modern computers, allows one to follow the diffusion of millions of independent (or even interacting) particles over physically meaningful distances. The approach is quite simple. One simply records the position x of the analyte as a function of time t and then estimates the mobility:

$$\mu = \frac{1}{\epsilon} \lim_{t\to\infty} \frac{\langle x(t)\rangle}{t} \tag{5}$$

where ϵ is the dimensionless field intensity. In absence of a field one can estimate the diffusion coefficient as

$$D = \lim_{t\to\infty} \frac{\langle x(t)^2\rangle}{2t} \tag{6}$$

Lattice Monte Carlo simulations can also provide information about the short time dynamics of the particles. However, when only the low-field steady-state regime (D of μ) of an isolated particle is of interest, we demonstrated in part I of this series that lattice simulations are not necessary since the Monte Carlo algorithm can in fact be solved exactly for the mobility (or for the diffusion coefficient) in the zero-field limit.[1,7] In other words, we find directly μ or D without recording x as a function of time. This greatly simplifies the analysis since we then obtain exact values. However, our method is only useful for isolated analytes in the zero-field limit.

A. The Lattice Random-Walk Model. In the lattice random-walk model, the particle moves by making discrete jumps of length $L = 1$ (the lattice parameter) and duration $\tau = 1$ (in scaled units). For a rigid particle (which can be of any desired shape; note however that particle rotation is not allowed) evolving on a three-dimensional cubic lattice with an electric field ϵ pointing in the $+x$ direction, the probabilities for the next jump to be in the various possible directions ($\pm x$, $\pm y$, and $\pm z$) are, to first order in ϵ, given by[1]

$$p_{\pm x} = \frac{1 \pm \epsilon}{6} + O(\epsilon^2), \quad p_{\pm y} = p_{\pm z} = \frac{1}{6} \tag{7}$$

The rules for this model are quite simple: at each time step the particle moves to one of the six adjacent sites according to the probabilities given by eq 7. However, since a particle cannot overlap with an obstacle (representing a gel fiber), a jump leading to this situation is rejected and the particle returns to its previous position. Note that the current time is increased by the time step ($\tau = 1$) even when the jump is rejected. The jump rejection rule models the steric (hard core) interactions between the analyte and the gel fibers. Other types of analyte–fiber interactions are not taken into account but can also be included.[5]

B. Exact Mobilities. The mobility μ is defined as the velocity v of the particle divided by the intensity ϵ of the applied field (eq 5). Consider a particle of mass M (where M is the number of lattice cells occupied by the particle) evolving on a lattice of size $s \times s \times s$ (using periodic boundary conditions). We first calculate the steady-state probability of presence (n_i) of the particle on each of the available sites (defined as the sites where the center of mass of the particle can be placed without having any part of the particle overlapping with gel fibers). Since the probabilities n_i are coupled to each other (because of the jump dynamics), the problem can be reduced to the solution of a large system of linear equations. We then calculate the mean local velocity of the particle on each site (v_i). This step is straightforward since the latter depends only on the occupancy (by an obstacle) of the nearest-neighbor sites.[1] The average velocity of the particle is then given by $v = \sum_i n_i v_i$. The reader can consult parts I–V of this series[1-5] as well as refs 7 and 8 for more details.

Since we are interested in the low-field limit $\epsilon \to 0$, all our calculations are carried to first order in ϵ, and we drop all higher order terms. Recently, we found that we can actually eliminate the need for an arbitrary (finite) value of ϵ in the case of a vanishing electrical field.[7,8] The calculation of the exact mobility is then reduced to the solution of a purely numerical (no reference to the field parameter ϵ) system of S linear equations (where $S \le s^3$ is the number of available sites) of the form (we use the Dirac notation where matrices are represented by uppercase letters, scalars by lowercase letters, and row and column vectors by respectively bras and kets):

$$A_{ij}|n_\epsilon\rangle = -A_\epsilon|n_I\rangle \tag{8}$$

where A_I, A_ϵ, $|n_I\rangle$, and $|n_\epsilon\rangle$ are the field-independent (subscripts I) and field-related (subscripts ϵ) terms of the transition matrix $A = A_I + \epsilon A_\epsilon$ and probability vector $|n\rangle = |n_I\rangle + \epsilon|n_\epsilon\rangle$. Note that the only unknown here is the probability correction term $|n_\epsilon\rangle$. Therefore, with our approach, the problem of finding the zero-field mobility of an analyte is reduced to the solution of a (large) system of linear equations. This system of linear equations can be directly solved using, e.g., Maple or Mathematica, in which case the mobility can be expressed in terms of a (huge) rational fraction or with a number of well-known numerical algorithms integrated within a lower level language (e.g., Fortran, C) program. With our homemade Fortran program (which automatically writes and solves the linear equations), we have been able to solve problems corresponding to lattices as large as 80 × 80 × 80 on standard Pentium-based workstations. Once $|n_\epsilon\rangle$ is found, the resulting scaled mobility can easily be computed as

$$\mu^* = \frac{v}{\mu_0 \epsilon} = \frac{\langle v|n\rangle}{\mu_0 \epsilon} = \frac{\langle v_I|n_\epsilon\rangle + \langle v_\epsilon|n_I\rangle}{\mu_0} \tag{9}$$

where μ_0 is the free (no obstacle) mobility of the particle. We refer the reader to refs 7 and 8 for a complete derivation of the preceding equations.

C. Diffusion Problems. It turns out that our approach can also be used to study diffusion problems since the zero-field mobility is related to the diffusion coefficient through the Nernst–Einstein relation:

$$D^* = \frac{D}{D_0} = \lim_{\epsilon \to 0} \frac{\mu}{\mu_0} \tag{10}$$

where D and D_0 are respectively the diffusion coefficients of the analyte with and without obstacles. Therefore, it is possible to reinterpret all the data in the current article as being related to the diffusion of spherical particles in quenched gels when the hydrodynamic interactions are neglected. Obstructed diffusion is of great interest in a large number of physical, biological, and chemical problems.[16–20] Numerous groups have studied this problem, and an impressive number of analytical and empirical theories, often contradicting one another, have been developed. Amsden recently reviewed different models and concluded that the obstruction models in general provided the best agreement to the experimental data for heterogeneous hydrogels.[17] But even when only steric interactions are considered, many competing theories still remain. Apart from the standard Ogston model, one of the most often used is probably the stretched exponential:[21]

$$D^* = e^{-a\phi^b} \tag{11}$$

where both a and b are constants. In his review, Amsden concluded that for heterogeneous gels the stretched exponential and the very simple Tsai and Streider model[18]

$$D^* = \frac{1}{1 + \frac{2}{3}\phi} \tag{12}$$

were the most consistent with the literature data.

Finally, the diffusion problem can also be related to other transport properties. For example, many groups have studied the electrical properties (i.e., the conductivity) of a conductor containing nonconducting patches (e.g., holes) using the diffusion algorithm.[19]

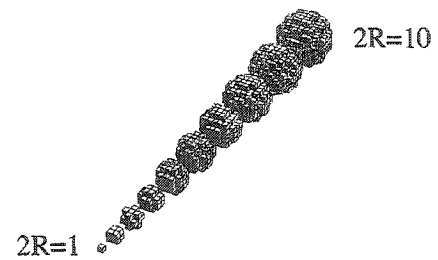

Figure 1. Spherical particles (on a cubic lattice) for diameters $2R$ varying from 1 to 10.

D. Random Systems. Our method allows one to obtain the exact mobility of the analyte for any specific finite size lattice system (using periodic boundary conditions) of any dimensionality ($d \geq 2$). For periodic systems of obstacles, this means that one can obtain the exact mobility in one iteration. However, the situation is different if there is any degree of randomness in the obstacle distribution. Using our approach, it is possible to find the exact mobility for specific realizations of the disorder, but we then need to average over various realizations to yield a meaningful mobility $\mu^*(C)$ or diffusion coefficient $D^*(C)$. This introduces a statistical error and explains why an uncertainty will be associated with the mobilities for the random systems. We also need to be careful with finite size effects. When calculating an average mobility for a disordered system, we are usually interested in the thermodynamic limit (an infinite system, $s \to \infty$). To obtain reliable results, the system has to be sufficiently large so that finite-size effects are negligible in comparison with the uncertainty resulting from the ensemble averaging process. For a complete discussion on these topics, see ref 8.

E. Modeling Spheres on a Cubic Lattice. For our system to be the most realistic possible, we chose to give the diffusing particle a "spherical" shape (and the gel fibers a "cylindrical" shape). Since the particles are evolving on a cubic lattice, our "spheres" are rather peculiar. Figure 1 shows the shape of our spherical particles (on a cubic lattice) for diameters $2R$ varying from 1 to 10. To build a pseudospherical analyte of size $2R$, we first center the particle (at the center of a unit cube for odd diameters and on a lattice site for even diameters) and we add the unit cubes whose centers are within a distance R of the starting position. The particles obviously become perfect spheres in the $R \to \infty$ limit.

Note that, for the calculation of the mobility, the problem of a particle of radius R diffusing in a gel with cylindrical fibers of radius r is equivalent to the problem of a particle with an effective size $r' = r + R$ diffusing in a gel with infinitely thin fibers (or vice versa). The relevant parameter of the problem is thus the excluded volume $\phi(R,r,C)$, which corresponds to the fraction of the volume not accessible to the analyte when the latter is reduced to a pointlike object. When calculating the mobility, we will use the simple procedure[22] of replacing a given system by a pointlike analyte and gel fibers of effective size $r' = r + R$. To obtain the results in term of "real" system parameters (R, r, and C), the relation between the excluded volume ϕ, the particle size R, the gel fiber size r, and the gel concentration C needs to be found. This relation can be very simple for periodic

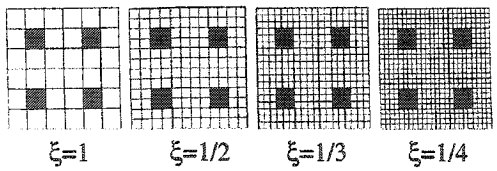

Figure 2. Transformation of a simple lattice problem as the mesh size ξ is decreased. The "gel" is made of isolated square obstacles placed periodically; the concentration C (or volume fraction ϕ) is $^1/_9$.

structures but can become quite complicated when considering complex gels. The original Ogston paper gives an example of such a calculation,[9] but real gels are different because they are cross-linked.

Note that it is not clear what a pointlike object corresponds to on a lattice. For instance, on a two-dimensional square lattice, a lattice site can be seen either as a pointlike object (i.e., a lattice point vertex) or as a 1 × 1 plaquette. While important for small analytes and fibers, this distinction becomes irrelevant in the continuum limit. In the following we will consider that the migrating analyte is a pointlike object (a lattice point vertex) and that the excluded volume ϕ is the fraction of lattice sites inaccessible to the analyte.

F. The Continuum Limit. The mobility (or diffusion coefficient) generally depends on the type of lattice used. This is so because the lattice amplifies the effect of the particle and obstacle shapes and modifies the correlation between consecutive events. To obtain experimentally relevant results, we need to consider the continuum limit, i.e., the limit where the size of the lattice parameter is infinitely small in comparison with the size of the analyte and obstacles. In this limit, the results are independent of the lattice type and correspond to the ones obtained with off-lattice Monte Carlo simulations. These two conditions are met, and our method thus provides valid and very precise numerical data with much less computing time.

In a separate article, we discuss a simple method to reach the continuum limit.[23] The procedure is to progressively decrease the "mesh size" ξ of a given problem, i.e., to decrease the relative size of the lattice parameter while keeping R and r constant. For example, let us consider the problem shown in Figure 2. In this system, a pointlike particle is migrating through a two-dimensional gel made of isolated square obstacles placed periodically. The separation between the obstacles is set to twice their linear size, resulting in a gel concentration (volume fraction) $\phi = C = {}^1/_9$. With the effective radius set at $r' = {}^1/_2$, the mesh size ξ is then reduced to zero. Figure 2 shows different views of the gel system for decreasing ξ while Figure 3 shows the resulting reduced mobility μ^* as a function of ξ for a pointlike analyte. The mobility converges toward $\mu^* = 0.922(1)$ in the $\xi \to 0$ (continuum) limit.

To obtain the dependence of the mobility upon the excluded volume ϕ (or the obstacle concentration C), one needs to repeat the procedure for different values of excluded volumes ϕ and then fit the ($\xi \to 0$) extrapolated mobility data. Because we did not have any specific mathematical formula to use to fit our numerical data, we chose to use the general polynomial form

$$\mu^*(\phi) = 1 + \sum a_i \phi^i \qquad (13)$$

Since we are mainly interested in the low concentration limit $\phi \ll 1$, only the first few coefficients are relevant. To obtain the a_i coefficients with more accuracy, we actually fit the function

$$g = \frac{\mu^*(\xi,\phi) - 1}{\phi} \qquad (14)$$

In this case, a_1 correspond to the ordinate axis, a_2 to the slope, and a_3 the curvature of the plot. This also ensures that the expansion in integer powers of ϕ is valid. For example, if there were a $\phi^{1/2}$ term in the $\mu(\phi)$ expression, the g function would actually diverge at $\phi = 0$.

Another approach to reach the continuum limit consists of finding the dependence (also in a polynomial form) of the mobility $\mu^*(\xi,\phi)$ upon the excluded volume ϕ for a large number of mesh sizes ξ and then estimate the resulting polynomial coefficients $a_i(\xi)$ in the $\xi \to 0$ limit. While less intuitive, this latter approach gives better results for small excluded volumes. For the Ogston hypothesis to be correct (eq 1), we must have $a_1 = -1$ and $a_{i\geq 2} = 0$.

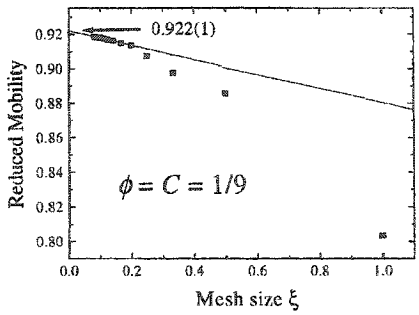

Figure 3. Mobility of a pointlike analyte as a function of the mesh size ξ for the system shown in Figure 2.

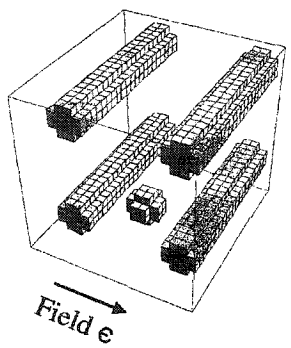

Figure 4. A three-dimensional periodic gel made of straight, parallel, and infinitely long fibers of radius $r = {}^1/_4$. There is no fiber aligned in the field direction. An analyte of radius $R = {}^1/_4$ is also shown. The mesh size is $\xi = {}^1/_8$.

III. Straight Fibers Perpendicular to the Field

Figure 4 shows a particle migrating in a "gel" made of straight, infinitely long parallel fibers. While the system is not a good representation of a gel, its symmetry of translation (the fibers are placed periodically) allows us to reduce it to the periodic two-dimensional system shown in Figure 5a. (We limit our study to the migration perpendicular to the gel fibers.) Since two-dimensional systems are computationally much easier to study than three-dimensional ones, this special case is a useful starting point for our investigation.

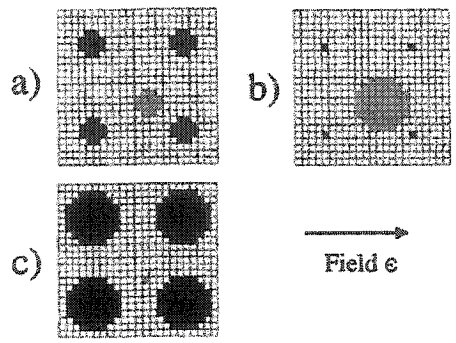

Figure 5. (a) Two-dimensional representation of the system shown in Figure 4. This problem is equivalent to that of a particle with an effective size $R' = r + R = 1/2$ diffusing in a gel with infinitely small fibers (b) or to the one of a pointlike particle and gel fibers of effective size $r' = r + R = 1/2$ (c). Note that, for visual reasons, the pointlike objects are shown as 1 × 1 plaquettes. The mesh size is $\xi = 1/8$.

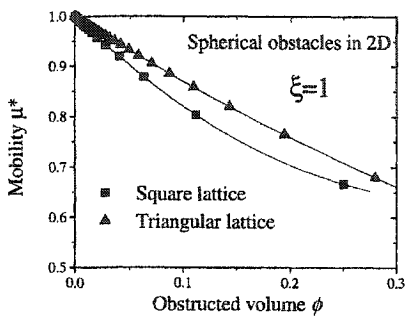

Figure 6. Mobility μ^* as a function of the excluded volume ϕ for a system made of two-dimensional periodic obstacles, using a square and a triangular lattice (in both cases the mesh size is $\xi = 1$). The solid lines are the best third-order polynomial fits.

A. Obtaining the Mobility. As briefly discussed in section IIE, when one is only interested in the mobility, the system shown in Figure 5a is formally equivalent to those of Figure 5b,c. Note that because of the imperfections of our lattice spheres, this equivalence will only be exact in the continuum limit ($\xi \to 0$).

We will now focus on finding the dependence of the mobility of a pointlike analyte upon the excluded volume ϕ (in terms of a polynomial form) for different mesh sizes (ξ). The procedure is the following. First, a mesh size ξ is chosen. Then the zero-field mobility of the particle is calculated exactly, using the method described in section IIB and refs 7 and 8, for increasing separations between the gel fibers (i.e., for decreasing excluded volume fractions ϕ). The excluded volume ϕ corresponds to the proportion of sites occupied by the effective fibers. Finally, a polynomial fit of the form

$$\mu^*(\xi,\phi) = 1 + \sum a_i(\xi)\phi^i \qquad (15)$$

is used to describe the dependence of the mobility upon the excluded volume ϕ. Figure 7 shows an example of such fit for a system with a lattice parameter $\xi = 1$, using a triangular and a square lattice. As expected, the two lattices give different results except in the trivial case $\phi = 0$. For all excluded volumes ϕ, the analyte has a larger mobility on the triangular lattice because of the larger lattice coordination number; i.e., the analyte has more ways to avoid consecutive collisions with an obstacle. In both cases, the curvature is positive, a characteristic of periodic gels.

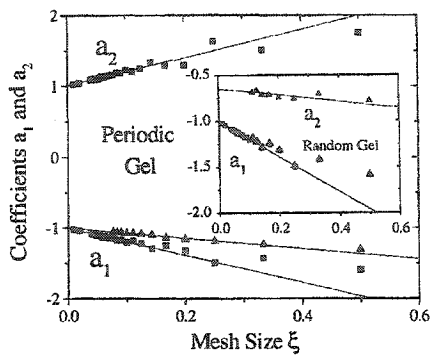

Figure 7. Coefficients $a_1(\xi)$ and $a_2(\xi)$ vs the mesh size ξ for a system made of two-dimensional periodic obstacles. The extrapolated values are $a_1(0) = -1.003(6)$ and $a_2(0) = +1.01(5)$ for the square lattice and $a_1(0) = -1.00(1)$ for the triangular lattice Inset: coefficients $a_1(\xi)$ and $a_2(\xi)$ for 2D isolated obstacles placed randomly, along with the a_1 data for the periodic obstacles (both results correspond to cases with a square lattice).

B. The Continuum Limit. The procedure described in section IIIA has been carried out for mesh sizes ξ varying from 1/100 to 1 on square and triangular lattices. Figure 7 shows the first coefficient a_1 for square and triangular lattices as a function of the mesh size ξ. The fluctuations of these very precise values can be explained by the roughness of our lattice "spheres" (our gel fibers will only take the perfect cylindrical shape in the $\xi \to 0$ limit). As expected, the results for the first coefficient is independent of the lattice type in the continuum limit, and the results converge toward the same value ($a_1(\xi \to 0) = -1.002(8)$) for both lattices. Similarly, we obtain $a_2 = +1.01(5)$ for the square lattice (although less precise, the results for the triangular lattice agree with this value; not shown). In fact, the extrapolated value for the third coefficient a_3 (not shown) also converges toward a value of -1 (however, the uncertainties are much larger). These results seem to indicate that an excellent description of the dependence of the mobility upon the obstructed volume (for small values of ϕ) is provided by the simple formula

$$\mu^*(\phi) = \frac{1}{1+\phi} \simeq 1 - \phi + \phi^2 - \phi^3 + \ldots \qquad (16)$$

This can be verified in Figure 8 where the inverse of the mobility is plotted as a function of the excluded volume for various mesh sizes ξ. Simple linear relations provide excellent agreement with the data, especially for small mesh sizes, for excluded volumes as large as $\phi \cong 20\%$. Furthermore, the data become closer to the relation given by eq 16 as the mesh size ξ decreases, indicating that it is indeed the correct relation in the continuum limit. This result, which has been predicted theoretically in ref 18 using variational principles, agrees with the OMRC model ($\mu = 1 - \phi$) to first order. Of course, this formula is not valid for large values of ϕ since it does not predict a percolation threshold. (For instance, eq 16 predicts $\mu = 1/2$ at $\phi = 1$, while we must have $\mu = 0$ when $\phi \geq \pi/4$ for our system of cylindrical fibers.) Nevertheless, it would give essentially perfect fits for all realistic "gel concentrations" (e.g., $\phi < 20\%$) in the continuum limit. In a separate article,[23] we showed that near the percolation threshold $\phi = \phi^* =$

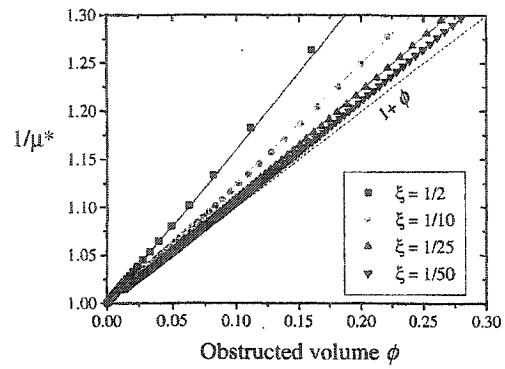

Figure 8. Inverse mobility $1/\mu^*$ vs the obstructed volume ϕ for various mesh sizes ξ. The solid lines are linear fits, and the dashed line is eq 16, the suggested asymptotic result for the $\xi \to 0$ continuum limit.

$\pi/4$ the data agree with a power-law decay, and we proposed a simple interpolation function which gives excellent agreement with our data for all values of the obstructed volume ϕ. We also showed that eq 16 can be generalized to the case of "hyperspherical" periodic obstacles in d dimensions:

$$\mu^*(\phi) = \frac{1}{1 + \dfrac{1}{1 + d}\phi} \tag{17}$$

for low values of excluded volume.

C. Randomly Placed Fibers. In a previous part of this series,[1] we reported that adding randomness in the distribution of obstacles does not affect the first coefficient (a_1) but does change the second one (a_2). In fact, we showed that, in the case of isolated square obstacles in two dimensions, the sign of the second coefficient actually changes from positive to negative as the degree of randomness is increased. However, all our calculations were done using a single mesh size $\xi = 1$. To verify that this effect is still present in the continuum limit, we repeated the calculations for various mesh sizes. The inset of Figure 7 shows the first two coefficients as a function of the mesh size for a two-dimensional gel made of randomly placed circular obstacles (or, equivalently, for the system shown in Figure 4 but with randomly distributed parallel fibers). The data for the first coefficient (a_1) of the periodic gel shown in Figure 4 were also added to the plot. As expected, the randomness does not affect the first coefficient, and the two sets of data coincide perfectly. However, the second coefficient converges to a negative value: $a_2(\xi \to 0) = -0.66(2)$. Thus, the effect previously observed was real; i.e., it was not a lattice artifact: randomness does change the sign of the second coefficient a_2.

D. Ferguson Plots and Gel Parameters. Following our previous work,[2-4] we now analyze our data in terms of the standard OMRC model. First let us define the effective retardation coefficient as

$$K(R) = -\lim_{C \to 0} \frac{\partial \mu^*(C)}{\partial C} \tag{18}$$

For this system of parallel straight fibers, the excluded volume of the analyte is given exactly by

$$\phi(C) = \frac{(R + r)^2}{r^2} C \tag{19}$$

Substituting this relation into eq 13, we obtain

$$\mu^* = 1 + \sum a_i(r') \frac{(R + r)^{2i}}{r^{2i}} C^i \tag{20}$$

In the continuum limit we have $a_1(\xi \to 0) = -1$; thus

$$K(R) = -\lim_{C \to 0} \frac{\partial \mu^*(C)}{\partial C} = \frac{(R + r)^2}{r^2} \tag{21}$$

According to these results, finding the value of the fiber size by extrapolating $K^{1/2}$ to negative values of R until $K^{1/2} = 0$ is thus perfectly valid as long as the fiber concentration is kept small.

For this simple gel, the concentration is given by

$$C = \frac{\pi r^2}{(2a(C) + 2r)^2} \tag{22}$$

where $2a(C)$, the pore diameter, is trivially given by the separation between two consecutive obstacles. (This is the size of the largest particle that would have a nonzero mobility in this system.) For small concentrations ($a(C) \gg r$), we thus have $a(C) \propto 1/\sqrt{C}$, which is consistent with the OMRC theory and Ogston's calculation.[9] Substituting this result into eq 20, we get

$$\mu^* = 1 - \frac{\pi(R + r)^2}{4a^2} + \ldots \simeq e^{-\pi(R+r)^2/4a^2} \tag{23}$$

which is the main result of the OMRC model (eq 2) although our definition of the retardation factor K slightly differs from that given in eq 4. Therefore, although OMRC's fundamental assumption eq 1 is invalid, the data analysis procedure based on this model remains useful in practice.

IV. Three-Dimensional Gels

We now look at more realistic three-dimensional systems where the fibers are not restricted to point in only one direction. A prediction for the dependence of the mobility upon the excluded volume can be made using a simple argument. The previous section demonstrated that when the gel fibers are placed perpendicularly to the movement of the particle, the mobility of the particle can be expressed as (at least for realistic gel concentrations)

$$\mu^* = \frac{1}{1 + \phi(C)} \tag{24}$$

Since fibers parallel to the motion of the particle will not affect its net migration, we can argue that the reduced mobility of the analyte should be (at least as a first approximation) given by

$$\mu^* = \frac{1}{1 + \dfrac{2}{3}\phi(C)} \tag{25}$$

when $^1/_3$ of the gel fibers are parallel to the motion. Note that this relation is equivalent to the Tsai and Streider equation (12).

Macromolecules, Vol. 34, No. 10, 2001 Ogston Model of Gel Electrophoresis **3443**

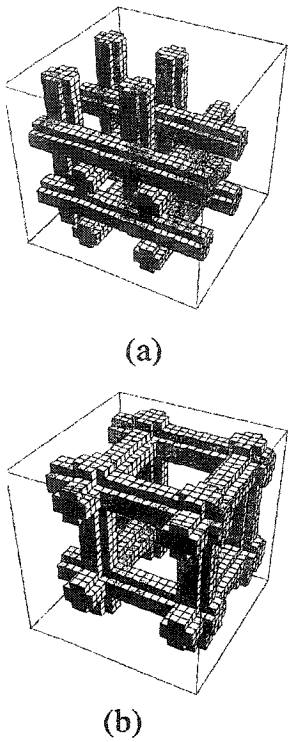

Figure 9. Two periodic three-dimensional gels with straight orthogonal fibers. (a) Without cross-link. (b) The gel forms a cross-linked network with a cagelike structure.

A. Periodic Gels. Figure 9 shows two periodic gels formed of straight fibers placed along the three orthogonal axis. In the first case (Figure 9a), each fiber follows an axis placed at the center of two other orthogonal fibers. Therefore, this gel is not cross-linked. In the second case (Figure 9b), three orthogonal fibers share one or more sites (depending on the size of the fibers) so that the gel forms a network with a cagelike structure.

As in section III, the dependence of the mobility upon the excluded volume ϕ was calculated in terms of a polynomial for decreasing mesh sizes ξ. As expected, the first coefficient (a_1) of the polynomial expression (eq 13) is identical for the two gels. In the low excluded volume limit the number of cross-links is very small and does not affect the migration of the analyte. The results for a_1 for the gel without cross-links (Figure 9a) are shown in Figure 10 as a function of ξ. The data for the gel with cross-links (Figure 9b) agree with Figure 10 (not shown). Again, the small fluctuations are due to the imperfect lattice "spheres". The extrapolation to the continuum limit ($a_1(\xi \to 0)$) is remarkably close to the predicted value of $-2/3$. For larger values of excluded volume ϕ, the specific geometry of the gel is important: this is why the two gels have different coefficients a_i for $i > 1$. This can be seen in the inset of Figure 10 where the extrapolated mobility $\mu^*(\xi \to 0)$ is plotted as a function of the total obstructed volume ϕ. While the mobility for the gel without cross-links (Figure 9a) follows nicely eq 25 for obstructed values as large as 10%, the mobility for the cross-linked gel (Figure 9b) diverges from eq 25 for relatively small obstructed volumes (~5%). In fact, for the latter gel, the sign of the second coefficient a_2 is different from the one predicted by eq 25! We thus see

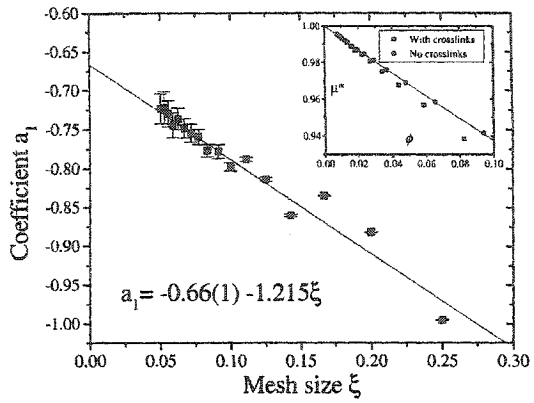

Figure 10. First coefficient of the polynomial expression of the dependence of the mobility upon the excluded volume for the gel shown in Figure 9a. The $\xi \to 0$ extrapolated value is $a_1 = -0.66(1)$. Inset: reduced mobility μ^* vs the total obstructed volume ϕ for the gels shown in Figure 9. The line is eq 25.

that the structure of the gel has an important effect on the dependence of the mobility upon the excluded volume. Therefore, a general relation describing the dependence of the mobility upon the excluded volume ϕ, independent of the gel structure, can only give rough estimates. This is a clear demonstration of the failure of the OMRC hypothesis (eq 1). This also shows that eq 25 is not general but corresponds to the precise gel shown in Figure 9a.

B. Random Gels. Although instructive, all the cases studied until now (2D systems, periodic systems, straight fibers, etc.) were probably poor representations of gel electrophoresis. We now look at the case of two different random gels. In the first one, the gel fibers are placed randomly in space but kept straight and parallel to the x, y, and z axes. This type of un-cross-linked gel is very close to the one originally proposed by Ogston.[9] Figure 11a shows an example of such a system.

The second one is the most realistic one since it is formed of irregular cross-linked fibers placed along random directions (Figure 11b). To generate such a gel, we first join two sites, randomly chosen, by a biased random walk. During this random walk, the "jumping" probability (along one of the orthogonal axis) is simply given by the ratio of the number of sites separating the two ends along this direction to the total separation. After completion of the first fiber, we choose two occupied sites (already part of the gel) and join them using the same rules but forcing them to go out of the primitive cell via the periodic boundary conditions (PBC). This last step is repeated until the right concentration (previously chosen) is obtained. We finally increase the fibers size by a factor r'/ξ in order to obtain the right mesh size. This leads to a connected network of "cylindrical" fibers with somewhat random shapes but still fairly rigid. While this gel still suffers from many imperfections, it is clearly the most realistic representation of a true gel that we have studied.

As we did for the other gels, we plot the coefficient a_1, which characterizes the low-concentration limit, as a function of the mesh size ξ (Figure 12). For comparison, the data for the non-cross-linked periodic gel described in the previous section were added to the plot. We note that, for both random gels, the values of the a_1 coefficient are apparently identical to the ones obtained

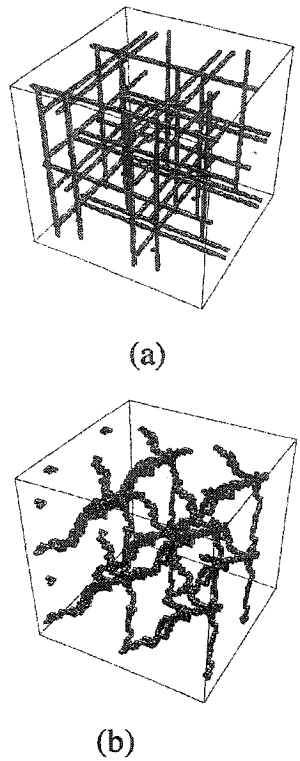

Figure 11. Two types of random three-dimensional gels. (a) Straight fibers placed randomly along the three orthogonal axis. (b) Gel formed of irregular, cross-linked fibers placed along random directions. In both cases, the primitive cell (of periodicity $s = 30$) is repeated eight times for a better view.

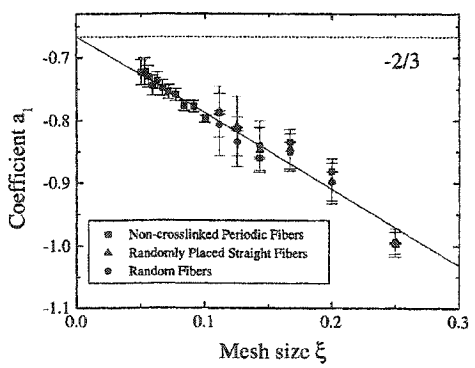

Figure 12. First coefficient (a_1) of the polynomial expression of the dependence of the mobility (μ^*) upon the excluded volume ϕ for the gels shown in Figure 11. The data for the periodic gel (Figure 9) are added for comparison. All extrapolated values are consistent with the predicted value of $-2/3$.

for the periodic gel, thus leading to an expected extrapolated value of $-2/3$. This confirms our previous results that the first coefficient changes with the shape of the obstacles but is independent of the distribution of the obstacles. Therefore, we expect to have $a_1 = 2/3$ for all representations of long stiff fibers, as long as the distribution of the fibers is isotropic. The higher coefficients ($a_{i\geq 2}$), however, are not universal and are strongly affected by the specific geometry of the gel.

C. Gel Parameters. Following section IIID, we now analyze the data using the method suggested by the OMRC model. For our first system (the non-cross-linked periodic gel shown in Figure 9a), the excluded volume is simply given by

$$\phi(C) = \frac{(R+r)^2}{r^2} C \tag{26}$$

leading to (using the fact that we have $a_1 = -2/3$)

$$K(R) = -\lim_{C\to 0} \frac{\partial \mu^*(C)}{\partial C} = \frac{2(R+r)^2}{3r^2} \tag{27}$$

For the other gels (Figures 9b and 11a,b), the presence of cross-links will slightly change the dependence $\phi(C)$ of the excluded volume upon the concentration. For low concentrations, however, eq 26 is a very good approximation. Therefore, the plot of the square root of the retardation coefficient K as a function of the particle radius R will lead to a straight line, and again the value of R at which $K(R) = 0$ will give the fiber radius r.

In the case of the non-cross-linked periodic gel (Figure 9a), the obstacle concentration can be expressed as

$$C \simeq \frac{3\pi r^2}{(2a(C) + 2r)^2} \tag{28}$$

For low concentrations ($a(C) \gg r$) we thus find $a(C) \propto 1/\sqrt{C}$, which is again consistent with the OMRC theory. Finally, substituting eq 2 into the polynomial fit, we get

$$\mu^* \simeq 1 - \frac{2\pi(R+r)^2}{4a^2} + \ldots \tag{29}$$

Again, we find a form very similar to the one used with the OMRC model (eq 2), although new numerical coefficients have appeared.

V. Conclusions

In this article we presented a study of pseudospherical analytes migrating in three-dimensional gels without hydrodynamic interactions. We showed that the use of a lattice to treat diffusion processes has an important impact on the numerical results. For example, the dependence of the mobility (or the diffusion coefficient since $\mu^* = D^*$ in the low-field limit) upon the excluded volume of the analyte changes drastically if we vary the mesh size of a given problem or if we change the lattice type (e.g., square vs triangular lattice). However, if one properly extrapolates toward the continuum limit, where the lattice parameter is infinitely small in comparison to all the other length scales, the results become independent of the lattice type and correspond to those of similar off-lattice simulations (but they require less CPU time). Our study of the continuum limit revealed that the geometry of the gel has a strong impact on the dependence of the mobility upon the excluded volume, thus confirming our previous work. If we express our results in terms of a polynomial expansion, we found that the first coefficient, which characterizes the low excluded volume limit, changes with the shape of the obstacles but is independent of the distribution of the obstacles. For example, we found $a_1 = -1$ for isolated cylindrical fibers perpendicular to the particle motion for both periodic and random distributions. For the case of an isotropic three-dimensional gel made of long fibers, we found the

universal value $a_1 = -2/3$. Since this result was insensitive to the presence of cross-links or randomness in the fiber distribution and that it seems to be valid even when we have tortuous fibers (as long as we keep the distribution isotropic), we believe that it will apply to any realistic gel. Note that this difference ($a_1 = -1$ vs $a_1 = -2/3$) is not only a dimensional one: for example, the case of isolated spherical obstacles in three dimensions gives $a_1 = -1/2$.[23] While the first coefficient (a_1) seems to be independent of the distribution of obstacles, it is not the case for the other coefficients $a_{i\geq 2}$. Even the second coefficient (a_2) is strongly affected by the specific geometry of the gel. For example, changing a simple periodic system to a random distribution or adding some cross-links can make the second coefficient to change its sign. The main assumption in the OMRC model, namely that the low-field mobility is directly proportional to the available volume $f = 1 - \phi$, is thus incorrect. The first coefficient is not, in general, equal to -1, and the higher ones are not equal to 0. However, for three-dimensional gels made of long stiff fibers, a modified relation, $\mu = 1 - 2/3\phi$, seems to be a good approximation, in the low excluded volume limit, for any type of gel.

Acknowledgment. The author thanks the C3.ca organization for computing resources. This work was supported by a Research Grant from the Natural Science and Engineering Research Council (NSERC) of Canada to G.W.S. and by scholarships from the Fonds pour la Formation de Chercheurs et l'Aide à la Recherche (Québec), NSERC, and the University of Ottawa to J.F.M.

References and Notes

(1) Slater, G. W.; Guo, H. L. *Electrophoresis* **1996**, *17*, 977.
(2) Slater, G. W.; Guo, H. L. *Electrophoresis* **1996**, *17*, 1407.
(3) Slater, G. W.; Treurniet, J. R. *J. Chromatogr. A* **1997**, *772*, 41.
(4) Mercier, J.-F.; Slater, G. W. *Electrophoresis* **1998**, *19*, 1560.
(5) Labrie, J.; Mercier, J.-F.; Slater, G. W. *Electrophoresis* **2000**, *21*, 823.
(6) Boileau, J.; Slater, G. W. *Macromolecules*, in press.
(7) Mercier, J.-F.; Slater, G. W. *J. Chem. Phys.* **1999**, *110*, 6050.
(8) Mercier, J.-F.; Slater, G. W. *J. Chem. Phys.* **1999**, *110*, 6057.
(9) Ogston, A. G. *Trans. Faraday Soc.* **1958**, *54*, 1754.
(10) Morris, C. J. O. R. *Protides of the Biological Fluids, 14th Colloquium*; Elsevier: New York, 1967.
(11) Rodbard, D.; Chrambach, A. *Proc. Natl. Acad. Sci. U.S.A.* **1970**, *65*, 970.
(12) Ferguson, K. A. *Metabolism* **1964**, *13*, 985.
(13) Tietz, D. *Advances in Electrophoresis II*, VCH: New York, 1988.
(14) Locke, D. R.; Trinh, S. H. *Electrophoresis* **1999**, *20*, 3331. In this recent theoretical study of the impact of the local variations of the electrical field around nonconducting obstacles, Locke et al. reported that the Ogston assumption should be valid in the limit of very small electrical fields and very dilute media, as well as in media without percolation limits. Similar studies are currently being done by our group and preliminary results indicate that local variations of the electric field do not change the analyte mobility in the low field limit and for an infinitely small analyte (submitted for publication).
(15) Slater, G. W.; Rousseau, J.; Noolandi, J.; Turmel, C.; Lalande, M. *Biopolymers* **1988**, *27*, 509.
(16) Trinh, S. H.; Arce, P.; Locke, D. R. *Transport Porus Media* **1999**, *1395*, 1.
(17) Amsden, B. *Macromolecules* **1998**, *31*, 8382.
(18) Tsai, D. S.; Strieder, W. *Chem. Eng. Commun.* **1986**, *40*, 207.
(19) Schlicht, L.; Ilgenfritz, G. *Physica A* **1995**, *227*, 239.
(20) Saxton, M. J. *Biophys. J.* **1993**, *64*, 1766.
(21) Johansson, L.; Elvingston, C.; Lofroth, J. E. *J. Chem. Phys.* **1993**, *30*, 7471.
(22) Kim, I. C.; Torquato, S. *J. Chem. Phys.* **1992**, *96*, 1498.
(23) Mercier, J.-F.; Slater, G. W. *J. Chem. Phys.* **2000**, *110*, 6057.

MA001544O

ARTICLE III

J. F. Mercier, F. Tessier and G. W. Slater.

An exactly solvable Ogston model of gel electrophoresis: VIII.

Nonconducting gel fibers, curved field lines, and the Nernst-Einstein relation.

Electrophoresis, 22: 2631–2638, 2001.

Corrections

1. In the text, (C) should read f(C) on page 43 (twice), 44 (four times), 45 (twice), 46 (six times), 47 (once) and 48 (twice).

   e.g. On page 43, first paragraph: "... the fractional volume (C) (i.e., to the fraction ..." should be "... the fractional volume f(C) (i.e., to the fraction ..."

2. Equation 2 should read:

$$\mu = \frac{1}{\varepsilon} \lim_{t \to \infty} \frac{\langle x(t) \rangle}{t}$$

3. Reference 20 should read:

   Trinh, S, H. Arce, P., Locke, B. R., *Transp. Porus Media* 2000, *38*, 241-259.

Electrophoresis 2001, 22, 2631–2638 2631

Jean-François Mercier
Frédéric Tessier
Gary W. Slater

Department of Physics,
University of Ottawa,
Ottawa, Ontario, Canada

An exactly solvable Ogston model of gel electrophoresis: VIII. Nonconducting gel fibers, curved field lines, and the Nernst-Einstein relation

In this article, we examine the low-field electrophoretic migration of infinitely small analytes in dilute sieving media made of nonconducting gel fibers. Using an Ogston obstruction model, we show that the electrophoretic mobility is not affected by the presence of curved field lines. In other words, the Nernst-Einstein relation between the mobility and the diffusion coefficient is valid regardless of the electrical properties of the gel fibers. Although this finding may greatly simplify the development of obstruction models of electrophoretic sieving, it also represents a critical test for any analytical or computational approach.

Keywords: Ogston model / Nernst-Einstein / Diffusion / Mobility / Curved field lines EL 4515

1 Introduction

1.1 General aspects

Over the past several years, we have developed a new lattice model to study the gel electrophoresis of various types of analytes [1–7]. While very simple at the beginning – it was first restricted to two-dimensional systems, periodic obstacles, cubic analytes, and coarse-grained lattices – our model has evolved considerably and we can currently treat spherical analytes migrating through realistic three-dimensional gels in the continuum limit (so that we avoid the artifacts related to the presence of the underlying lattice) [7]. Originally, our goal was to verify the fundamental assumption of the Ogston-Morris-Rodbard-Chrambach (OMRC) model for gel electrophoretic sieving [8–10], namely that the low-field reduced mobility $\mu^*(C)$ of an analyte is equal to the fractional available volume (C) (*i.e.*, to the fraction of the total gel volume that is made of pores large enough to host the analyte):

$$\mu^*(C) \equiv \frac{\mu(C)}{\mu_0} = f(C) = 1 - \phi(C) \tag{1}$$

where μ_0 is the free solution (no obstacle) mobility, $\phi(C)$ is the (fractional) excluded volume and C is the obstacle (or gel) volume/volume concentration. Note that the mobility μ of the analyte is defined as:

$$\mu = \frac{1}{\varepsilon} \lim_{t\to\infty} \frac{<x(t)}{t} \tag{2}$$

where ε is the dimensionless field intensity.

We studied many different sieving gel structures [1–7], and our results clearly indicate that the OMRC assumption is inaccurate, except for the nonrealistic case where the gel constraints (the obstacles) are reset randomly at each time step (corresponding to a mean field approximation or an annealed gel) [1]. In fact, our studies revealed that the geometry of the gel has a strong impact on the dependence of the mobility upon the excluded volume $\phi(C)$; in other words, the mean-field geometric parameter $(C) = 1-\phi(C)$ is not sufficient to describe the precise sieving properties of a gel even when only steric interactions exist.

Although these conclusions are not unexpected since random walks in disordered systems are notoriously hard problems, especially near the percolation threshold, they have (and continue to) lead to controversy [11, 12]. In this article, we will review some of the critical aspects of the problem and we will address a recent criticism [12] that indeed represents an acid test for all modeling approaches. In particular, we will show that our numerical model can be generalized to include the curved field lines that exist when the obstacles (*e.g.*, the gel fibers) are not conducting. Our results will then demonstrate that for infinitely small analytes, the low-field mobility is unaffected by such effects. Therefore, we conclude that our previous results are quite general, that the Nernst-Einstein relation is valid in the presence of nonconducting fibers, and that the OMRC model does not correctly predict the result of electrophoretic sieving.

Correspondence: Dr. Gary W. Slater, Department of Physics, University of Ottawa, 150 Louis-Pasteur, Ottawa, Ontario, K1N 6N5, Canada
E-mail: gslater@science.uottawa.ca
Fax: +613-562-5190

Abbreviation: OMRC, Ogston-Morris-Rodbard-Chrambach

0173-0835/01/1308–2631 $17.50+.50/0

1.2 Theoretical elements for Ogston obstruction models of gel sieving

1.2.1 The physical mechanisms at play

For a given class of nondeformable particles, models of gel electrophoresis may take into account several physical elements, including: (i) steric analyte/fiber interactions; (ii) solvent-mediated hydrodynamic interactions between the analyte and the fibers; (iii) various ionic effects (such as the electroosmotic flow); (iv) the exact structure of the gel, *i.e.* the spatial distribution of gel fibers and their cross-links (if any); (v) specific analyte/fiber interactions (attractive or repulsive); (vi) the intensity and the local direction of the electric field inside the gel; (vii) the gel dynamics if the gel fibers are not perfectly rigid; (viii) any other physical parameter that may impact the separation. Here, we implicitly assume that the system is homogeneous, *i.e.*, we do not consider nonideal system-dependent conditions (*e.g.*, temperature gradients). Of course, some of these parameters are more important than others, and their relative importance may vary from system to system. In the case of deformable analytes (such as DNA molecules), the reduced conformational phase space available to the analyte in the gel plays an important role and may lead to entropic trapping phenomena [6, 13–17].

No existing model includes all of these elements. In fact, it would be useless to include them all because we do not know the value of the microscopic parameters that would be required to make predictions. Fitting data with a complex theory that includes dozens of unknown parameters is not a useful exercise. Instead, research scientists have been trying for the past 35 years or so to explain experimental data using the smallest possible subset of parameters (or physical mechanisms). What distinguishes the existing electrophoretic sieving models can be grouped under three headings: (i) the physical mechanisms taken into account in the model; (ii) the theoretical method used to represent the selected physical mechanisms; (iii) the mathematical techniques used to solve the resulting equations. One of the difficulties in developing models is to establish good tests of their validity. In many cases, the error bars on experimental data or/and the mathematical approximations required to make predictions do not allow us to draw clear conclusions. In the case of the OMRC model, for example, the fact that it is not generally possible to measure the fractional volume (C) means that one cannot test Eq. (1) directly.

1.2.2 Ogston and the OMRC obstruction model(s)

Given the description provided in the previous subsection, we will now address two key questions: What do we mean by an "Ogston-like" model? And then, what is the OMRC model? We propose that a model should be called an "Ogston" or "Ogston-like" model when it reduces gel electrophoresis to the following three elements: (i) analytes and gel fibers/obstacles interact only through steric interactions (hard core excluded volume effects); (ii) the field intensity is low enough that we can consider the system to be close to local equilibrium; (iii) the analyte (or its effective representation) is not deformable. These three elements are clearly the historical ones taken explicitly (or implicitly) into account by the scientists who developed the standard OMRC model. The latter is thus defined by the additional fact that it uses Eq. (1) to estimate the impact of these three physical elements on the electrophoretic mobility $\mu^*(C)$. Hydrodynamic interactions, ionic effects, specific analyte-fiber interactions, and the dynamics of the gel are all neglected. The electroosmotic flow is simply an additive correction.

A more subtle question is perhaps whether the gel structure and the resulting direction of field lines inside the gel are implicitly part of the OMRC model. Equation (1) strongly suggests that neither effect is present since the result $\mu^*(C) = (C) = 1-\phi(C)$ predicts that all gels offering the same available volume (C) (or blocking the same excluded volume $\phi(C)$) to the given analyte will lead to the same electrophoretic mobility $\mu^*(C)$, no matter what the detailed gel structure is. However, sieving structures differ in many ways. Some are more periodic than others. Some are more homogeneous than others. Some are cross-linked more heavily than others. Some have numerous dead-ends and short-length scale fractal structures [17], while others are more regular. These differences affect the tortuosity of the path followed by the analyte as well as the field lines pattern (if the fibers are not conducting), regardless of the value of (C).

In the OMRC model, one often uses Ogston's famous result

$$\mu^*(C) = f(C) = e^{-KC} \tag{3}$$

where the so-called retardation coefficient K is a function of the physical size (and shape) of the analyte. Many authors have proposed modifications to Eq. (3) to take into account various geometric factors (*e.g.*, the elongated shape of certain analytes), but the final result is always substituted into Eq. (1). Therefore, we should indeed consider Eq. (1) (and not Eq. (3)) to be the fundamental equation that defines the OMRC model. It is inter-

Electrophoresis 2001, *22*, 2631–2638

esting to note in passing that Ogston's Eq. (3) has been derived for a gel made of uncross-linked gel fibers. Therefore, we should certainly consider Eq. (3) to be a convenient semiempirical formula based on a zeroth order model of gel electrophoresis and gel structure.

1.2.3 Improved Ogston models

The fact that Ogston models keep only three elements in the problem (steric interactions, low-fields, hard analytes) is not the main issue. It is actually a very realistic approach and, indeed, it is the one that we have also taken. Unfortunately, the OMRC model further assumes that the fractional available volume (C) takes into account all of these effects. This is the weak part. This is simply not a viable method to treat the physics of the problem. Whether the mathematical methods used to calculate (C) are adequate (they are) is not relevant here. In their recent paper, Trinh and Locke [12] also concluded that while the three elements of the Ogston models make sense, we still need a better theoretical method to represent the physics of the problem. Their approach includes the field lines and the obstacles, and the resulting equations are fundamental differential equations. In our case, we introduce essentially the same ingredients (the curved field lines are treated in this article), but we use a lattice (discrete) representation of the space. In principle, these two approaches should be identical in the limit where the field is very weak and the lattice mesh very (infinitely) small. However, Trinh and Locke [12] use a completely different mathematical technique to solve the resulting equations, a method called "volume averaging" [19] which has been shown to give superb results in the case of free diffusion [20]. Using a lattice allows us to obtain numerically exact results for a wide variety of systems. Let us now summarize our previous findings.

Since we did not have any specific mathematical formula to use to fit our exact numerical data, we chose to use the general polynomial form

$$\mu^*(C) = 1 + a_1\phi + a_2\phi^2 + a_3\phi^3 + \ldots \quad (4)$$

where $\phi = \phi(C)$. We found that the first coefficient a_1, which characterizes the low-excluded volume limit, changes with the shape of the obstacles (but is independent of the geometry of the gel), and that the other coefficients are strongly affected by the specific geometry of the obstacles and the gel. Therefore, the OMRC universal assumption that $\mu^*(C) = 1 - \phi(C)$ is incompatible with all of our previous results, even though the data analysis method based on this model (mostly the so-called Ferguson plot [21, 22]) leads to realistic mean pore sizes and fiber radii estimates [2, 7].

More recently, we have designed a method to reach the continuum limit [23]. In this way, we have been able to demonstrate that our conclusions were not artifacts due to the presence of the underlying lattice [7]. This was a critical step in establishing the validity of the conclusions reached in our previous articles. In fact, our results agree perfectly with a number of theories for the electrical conductivity of heterogeneous media [24], and for the diffusion coefficient of random walkers in systems with obstacles [25, 26]. Therefore, once the elements to be included in the model are identified, our approximation-free mathematical approach does indeed provide extremely accurate results.

1.2.4 The field line problem

However, it should be noted that our model has always assumed that the field was homogeneous and not affected by the gel fibers, *e.g.*, the field lines simply went through the gel fibers as if the latter and the solvent had the same conducting properties (Fig. 1b). In their recent article, Locke and Trinh [12] criticized this assumption and made the reasonable claim that it is important to consider the electrical conductivity properties of the fibers even in the low-field limit [12]. More precisely, they claimed that our previous results did not agree with Eq. (1) because we failed to take this element into account. Using the averaging method, they predicted that the electrophoretic mobility of an infinitely small analyte migrating in a dilute medium can be expressed as:

$$\mu^*(C) = f(C) + S_1 \quad (5)$$

where S_1 is a function of the local electrical field and geometry. In the case where the fibers are nonconducting (Fig. 1c), Locke and Trinh found that the value of S_1 is identically zero. Therefore, in this limit, the ORMC assumption should be valid. In fact, Locke and Trinh go even further and claim that the diffusion coefficient $D(C)$ is then given by:

$$\frac{D(C)}{D_0} \equiv D^*(C) = f(C) - S_2 + S_3 \quad (6)$$

where S_2 is a function of the local geometry and S_3 is a function of the local electrical field and geometry. In the zero-field limit and for low gel concentrations, they found that both terms, S_2 and S_3, become negligible. This thus leads to $D^*(C) \cong f(C)$, which is essentially a version of Eq. (1) for diffusion problems.

These authors also claim that Monte Carlo simulations actually support Eq. (6) in the limit where it reduces to $D^*(C) = f(C)$. However, zero-field Monte Carlo simula-

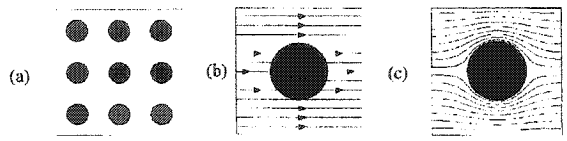

Figure 1. Sieving system made of periodic circular obstacles, (a) The primitive cell is repeated nine times, (b) The electric field lines are not affected by the gel fibers and the field is uniform everywhere, (c) The gel fibers are nonconducting and the field lines curve around the obstacles.

tions of particle diffusion among fixed obstacles are well-known to give results in strong disagreement with this prediction [20, 24, 25]. For instance, such a study, published by the very same group, showed that the diffusion coefficient does not follow a universal curve $D^*(C) = (C)$, but that it instead depends on the medium architecture [20]. In fact, their main conclusion was that for a point-like analyte with no electrical field, in "both 2D and 3D media, there are three factors which can affect the effective diffusion coefficients: the geometry of the obstacles, the arrangement of the obstacles, and the dimension of the media" [20]. Indeed, their Figs. 6 and 8 clearly demonstrate that the shape and distribution of the obstacles have a strong impact on the value of $D^*(C)$ for a fixed value of the available volume (or porosity) $f(C)$ [20]. Our own data agree nicely with those of [20] and convincingly demonstrate that $D^*(C) = (C) = 1 - \phi(C)$ is wrong in the case of diffusion, even in the low-concentration, zero-field limit. In all three-dimensional cases, for instance, we and other authors found that the first order coefficient a_1 in Eq. (4) is not equal to −1, as the OMRC model would predict. Therefore, Trinh and Locke's diffusion arguments in [12] and [20] are contradictory.

1.2.5 The Nernst-Einstein relation

The main question is thus whether taking into account curved field lines (Fig. 1c) can restore Eq. (1) and/or invalidate our previous data and conclusions. This question may actually have even deeper consequences, as we shall now explain. First, let us write the scaled Nernst-Einstein relation:

$$\mu^*(C) = D^*(C) \tag{7}$$

where

$$D = \lim_{t\to\infty} \frac{< x(t^2) >}{2t}. \tag{8}$$

Equation (7) is indeed identical to the first two terms of Eq. (3) in [12]. This is a fundamental law of thermodynamics that must be valid near equilibrium, *i.e.*, for low-field intensities. On the one hand, our previous work has clearly established that the relation $\mu^* = D^*$ is valid when the field lines are parallel to each other [26, 27]. On the other hand, Monte Carlo simulations have also clearly demonstrated that the Ogston-like relation $D^*(C) = (C)$ is not valid when the field is zero, as we have just discussed. Together, these two demonstrated and indisputable facts lead us to the inevitable conclusion that $\mu^*(C) \neq f^*(C)$, *i.e.*, that Eq. (1) is invalid. In fact, if Eq. (1) was valid, the Nernst-Einstein relation would be violated in the presence of parallel field lines of arbitrarily low intensities. Our results thus satisfy this law of thermodynamics for conducting obstacles/fibers.

However, we are not aware of any proof that the same conclusions apply to curved field lines and nonconducting obstacles/fibers. This is in essence the challenge presented in Trinh and Locke's article [12]. However, there is something more fundamental about this challenge. As discussed in the previous subsection, the relation $D^*(C) = (C)$ is not valid in the absence of a field. Therefore, if the Ogston fundamental relation $\mu^*(C) = (C)$ was valid in the presence of curved field lines (this is the main claim of Trinh and Locke), the Nernst-Einstein relation Eq. (7) would automatically be violated. Although, it seems logical to believe that the nature of the field lines should not matter much in the zero- or low-field limit, we could not find any previous article that tested this crucial issue. In this article, we numerically calculate the mobility of a point-like analyte in a simple periodic system and show that the curvature of the field lines have no impact on the low-field mobility. Therefore, the Nernst-Einstein relation is not violated and the Ogston relation $\mu^*(C) = (C)$ is invalid even for nonconducting gel fibers.

2 Methods

The numerical mobilities were obtained using a lattice model in which the migration of the point-like analyte is represented by a biased random-walk on a finite-size lattice (with periodic boundary conditions) where certain sites are forbidden (the gel fibers). This type of computational model usually implies Monte Carlo simulation methods. However, we demonstrated previously [1–7] that such simulations are not necessary since the Monte Carlo algorithm can in fact be rewritten as a set of linear equations which can be solved exactly for the mobility in the zero-field limit. The reader can consult [27, 28] for detailed explanations of this numerical procedure. In order to avoid lattice-dependent effects, our calculations were done in the continuum limit, *i.e.*, in the limit where the size of the lattice parameter is infinitely small compared to the size of the obstacles (this also insures that the

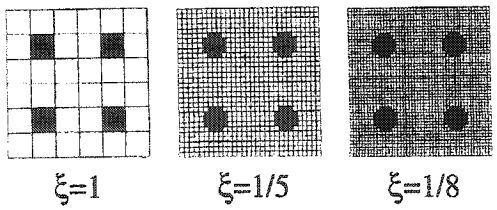

Figure 2. Transformation of a simple lattice problem as the mesh size ξ is decreased. The "gel" is made of isolated circular obstacles placed periodically, as described in Fig. 1.

analyte is indeed a point-like object). This is achieved by progressively decreasing the mesh size of the system until clear asymptotic values (*e.g.*, asymptotic mobilities) were obtained [22]. Figure 2 shows how a given problem (isolated circular obstacles placed periodically, Fig. 1) was transformed as the mesh size ξ was decreased.

In the case of conducting fibers or obstacle-free systems, the electric field ε is uniform and simply given by: $\varepsilon = \varepsilon_0 = U/L$, where U is the potential drop between the ends of the unit cell of length L. With nonconducting fibers, however, the field ε is no longer uniform (nor is it pointing in the x-direction everywhere); for example, the field is higher between two close obstacles because the latter compress the field lines (Fig. 1c). Experimentally, the field intensity is always defined as $\varepsilon_0 = U/L$ since a fixed potential U is applied between the two electrodes. Here, we take the same approach: all systems will be compared at constant potential U or effective field intensity $\varepsilon_0 = U/L$. Therefore, the mobility is defined as:

$$\mu = \frac{1}{\varepsilon_0} \lim_{t\to\infty} \frac{< x(t) >}{t}. \qquad (9)$$

To calculate the local field $\vec{\varepsilon}\,(x, y)$ at each lattice site (x, y), the Laplace equation is solved numerically using a standard numerical relaxation method [29] on a grid. Note that for the nonconducting fibers ε_0 is not equal to the spatially averaged electric field $\iint dx\, dy\, \varepsilon_x(x, y)/L^2$.

3 Results

Figure 1a shows a system made of periodic circular gel fibers. This will be our main model system for investigating the role of the field lines. Since the validity of both the Nernst-Einstein relation and the OMRC hypothesis Eq. (1) should not depend on the nature of the gel structure (this was also suggested by Trinh and Locke [12]), the use of a periodic system will greatly simplify the analysis. Note that this can be seen as either a two-dimensional model with round obstacles or a three-dimensional system with infinitely long and parallel fibers, as demonstrated by Mercier and Slater [7]. To evaluate the effect of the curvature of the field lines, we thus numerically calculated the mobility of a point-like particle for both straight (Fig. 1b) and curved (Fig. 1c) field lines. Some results are shown in Fig. 3 where the scaled mobility $\mu^*(C)$ is plotted as a function of the mesh size ξ for different fractional available volumes $= 1 - \phi$. Note that because we have a point-like analyte, the separation between obstacles and the obstacle radius do not play separate roles: the fractional volume ϕ fully defines the system. For large mesh sizes ξ, the mobility is slightly larger for curve field lines. This is so because the lattice is too "coarse" to give a reliable representation of the local field pattern, especially in the regions where the field changes rapidly. However, the two sets of data (straight and curved field lines) get closer as the mesh size is decreased, and the extrapolated values for infinitely small mesh sizes, corresponding to the physically relevant continuum limit ($\xi \to 0$), are identical for all excluded volumes ϕ. Therefore, for this system, the electrical properties of the gel fibers have no impact on the mobility of small analytes in the vanishing field limit; straight and curved field lines give exactly the same mobility in the continuum limit. Since we previously demonstrated that this mobility does not satisfy $\mu^* = 1-\phi$, we conclude that the fundamental hypothesis of the OMRC model is not valid in presence of nonconducting gel fibers either.

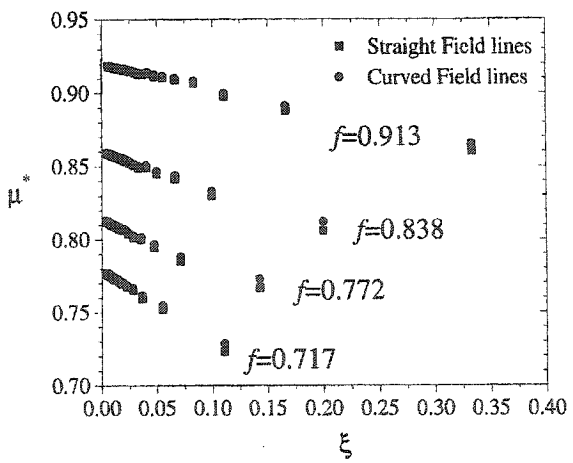

Figure 3. Reduced mobility $\mu^*(C)$ of a point-like analyte as a function of the mesh size ξ for both straight (Fig. 1b) and curved (Fig. 1c) field lines. The data for four different fractional available volumes (C) are shown. The mobilities were calculated using our numerical procedure and verified with MC simulations.

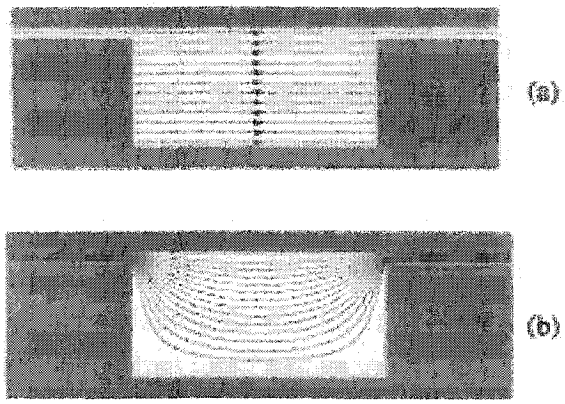

Figure 4. Primitive cell of a channel periodically narrow and large, (a) The electric field lines are not affected by the constraints and the field intensity is uniform everywhere, (b) The walls are nonconducting and the field lines curve around the corners.

We have repeated our calculations for a large number of systems, in two and three dimensions (see Fig. 4 for an example of a completely different system based on the microfluidic structure recently studied by Craighead's group [30]). For all systems studied, the low-field limit of the mobility was identical for both straight (Figs. 1b and 4a) and curved (Figs. 1c and 4b) field lines in the zero-field limit. Therefore, this conclusion is not an artifact of the relatively simple periodic system studied above, but is indeed quite general.

4 Discussion

It could be argued that the equality between the mobilities for straight and curved field lines is trivial because the problem is always reduced to one of pure diffusion in the zero-field limit. However, numerically the situation is not that simple. Let us examine this issue using our lattice model. On a lattice, the mean velocity $\bar{v}$ of an analyte can be expressed as the weighted average of the local velocities v; on each site:

$$\bar{v} = \sum_i v_i n_i, \tag{10}$$

where the sum is over all the sites that the analyte can occupy. Here, n_i is the probability of occupying site i in the steady-state [1]. When the field lines are straight (Fig. 1b), the local velocity v_i is identical on all sites (the field is uniform), except for those sites that are forming the perimeter of the obstacles since the analyte is prevented to move in the direction of the obstacle by the steric forces. However, the probability of presence n_i is quite inhomogeneous in this case. Indeed, the analyte has a greater probability of being "in front of an obstacle" because it bounces on it when drifting in the field direction (see Fig. 5a), while there is a depletion shadow behind the obstacle. The mean electrophoretic velocity $\bar{v}$ is thus a combination of surface-velocity and bulk-occupation effects.

We have quite a different situation when the gel fibers are nonconducting and the field lines curve around them (Fig. 1c). The site occupation probability n_i is then spatially uniform because the "bouncing" effect is perfectly balanced by the curvature of the field lines. However, the local velocity v_i is very inhomogeneous because the field varies from site to site, being higher between two obstacles where the field lines are compressed (see Fig. 5b). Therefore, the mean velocity $\bar{v}$ is directly related to the mean local field intensity in the system (*i.e.*, the spatially averaged field intensity). It turns out that in the low-field limit, the two calculations, corresponding to straight and curved field lines, give exactly the same result although all the mathematical steps are quite different.

Of course, the fact that the curvature of the field lines does not change the mobility in the low-field limit means that the Nernst-Einstein relation is valid regardless of the electrical properties of the gel fibers or obstacles that define the electrophoretic medium. This is a major result since it allows us to use the simplest possible model. For our study, we find that the calculations were much easier and less computer-intensive with parallel field lines. However, with curved field lines, the problem is essentially reduced to the solution of the Laplace equation. This is a very standard problem and many algorithms [29] have been developed to solve it. For very large or complex systems, and with the right algorithm, it might even be advantageous to work with the curved field lines.

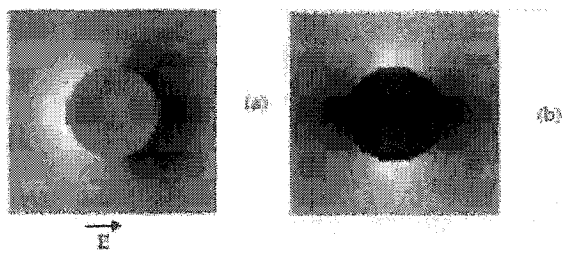

Figure 5. (a) Probability of occupation for a point-like analyte migrating on the lattice shown in Figs. 1a and 1b, *i.e.*, with straight field lines. The white lattice sites are the most probable and the black ones are the least probable. (b) Local x-velocities of the analyte when the field lines curve around the obstacles (Fig. 1c). The white sites represent the high-velocity sites while the black ones represent the low-velocity sites.

It seems that the fact that the curvature of the field lines has no impact on the zero-field mobility has been known (or at least used) for a long time. For example, many groups have been studying the electrical conductivity of various systems with nonconducting domains by comparing it to the unbiased random-walk (diffusion) problem in the same system (see, *e.g.*, [24]). The Monte Carlo diffusion coefficient thus obtained (with no field) is then assumed to be directly proportional to the electrical conductivity in the original problem (which obviously had curved field lines). Also, it should be noted that even though the electrical conductivity is related to the free diffusion coefficient, no one has claimed that a single formula (such as the ORMC $\mu^* = 1-\phi$) could possibly predict the conductivity of a sample regardless of the geometry and distribution of the nonconducting domains.

Since the curved field lines do not change the mobility in the low-field limit, the general conclusions of our previous articles are perfectly valid and do apply to realistic nonconducting fibers as well [1–7]. In particular, we stress the fact that the geometry of the gel has a strong impact on the dependence of the mobility upon the excluded volume $\phi(C)$ even in the low-obstruction limit, a result that is fully supported by Monte Carlo simulations [20, 24, 25]. In other words, the geometric parameter $(C) = 1-\phi(C)$ is not sufficient to describe the precise effect of the geometry and topology of a sieving matrix.

When our numerical results were expressed in terms of a polynomial expansion of the excluded volume $\phi(C)$ (see Eq. 4), we found that the first coefficient (a_1), which characterizes the low-concentration limit, changed with the shape of the obstacles but was not affected by the structure of the gel [7]. Note that the OMRC model then predicts the universal value $a_1 = -1$. For example, we found $a_1 = -1$ for isolated circular two-dimensional obstacles (Fig. 1), $a_1 = -2/3$ for the case of a three-dimensional gel made of infinitely long fibers and $a_1 = -1/2$ for isolated spherical obstacles in three dimensions. Furthermore, the higher coefficients $a_{i\geq 2}$ were not equal to zero, as predicted by the OMRC model, but were instead strongly dependent upon the gel structure that was selected.

5 Conclusion

Our numerical results establish that, for a point-like analyte, the dependence of the mobility upon free volume is not affected by the field line distortions. Therefore, the Nernst-Einstein relation is valid even in the presence of curved field lines, and the OMRC hypothesis, Eq. (1), is invalid. This is consistent with Monte Carlo simulation studies of particle diffusion in inhomogeneous systems [20, 24, 25], but it conflicts with the recent work of Locke and Trinh [12]. In particular, we have demonstrated that curved field lines do not validate Eq. (1), the main claim in [12]. Therefore, the geometric parameter (C) is not sufficient to describe the precise sieving properties of a gel, even for low gel concentrations. Since the volume averaging method gives excellent results in the absence of a field [20], we must conclude that the Locke and Trinh generalization of the method for the mobility in the presence of an electric field is not reliable.

Of course, these conclusions are only valid for a point-like analyte and a vanishingly low-electric field intensity. At high fields, the whole picture changes since the Nernst-Einstein relation is expected to be violated. For larger analytes, the field is not homogeneous inside the analyte and these gradients can induce rotations; in the case of flexible analytes, such as polymers, these gradients will even lead to conformational changes. These problems are certainly of great interest since real analytes are not point-like and useful electric fields are not always negligible. We are currently looking at these fundamental issues.

The authors would like to thank Marc P. Pépin, as well as Profs. Anthony Day, Hyuk Yu, André-Marie Tremblay, Georg Ilgenfritz, Dietrich Stauffer, Bruce Locke, Ras Pandey, and Pedro Arce for useful discussions. This work was supported by a Research Grant from the Natural Science and Engineering Research Council (NSERC) of Canada to GWS and by scholarships from NSERC and the University of Ottawa to JFM and FT.

Received February 5, 2001

6 References

[1] Slater, G. W., Guo, H. L., *Electrophoresis* 1996, *17*, 977–988.
[2] Slater, G. W., Guo, H. L., *Electrophoresis* 1996, *17*, 1407–1415.
[3] Slater, G. W., Treurniet, J. R., *J. Chromatogr. A* 1997, *772*, 41–48.
[4] Mercier, J.-F., Slater, G. W., *Electrophoresis* 1998, *19*, 1560–1565.
[5] Labrie, J., Mercier, J.-F., Slater, G. W., *Electrophoresis* 2000, *21*, 823–833.
[6] Boileau, J., Slater, G. W., *Electrophoresis* 2001, *22*, 673–683.
[7] Mercier, J.-F., Slater, G. W., *Macromolecules* 2001, *34*, 3437–3445.
[8] Ogston, A. G., *Trans. Faraday Soc.* 1958, *54*, 1754–1756.
[9] Morris, C. J. O. R., *Protides of the Biological Fluids, 14th Colloquium*, Elsevier, New York 1967, pp. 543–551.
[10] Rodbard, D., Chrambach, A., *Proc. Natl. Acad. Sci. USA* 1970, *65*, 970–977.
[11] Tietz. D., *Electrophoresis* 1995, *16*, 460–461.
[12] Locke, B. R., Trinh, S. H., *Electrophoresis* 1999, *20*, 3331–3334.

[13] Baumgartner, A., Muthukumar, M., *J. Chem. Phys.* 1987, *87*, 3082–3087.

[14] Muthukumar, M., Baumgartner, A., *Macromolecules* 1989, *22*, 1937–1945.

[15] Muthukumar, M., Baumgartner, A., *Macromolecules* 1989, *22*, 1941–1949.

[16] Slater, G. W., Wu, S. Y., *Phys. Rev. Lett.* 1995, *75*, 164-167.

[17] Rousseau. J., Drouin, G., Slater, G. W., *Phys. Rev. Lett.* 1997, *10*, 1945–1948.

[18] Maaloum, M., Pernodet. N., Tinland, B., *Electrophoresis* 1998, *19*, 1606–1611.

[19] Locke, B. R., Trinh, S. H., *Ind. Eng. Chem. Res.* 1998, *37*, 615–625.

[20] Trinh, S. H., Arce, P., Locke, B. R., *Transp. Porous Media* 1999, *1395*, 1–19.

[21] Ferguson, K. A., *Metabolism* 1964, *13*, 985–1002.

[22] Tietz, D., *Advances in Electrophoresis II*, VCH, New York 1988, pp. 109–169.

[23] Mercier, J.-F., Slater. G. W., *J. Chem. Phys.* 2000, *113*, 9109–9112.

[24] Schlicht, L., Ilgenfritz, G., *Physica A* 1995, *227*, 239–245.

[25] Amsden, B., *Macromolecules* 1998, *31*, 8382–8395.

[26] Tsai, D. S., Strieder, W., *Chem. Eng. Commun.* 1986, *40*, 207–214.

[27] Mercier, J.-F., Slater, G. W., *J. Chem. Phys.* 1999, *110*, 6050–6056.

[28] Mercier. J.-F.. Slater, G. W., *J. Chem. Phys.* 1999, *110*, 6057–6065.

[29] Press, W. H., Vetterling, W. T., Teukolsky, S. A., Flannery, B., *Numerical Recipes in Fortran 77*, 2nd Ed., Cambridge University Press, Cambridge 1996, pp. 854–880.

[30] Han, J.. Turner, S. W., Graighead, H. G., *Phys. Rev. Lett.* 1989, *83*, 1688–1691.

ARTICLE IV

J. F. Mercier, G. W. Slater and P. Mayer.

Solid phase DNA amplification: a simple Monte Carlo lattice model.

Biophysical Journal, 85: 2075–2086, 2003.

Corrections

1. On page 56, third paragraph of the second column. "... its free end tends to move away form the surface ..." should read " ... its free end tends to move away from the surface ..."

2. In the legend of FIGURE 11 , "When $s > s^* \approx 41\%$ ..." should read: "When $s < s^* \approx 41\%$ ..."

3. On page 59, second paragraph, " ... Apart form the obvious fact ..." should read .." ... Apart from the obvious fact ..."

Biophysical Journal Volume 85 October 2003 2075–2086

Solid Phase DNA Amplification: A Simple Monte Carlo Lattice Model

Jean-Francois Mercier,* Gary W. Slater,* and Pascal Mayer†
*Department of Physics, University of Ottawa, Ottawa, Ontario, Canada; and †Manteia Predictive Medicine S.A., Coinsins, Switzerland

ABSTRACT Recently, a new way to amplify DNA, called solid phase amplification (SPA), has been introduced. SPA differs from the traditional polymerase chain reaction (PCR) in the use of surface-bound instead of freely-diffusing primers to amplify DNA. This limits the amplification to two-dimensional surfaces and therefore allows the easy parallelization of DNA amplification in a single system. Furthermore, SPA could provide an alternate route to DNA target implantation on DNA chips for genomic studies. Standard PCR processes are usually characterized (at least initially) by an exponential growth and a broad population distribution, and they are well described by the theory of branching processes, wherein a generating function can be used to obtain the probability distribution function for the population of offspring. This theoretical approach is not appropriate for SPA because it cannot properly take into account the many-body (steric) and geometric effects in a quenched two-dimensional environment. In this article, we propose a simple Lattice Monte Carlo technique to model SPA. We study the growth, stability, and morphology of isolated DNA colonies under various conditions. Our results indicate that, in most cases, SPA is characterized by a geometric growth and a rather sharp size distribution. Various non-ideal effects are studied, and we demonstrate that such effects do not generally change the nature of the process, except in extreme cases.

INTRODUCTION

Since its invention in 1983, the polymerase chain reaction (PCR) has transformed molecular biology by allowing researchers to make unlimited copies of a single DNA fragment in a matter of hours. PCR is usually performed by first mixing the necessary components in a vial. The amplification then takes place in all of the available volume. Usually, only one target sequence is amplified for each PCR experiment. This means that if different DNA strands are amplified simultaneously (i.e., Multiplex PCR), they have to be separated afterward (using, for example, gel electrophoresis; see Pang et al., 2002). Recently, a new type of DNA amplification, called solid phase amplification (SPA), has been introduced by two different groups: Adessi et al. (2000) and Bing et al. (1996). By attaching the primers to a solid surface, SPA allows an amplification limited to a well-defined two-dimensional area. Since it results in a spatially located amplification, it is possible to amplify a large number of different DNA strands in the same experiment (i.e., onto the same solid surface) without mixing them. This characteristic could be very useful for the design of DNA chips.

It is common to make use of the theory of branching processes to model PCR (Peccoud and Jacob, 1996). In this framework, a generating function provides the probability distribution function for the number of offspring, given the initial number of molecules and the total number of PCR cycles. However, the theory of branching processes is not appropriate in the case of SPA because it cannot take into account the many-body interactions in a quenched environment such as molecular crowding (a chain has less chance to produce an offspring when surrounded by other chains). Furthermore, such theories cannot provide any spatial or density information. In this article, we propose a simple approach to modeling SPA. We reduce the system to a lattice model where a given site can be either occupied by one DNA molecule or left empty. Monte Carlo techniques are then used to simulate the amplification process, i.e., the growth of the colony. The model is thus reminiscent of the models used for the growth of tumors and bacterial colonies (Eden, 1961; Meinhardt, 1982; Sams et al., 1997; Wagner et al., 1999; Williams and Bjerknes, 1972; Ziqin and Boquan, 1995).

This article is organized as follows. The next section describes and explains the PCR process and reviews the standard way to model PCR, the branching process theory. The following two sections then introduce the new technique of solid phase DNA amplification and our Monte Carlo lattice model and results, respectively. We end with our discussion and conclusions.

SOLUTION PCR

PCR is based on the activity of polymerase, a naturally occurring enzyme that acts on a single stranded DNA fragment (ssDNA) and generates its complementary strand. Two characteristics of polymerase make PCR possible. First, polymerase cannot copy a DNA chain without a short sequence of nucleotides to "prime" the process, i.e., to get the process started. This initial stretch of DNA is called a primer. The primers are generated synthetically and are designed to complement a specific sequence at one end of the target sequence (the section of the DNA fragment that needs to be amplified). The other essential characteristic of polymerase is that it can only act on one end (the 3′-end) of the primer. This comes from the structure of the sugar molecules used in the DNA double helix. In a PCR experiment, two primers are usually required (one for each strand). By

Submitted February 17, 2003, and accepted for publication May 15, 2003.
Address reprint requests to Gary W. Slater, 150 Louis Pasteur, University of Ottawa, Ottawa, ON, Canada K1N 6N5. Tel.: 613-562-5800 x6775; Fax: 613-562-5190; E-mail: gslater@science.uottawa.ca.

0006-3495/03/10/2075/12 $2.00

carefully choosing these two primers, it is possible to multiply a selected section of the total DNA fragment: only the section contained between the two primers (the target sequence) is then amplified (Fig. 1).

In a typical PCR experiment, the four necessary components—piece(s) of DNA, large quantities of the four nucleotides (adenine A, cytosine C, guanine G, and thymine T), large quantities of the two primers, and DNA polymerases —are mixed in an aqueous solution (the buffer, which is also used to maintain proper pH and salt concentrations). The PCR process itself usually consists of sequentially heating (to denature the double-stranded DNA), cooling down (to allow the primers to hybridize to the ssDNA fragments) and reheating the mixture (to allow the polymerase to complete the double helix). Those three steps are respectively called *denaturation*, *annealing*, and *extension* (see Fig. 1). After a few cycles, exact replicas of the target sequence have been produced. In the subsequent cycles, dsDNA of both the original molecules and the copies are used as templates. Solution PCR is thus characterized, at least initially (after a while, a lack of nucleotide and/or primer and/or enzyme can affect the growth rate), by an exponential growth. After several cycles, the pool is greatly enriched in pieces of DNA containing the target sequence. In ~1 h, as many as $n = 25$ cycles can be completed, giving up to a $2^{25} \simeq 67$-million-fold increase in the amount of the target sequence.

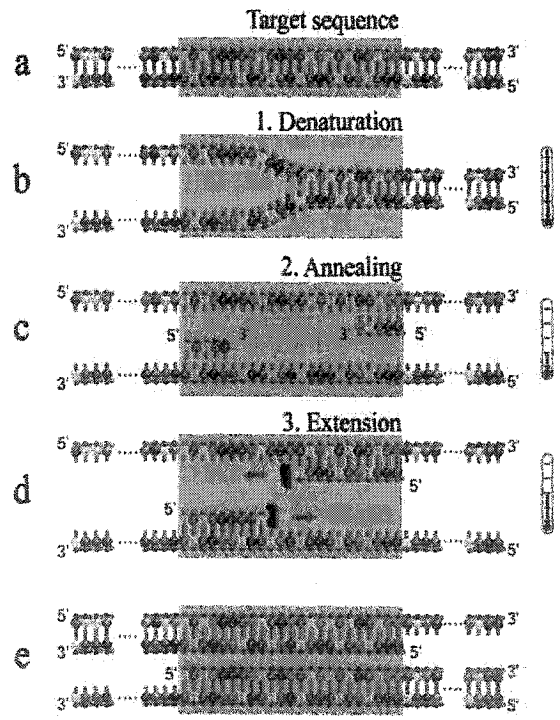

FIGURE 1 Representation of the PCR process. A dsDNA fragment is first heated (*a*) to break the molecule into its two complementary fragments (*b*). The solution is then cooled down to allow the primers to bind to their complementary sequences along the DNA fragments (*c*). Finally the solution is reheated to allow the polymerase to add nucleotides at the end of the primers and eventually make a complementary copy of the template (*d*). Because the polymerase can only act on one end of the DNA (the 3′ end), the solution quickly consists almost exclusively of DNA fragments corresponding to the target sequence located between the two selected primers (*e*).

In practice, however, PCR amplification is not perfect. For example, a PCR thermal cycle can finish before the polymerase has completely copied the DNA. The copy is then said to be a sterile molecule and it is unable to replicate in the following cycle. It is also possible that the molecule simply does not find a matching primer in the annealing phase. These phenomena slow down the growth of the population size. Therefore, the expected population grows like $\sim y^n$, with $y < 2$ (typically $y \simeq 1.9$; see Bing et al., 1996).

Nonspecific hybridization of the primer can also occur and can lead to the amplification of nonspecific PCR products. The case of a primer using the other primer as a template leads to the formation of primer-dimers (Brownie et al., 1997; Halford et al., 1999; Hogdall et al., 1999; Markoulatos et al., 2002; Nazarenko et al., 2002; Wabuyele and Soper, 2001). Because they contain both primer annealing sites, primer-dimers are valid templates and are amplified very efficiently. They may even become the predominant PCR product. To avoid mis-hybridization and the formation of primer-dimers, great care must be taken in the primer design and in the choice of experimental conditions. For example, too short a primer (primer lengths of 18–30 bases are optimal for most PCR applications), complementarity among the 3′ ends of the two primers, low annealing temperatures, high enzyme concentrations, and high primer concentrations have all been shown to increase the frequency of primer-dimer formation (Brownie et al., 1997; Markoulatos et al., 2002).

As previously mentioned, solution PCR leads, at least initially, to an exponential amplification of the target sequence. This is due to the fact that every molecule (the original ones as well as the copies) can be duplicated at each cycle. Solution PCR is thus characterized by the yield of the reaction, p, which is the probability that a DNA molecule produces a fertile copy during a cycle. The growth remains exponential as long as p stays constant. It is the case for the first cycles because PCR is usually carried out with a large excess of reagents (nucleotides, primers, and polymerases) such that the DNA molecules do not have to compete to copy themselves. After a while (typically 20 cycles), however, there are not enough reagents to satisfy all the DNA targets, and both the reaction yield p and the growth rate decrease.

Unless the reaction yield p is equal to 1 or 0, PCR is a random process. If we start with a single copy of the target, the population could be anywhere between 1 and 2^n after n amplification cycles. To simulate this amplification, a simple Monte Carlo procedure can obviously be useful. However, since PCR is intrinsically a simple discrete process, branching theory can also be used (Peccoud and Jacob, 1996). This straightforward, yet powerful theory allows one to quickly

obtain the mean value of the DNA population and the probability distribution of offspring using a generating function.

In the framework of the branching process theory, the discrete growth of a population is written in terms of the generating function (Bailey, 1963; Feller, 1968):

$$P(s) = \sum_{k=0}^{\infty} p_k s^k = p_0 + p_1 s + p_2 s^2 + p_3 s^3 + \ldots, \quad (1)$$

where p_k is the probability that one molecule gives rise to k molecules after one generation (i.e., after one PCR cycle in our case). The probability distribution for the population after n generations is given by the composition of the generating function over itself n times:

$$P_n(s) = P(P_{n-1}(s)), \quad (2)$$

where the coefficient of the s^k term is then the probability of having k molecules after n generations. Using this iterative approach, it is possible to obtain the exact probability distribution function for the population after n generations.

If the process is started with just one individual ($m_0 = 1$), the expected population size after n generations, M_n, is given by Bailey (1963) and Feller (1968) as

$$M_n = (P'(1))^n. \quad (3)$$

In the case of a larger initial number of molecules ($m_0 > 1$), each of them will, independently, give rise to a branching process. The probability-generating function for the n^{th} generation would thus be $(P_n(s))^{m_0}$. Therefore, the expected population size after n generations is $M_n = m_0 \times (P'(1))^n$ and the probability distribution function tends toward a Gaussian form when the initial copy number m_0 is increased (Feller, 1968).

During a PCR cycle, a molecule can either duplicate or not. The probabilities associated with those events are respectively denoted as p and $1 - p$. Therefore the generating function of a PCR cycle is reduced to

$$P(s) = (1 - p)s + ps^2. \quad (4)$$

The expected DNA population of a PCR amplification experiment starting with a single molecule is thus given by

$$M_n = (P'(1))^n = (1 + p)^n. \quad (5)$$

Using Eq. 2, it is possible to obtain the probability distribution function for the DNA population for arbitrary values of p. Fig. 2 shows three samples distributions obtained after $n = 10$ iterations. The population sizes (the x-axis) m_n were divided by the expected value ($m^* = m_n/M_n$) to make comparisons easier. The general shape of the distribution is almost independent of the number of cycles for $n \geq n^* \simeq 10$. In general, we see that the larger the value of p, the sharper the distribution. Also, for large values of p ($p \geq p^* \simeq 0.82$), the distribution is actually multimodal. This is due to the fact that the initial amplification is then critical: a failure of the original molecule to duplicate in the first cycle has a lasting impact. For large values of p, the distribution thus contains (at least) two peaks: one corresponding to the case where the initial amplification failed, and the other one (the larger one) where it was successful. As the amplification yield p approaches its maximum value ($p = 1$), other peaks progressively appear corresponding to the cases where one of the molecules failed to reproduce in the second cycle, then in the third cycle, and so on.

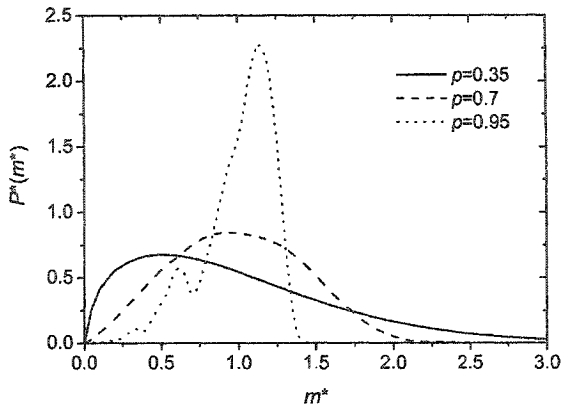

FIGURE 2 Probability distribution of the DNA population for different PCR amplification yields p (using $n = 10$). For $p \gtrsim 0.82$, the distribution is multimodal. The x-axis is the normalized (so the expected value is 1 for all p) size of the population ($M^* = m_{10}/M_{10}$) whereas the y-axis is the probability multiplied by the expected population size $P^*(M^*) = M_{10}P_{10}(M^*)$. The general shape of the distribution is almost completely independent of the number of cycles for $n \geq n^* = 10$. The distributions were obtained starting with a single initial molecule. The distribution tends to become Gaussian when the initial copy number is increased.

PCR is often used to detect substances that are present in very small concentrations (e.g., viral DNA). It is highly effective if one only wants to know if a given substance is present or not. A harder task is quantitative PCR (Q-PCR) where one's goal is to determine the initial number of molecules (m_0), given the final population (m_n) of a single experiment, the (estimated) amplification yield p, and the number of PCR cycles (n) (Boom et al., 2002; He et al., 2002; Stevens et al., 2002). Fig. 2 shows why Q-PCR is difficult in practice. When the amplification yield p is small, the probability distribution is broad and has a large standard deviation. On the other hand, when p is large, the distribution is multimodal. Note that Fig. 2 represents the extreme case where the initial number of molecules is 1. The situation is less critical when m_0 is larger. However, it is precisely when the number of initial molecules is very small and cannot be directly detected using other methods that PCR should be used! Furthermore, the final number of molecules is only known approximately and it is very hard to have a reliable value for the amplification yield p. Nevertheless, Q-PCR has been shown to be useful. It is used, for example, to provide

an estimate of the virus load during HIV and hepatic infections (Boom et al., 2002; Stevens et al., 2002).

SOLID PHASE AMPLIFICATION

The central idea of this novel method is to attach the 5′-end of the primers to a surface (silica, polystyrene bead, ...) instead of letting the primers freely diffuse in a bulk solution (see Fig. 3 *a*) (Adessi et al., 2000; Bing et al., 1996). The primers then form a very dense carpet (the density is $\sim 10^{11}$ primers per mm^2—Adessi et al., 2000—which corresponds to a mean distance of the order of ~5–10 nm between primers; note that this is similar to the contour length of a primer). In this context, the amplification can occur via two processes. First, a freely diffusing DNA target can be captured on the surface and then copied by the polymerase (see Fig. 3, *a–d*). This is called *interfacial amplification*. Note that the copy stays attached to the surface whereas the initial DNA molecule returns to the solution after the annealing step. After several DNA copies are attached to the surface via interfacial amplification, a second type of amplification can take place. In this case, the free end of the attached copy hybridizes to the primer (attached to the surface) complementary to its sequence, and the amplification process can start (see Fig. 3, *e–l*). It is important to note that this *surface amplification* process leaves both molecules attached to the surface, hence its name. Therefore, solid phase DNA amplification leads to the growth of a colony of

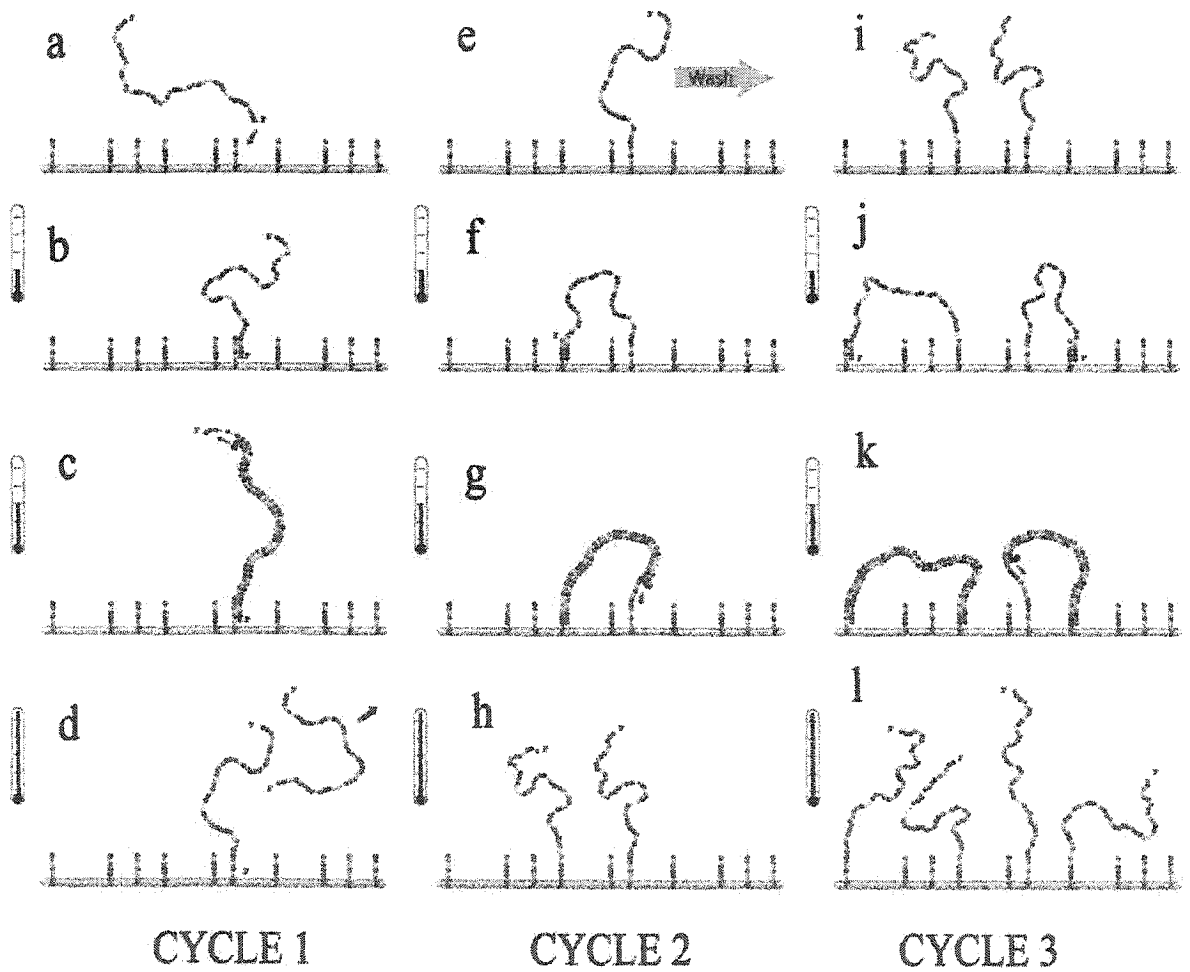

FIGURE 3 Representation of the solid phase amplification process. In the first cycle (*a-b-c-d*) the DNA is replicated by the interfacial amplification. The net result is that one ssDNA is now attached to the surface via the primer. The solution is then changed with a new one free of DNA targets. In the following cycles (*e-f-g-h* and *i-j-k-l*), only surface amplification is possible. This results in a spatially located DNA colony. Note that since a molecule always generates its complementary sequence in a thermal cycle, the two complementary branches will be present in the colony and two different types of primers have to be attached to the surface.

molecules attached to the surface and located in the same region. This characteristic could easily be exploited in the design of DNA microarrays.

The procedure for solid phase amplification can be separated in three distinct steps—annealing, extension, and denaturation—which are repeated in an iterative way. In the first cycle, interfacial amplification is the only type of amplification possible. The result of the first cycle is thus to obtain a certain number of target DNAs attached to the surface via the primers. In subsequent cycles, surface amplification is also possible since some of the target DNAs are now attached to the surface. However, when the two types of amplification process coexist, interfacial amplification is usually predominant (Adessi et al., 2000). Therefore, to obtain surface amplification, the initial solution has to be washed away and replaced with a solution free of DNA targets. Surface amplification is then the only amplification possible and the temperature cycles can be started again. The net result of a surface amplification event is to obtain a new ssDNA molecule attached to the surface in the immediate proximity of the initial strand (Fig. 3, *h–i*). Note that the length of the molecules used in SPA is typically 400 bases (contour length of ~170 nm). The radius of gyration in the hybridization phase (ssDNA) is thus ~15–20 nm which is larger than the mean distance between nearest-neighbor primers (~5–10 nm). Also, a typical DNA length is much larger than the persistent length of ssDNA (~10 bases or ~4 nm) but is similar to that of dsDNA (~150 basepairs or ~51 nm). Therefore, the molecule is very flexible in the hybridization phase, and has no problem bending to find matching primers. However, at the end of the elongation phase (when the molecule is completely double-stranded), it becomes quite rigid and must be under considerable bending stress.

Surface amplification results in an area covered with copies of both strands of the original DNA target. This can be seen as a DNA colony. The number of colonies depends on the number of DNA targets captured (via interfacial amplification) before the initial solution is washed. If different DNA targets are captured, many types of colonies will exist on the surface.

Two strategies can be used for primer implantation. Specific primers can be used so that the hybridization (and the amplification) is only possible for a specific DNA target. A chip can then be designed so that each sub-area is specific for one target, and it is possible to detect target sequences without using solution-based primer sets, hybridization, or electrophoresis (Bing et al., 1996). Another approach consists of adding, at both ends of the nucleic acid templates to be analyzed, the linker sequences complementary to the immobilized primers (Adessi et al., 2000). In this case, it is possible to amplify each template molecule irrespective of their actual sequence. Note that the colonies are then randomly arrayed. If the colonies are far enough from each other (favored by using a small concentration of DNA targets in the initial solution), each colony is amplified but remains isolated from the others (no merging occurs between neighboring colonies). SPA thus allows the parallelization of the DNA amplification process without any direct human intervention. In both scenarios, the actual growth of the colonies is similar.

The process described in Fig. 3 corresponds to the ideal case in which the primer cannot be removed from the surface. In reality, the successive heating and cooling of the solution can cause the primer to detach from the surface. A recent study (Adessi et al., 2000) showed that, even in the most suitable case, up to 50% of the primers had detached after 28 cycles. Of course, the primers can also detach after a DNA target has been "attached" to it. Therefore, after a couple of cycles, the solution can contain some free diffusing targets and primers. In this context, solution PCR followed by interfacial amplification is still possible in principle. However, experimental work (Adessi et al., 2000) showed that this process is negligible, perhaps because of the very small concentration of DNA targets and primers present in solution. It is also possible to avoid solution PCR completely by changing the chemical mix at each cycle.

The number of molecules in a given SPA colony does not increase exponentially (with the exception of the first few cycles) as in the case for solution PCR. The reason is molecular crowding. Two free molecules separated by less then their radius of gyration (R_g) will interact sterically with each other, and will tend to repulse each other. In SPA, a duplicated molecule (child), will always be in the vicinity of the original molecule (parent). Therefore, the parent molecule will not be able to bend and make a new molecule in the vicinity of its child and vice versa. When a molecule is completely surrounded by others, its free end tends to move away form the surface (like in a dense polymer brush; Currie et al., 2000; Netz and Schick, 1998; Skvortsov et al., 1999). Therefore, after a few cycles, a molecule at the center of the colony (which is thus surrounded by others) will have a smaller duplication probability (its free end is less likely to find a matching primer on the surface). Because of this phenomenon, a DNA colony should be characterized by a roughly constant density and should grow outwards, i.e., from its perimeter. Since only the perimeter can reproduce freely, the growth cannot be exponential.

Like in solution PCR, a SPA cycle can finish before the polymerase has completely copied the DNA, resulting in a sterile molecule. In solution PCR, this simply reduces the growth rate of the amplification. In SPA the impact can be more severe because the sterile molecule is attached to the surface and will interact sterically with its neighbor. When the edge of the colony is obstructed by sterile molecules, the latter can act as a fence and slow down, or even stop, the growth of the colony. Note that there is a certain (small) probability for a sterile molecule to become fertile again in subsequent cycles (the sterile molecule may rehybridize to a fertile molecule, allowing the polymerase to complete its DNA sequence).

SIMULATING SOLID PHASE AMPLIFICATION

As mentioned previously, the branching process theory is not appropriate for solid phase DNA amplification because it is based on the assumption that the amplification yield is the same for all molecules and remains unchanged over all cycles. Although somewhat realistic in the case of solution PCR, those assumptions are obviously not valid for SPA because of the many-body (steric) interactions (see Solution PCR). In this section, we propose a simple lattice Monte Carlo system to model SPA and we present simulation results.

The simplest possible system, where a molecule can only create a copy of itself on an empty lattice site immediately adjacent to its position (with a probability $0 < p \leq 1$), is considered in The Basic System. In the following subsections, the model is generalized to include sterile molecules (Sterilization) and molecules detaching from the surface (Detachment). In The Colony Density Profile, the model is further generalized to allow a greater density at the center of the colony. To do so, two alternatives are explored (adding a probability for a molecule to generate a copy of itself in between existing molecules and allowing more than one molecule to occupy each site of the lattice). In each case, the growth of the colony is examined as well as its stability and morphology.

As we shall see, a realistic representation of a SPA experiment must include many parameters. Also, while a lattice representation greatly simplifies the simulation, some important choices are still necessary regarding the algorithm itself. Choosing a good algorithm and a good set of parameters likely requires a combination of precise experimental data and microscopic simulations, e.g., detailed and extensive molecular dynamics or Brownian dynamics simulations of realistic chains attached to surfaces. Instead of trying all possible options and sets of parameters, educated guesses are made, allowing an overview of the possibilities and an understanding of the general phenomenon of SPA. Therefore, this work should not be seen as a final product, but rather as a starting point, aiming at guiding what needs to be done experimentally and in terms of microscopic simulations.

The basic system

The simplest way to model SPA is to use a lattice algorithm where each site can be either occupied by a ssDNA molecule or left empty (an empty site is actually occupied by several primers since the latter form a dense carpet). Fig. 4 shows a simple example of such a system. At each thermal cycle, a ssDNA molecule can either generate a copy on one of its empty nearest neighbor sites or stay inactive. Although very simple, this model better represents SPA than branching processes because it includes the essence of the molecular crowding phenomenon, i.e., when all the nearest neighbors of a molecule are occupied, the latter cannot produce further copies. The model thus assumes that the duplicated molecules are always roughly at the same distance from the original molecules and that once a molecule is surrounded by four others (we use a square lattice), its free end remains away from the surface so that it cannot duplicate.

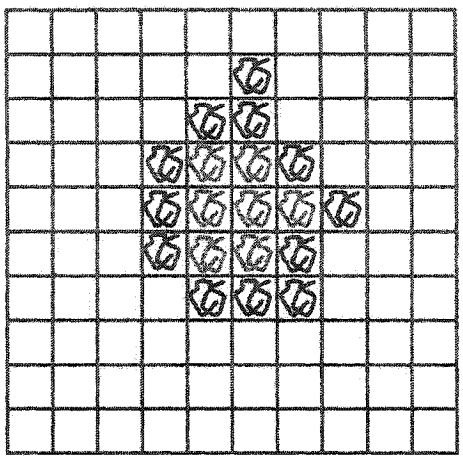

FIGURE 4 Example of an SPA representation on a square lattice system. A lattice site can be occupied by an ssDNA molecule or left empty. At each cycle, a molecule can either make a copy on one of the nearest neighbor empty sites or stay inactive. When all four nearest neighbor sites are occupied (molecules in *gray*), the molecule cannot produce copies anymore.

The simulation algorithm goes as follows. A molecule is first placed at the center of a square lattice. At each cycle, each molecule makes one attempt to copy itself into one of its empty nearest neighbor sites (if any). If more than one such site is available to a molecule, one of them is chosen randomly, but the molecule still has only one chance (per cycle) to make a copy. Therefore, two molecules can try to generate a copy onto the same site, but only one can be successful. Each attempt has a probability p of being successful. When a molecule is completely surrounded by others (i.e., all its nearest neighbors are occupied by other molecules), it cannot produce any more copies. Note that a colony is actually made of both strands of the original DNA target (see Solid Phase Amplification). We do not, however, distinguish between the two types.

Simulations were performed for up to 100 thermal cycles and were averaged over 100,000 colonies for each set of parameters. Fig. 5 shows the average size $M(n)$ of a colony (defined as the number of fertile molecules in the colony), as a function of the number n of thermal cycles, for various values of p (Fig. 5, *inset*, shows the average size of a colony after $n = 100$ iterations as a function of p). As expected, a larger value of p leads to a faster increase of the colony size. Also, the growth in the size of the population is slower than for solution PCR. This is so because once a molecule is surrounded by others, it stops copying itself (this is the molecular crowding issue that we mentioned previously). Therefore, apart from the very first few cycles, the colony

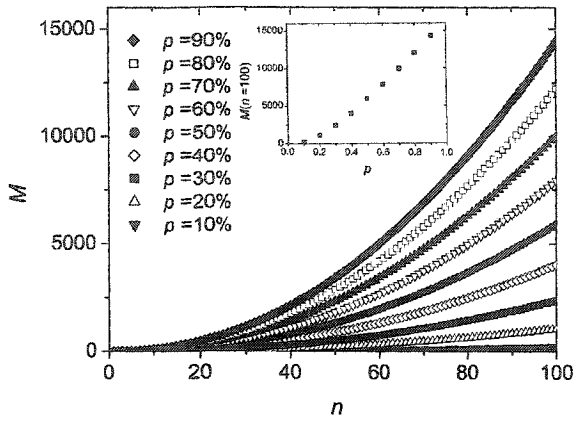

FIGURE 5 Average size M of the colony as a function of the number n of SPA cycles. Each colony starts with a single molecule. The data were averaged over 100,000 colonies for each set of parameters. A larger value of p leads to a faster increase of the colony size. *Inset*: Average size of a colony after $n = 100$ iterations as a function of p.

grows mostly from its perimeter. Since the radius r of the colony increases linearly with the number n of generations,

$$r(n) \sim n, \tag{6}$$

its surface area, $A(n)$, scales like

$$A(n) \sim r(n)^2 \sim n^2. \tag{7}$$

If we assume that most of the sites inside the colony are occupied, which is certainly the case for the "old" sites away from the colony perimeter, the colony grows in a geometrical manner:

$$M(n) \propto A(n) \sim n^2. \tag{8}$$

This can be verified on Fig. 6 where the evolution of the colony size ($M(n)$) is shown on a log-log graph. An asymptotic slope of 2 is clear for all values of p. The initial exponential growth ceases when the core of the colony reaches its maximum density of one molecule per lattice site.

Fig. 7 shows the distribution of colony sizes for $p = 10\%$ to $p = 90\%$ with 10% intervals. The distributions are much sharper than the one obtained for solution PCR (compare to Fig. 2). This is so because solid phase amplification is less sensitive to failures in the first few thermal cycles. When normalized, the standard deviation of the distributions decreases sharply when p increases (Fig. 7, *inset*), as one would expect.

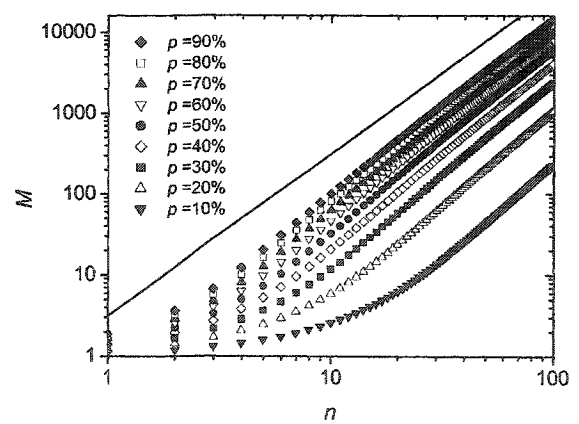

FIGURE 6 Average size M of the colony as a function of the number n of SPA cycles. Apart from the very first few cycles, the relation is linear for all values of p, and for large n, the slope approaches a value of 2 (*solid line*). Therefore the colony grows in a geometrical manner, $M(n) \propto n^2$.

Sterilization

As explained in the previous section, a thermal cycle can finish before the polymerase has completely copied the DNA strand, resulting in a sterile molecule. Such a molecule is unable to produce new copies because the DNA sequence at its free end does not correspond to the primer sequences on the surface. However, a sterile molecule still occupies space; therefore, it applies steric constraints to its neighbors and can prevent them from duplicating. Note that a sterile molecule can become fertile again in subsequent cycles if it rehybridizes with a fertile molecule.

The algorithm presented in the last section was modified to account for these phenomena. First, each new molecule is now assumed to have a probability s to be *born* sterile (the probability to generate a sterile molecule is thus ps). Note that a sterile molecule still occupies one lattice site, and therefore prevents a fertile molecule from occupying it. We thus make the approximation that a sterile molecule, with a smaller radius of gyration, has the same steric impact as a fertile one. Second, to account for the possible rehybridization of a sterile molecule, we assume that when a fertile

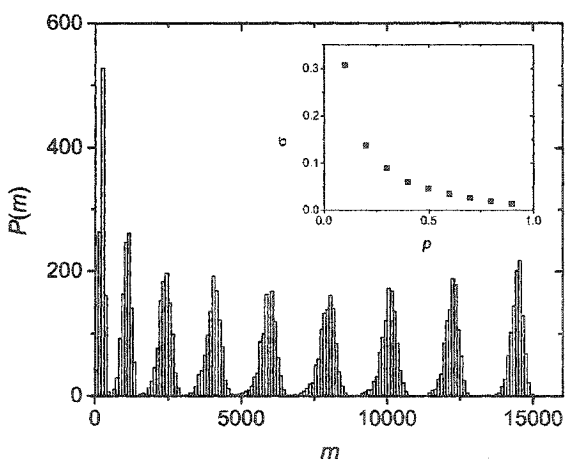

FIGURE 7 Distribution of colony sizes m for $p = 10\%$ to $p = 90\%$ (from *left* to *right*) with 10% intervals. All distributions are much sharper than that obtained by solution PCR (see Fig. 2). We used ensembles of 1000 colonies and $n = 1000$ cycles. *Inset*: Normalized standard deviation as a function of p.

molecule is completely surrounded by others (all its nearest neighbors are occupied), it tries to recombine with one of its neighbors (one of the four neighbors is chosen randomly). If this neighbor happens to be sterile, it has a probability r to complete its sequence, thus rendering it fertile (we also assume that all the fertile molecules can rehybridize with a sterile molecule even though only molecules that are its complement can actually do it). Note that both s and r are assumed to be constant during the simulation, i.e., from cycle to cycle.

Simulations were performed using this algorithm and the recombination mechanism was first assumed to be negligible ($r = 0$). The probability for a molecule to make a copy was set to $p = 0.4$, the number of thermal cycles to $n = 100$ and the results were averaged over 100,000 colonies. Since a sterile molecule is unable to copy itself, a larger probability s to obtain a sterile molecule results in a slower growth. This can be seen in Fig. 8, where the number of fertile molecules is plotted as a function of the number of cycles for various values of s. When $s \neq 0\%$, there is a finite probability that a colony simply stops growing because all the molecules on its perimeter turn out to be sterile. In principle, this could happen at any stage of the development of the colony. In reality, however, when $s < s^* \simeq 41\%$, the colony either stops growing after only a few cycles or grows indefinitely. As an example, the distributions of colony sizes are compared in Fig. 9 for $s = 0\%$ and $s = 20\%$. Apart form the obvious fact that the mean colony size decreases when s increases, there is apparently little difference between the two distributions. However, we note a little bump near the origin for the $s = 20\%$ case: this corresponds to the colonies that died young. As s is increased, the probability that the colony stops growing at a later stage increases, and when $s > s^* \approx 41\%$, the colony is doomed to die (the average size of the colonies converges to a finite value: $M(n \to \infty) \neq \infty$). This can be observed in Fig. 10 where the size distributions are plotted for $s = 40\%$ and $s = 50\%$. Those critical effects can also be seen on Fig. 11 where the fraction of colonies still growing after n cycles $\Omega g/\Omega$, is plotted as a function of the inverse of the number of cycles ($1/n$) for different values of s. When $s < s^* \approx 41\%$, the number of growing colonies converges to a finite value. Another important result is that when $s < s^*$ the growth of the colony remains geometric, i.e., we still have $M \sim n^2$. The actual value of s^* is expected to be equal

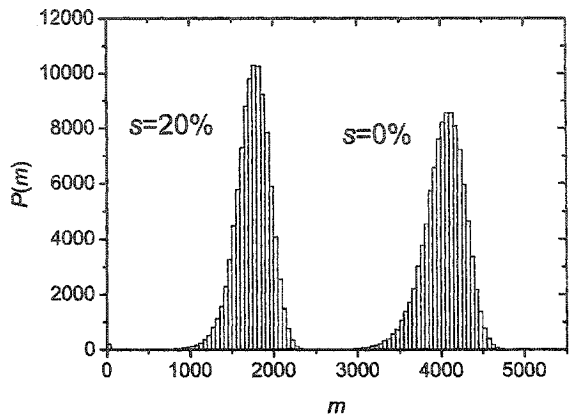

FIGURE 9 Distribution of colony sizes M for $s = 0\%$ and $s = 20\%$ ($p = 0.40$ in both cases). Apart from the obvious fact that the mean size of the colony is larger for $s = 0\%$, and the little bump at the beginning of the $s = 20\%$ curve (due to colonies that have stopped growing because all the molecules on their perimeter were sterile), there is little difference between the two distributions. The ensemble is made of 100,000 colonies and we allowed $n = 100$ cycles. We have $M_{0\%} = 4036$, $\sigma_{0\%} = 247$, and $M_{20\%} = 1745$, $\sigma_{20\%} = 217$. For $s = 20\%$, the total fraction of the "dead" colonies is 184/100,000 after 100 cycles.

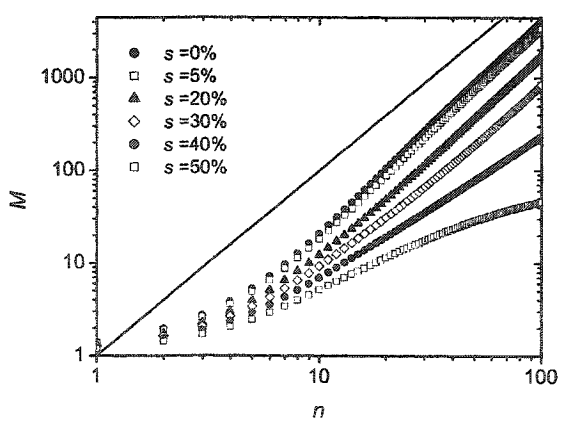

FIGURE 8 Average size M of the colony (number of fertile molecules) as a function of the number n of cycles for various values of s. The *solid line* corresponds to a geometric growth and has a slope of 2. A sterile molecule is not able to copy itself, therefore a larger probability s to generate a sterile molecule results in a slower growth. For each set of data, the results were averaged over 100,000 colonies and $p = 0.4$ was used.

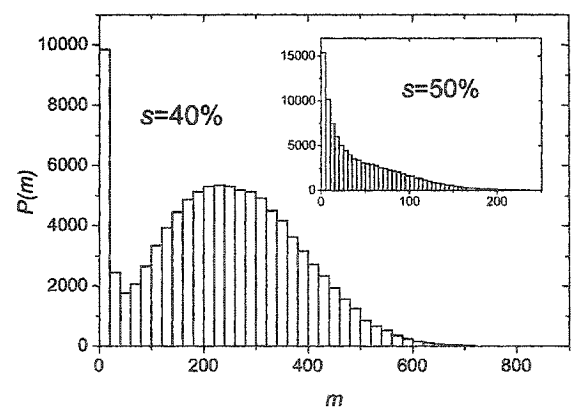

FIGURE 10 Distribution of colony sizes m for $s = 40\%$ and $s = 50\%$ (*inset*). The ensemble is made of 100,000 colonies and we used $n = 100$ cycles and $p = 0.40$. We have $M_{40\%} = 234$, $\sigma_{40\%} = 141$, and $M_{50\%} = 46$, $\sigma_{50\%} = 45$.

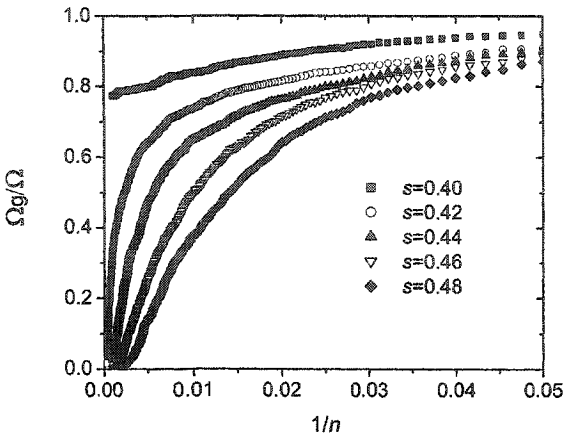

FIGURE 11 The fraction of colonies still growing after n cycles as a function of the inverse of the number of cycles $1/n$ for different values of s. Here, $\Omega = 1000$ is the initial number of colonies, and Ωg is the colonies that are still alive after n cycles. When $s > s^* \approx 41\%$, the number of growing colonies converges to a finite value.

to the site percolation threshold c^* of the given lattice. For the two-dimensional square lattice, we have $c^* = 0.407254$ (Stauffrer and Aharony, 1992), which is compatible with our value of $s^* \approx 41\%$.

When the probability r that a fertile molecule hybridizes with and completes a sterile molecule is not negligible, the impact of molecular sterility is less important. For example, we can see in Fig. 12 that the $s = 0.2$ curve gets closer to the $s = 0.0$ curve as r increases. The effect is very subtle, however, and the recombination mechanism can be neglected if s is not too large. For large values of s, however, rehybridization cannot be neglected because it is the only mechanism that ensures that a colony will not remain surrounded by sterile molecules forever. Rehybridization is then the key to continuous growth.

Note that sterile molecules can affect the shape of the colonies. While extremely symmetric when no or only a small fraction of the molecules are sterile, the colonies become more asymmetric when the fraction of the sterile molecules is increased (results not shown). This is so because a small number of consecutive sterile molecules can completely block a direction of growth for the colony. The colony then has to go around the blocked section, leading to an asymmetrical growth.

Detachment

Until now, we have assumed that a primer (or an attached molecule) cannot be removed from the surface. In reality, the successive heating and cooling phases can cause the primer to break away from the surface. The algorithm was further modified to include this rather dramatic effect: at each cycle a molecule now has a probability x of disappearing. It is further assumed that the number of primers remains high and that it is never a limiting factor. Therefore the probability of copying a molecule p is not affected by primer detachment, and remains constant. Furthermore, a site that has just been vacated by the detachment of a molecule cannot be distinguished from a site that has never been occupied. Note that it is also assumed that the detachment of a molecule occurs at the beginning of a thermal cycle in the denaturation phase when the solution is heated and that the probability x is independent of the number of cycles.

Fig. 13 shows the average size of the colony as a function of the number of cycles for various values of x. The probability for a molecule to make a copy was set to $p = 0.4$,

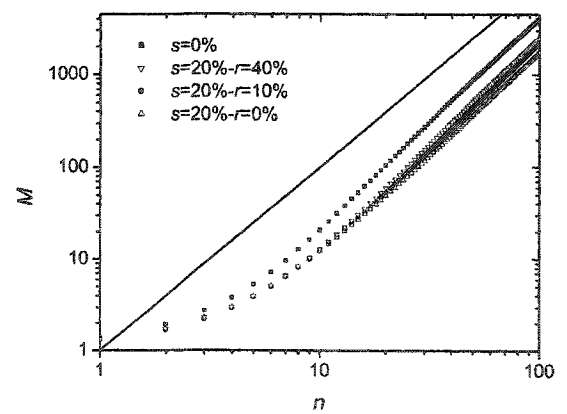

FIGURE 12 Average size M of the colonies as a function of the number n of cycles for various values of r. For each set of data the results were averaged over 100,000 colonies and $p = 0.4$ was used. When the probability r that a fertile molecule hybridizes and completes a sterile molecule is not negligible, the effect of the sterile molecules is a little less important: the $s = 0.2$ curve gets closer to the $s = 0.0$ curve as r is increased.

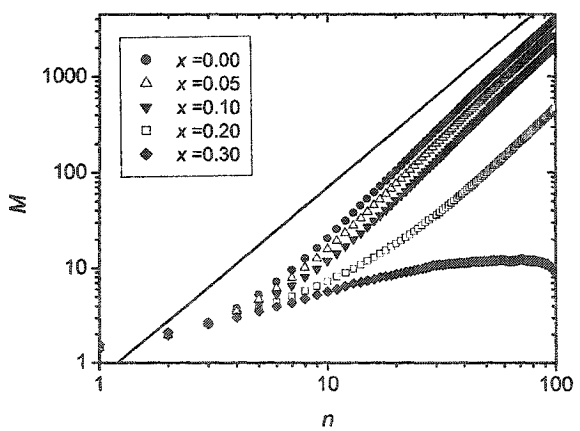

FIGURE 13 Average size of the colonies M as a function of the number n of cycles for various values of x, the probability for a molecule to break away from the surface. The *solid line* corresponds to a geometrical growth and has a slope of 2. For each set of data the results were averaged over 100,000 colonies and $p = 0.4$ was used.

the sterile molecules were neglected ($s = r = 0$), the number of thermal cycles was set to $n = 100$, and the results were averaged over 100,000 colonies. An increase in the probability of molecular detachment results in a decrease of the expected size of the colony. Furthermore, when x reaches a critical value (here $x^* \simeq 30\%$), the expected size of the colony actually decreases after it reaches a maximum. This means that the colonies are actually doomed to becoming extinct as the number of thermal cycles is increased; molecules simply disappear faster than they are created. Note that the data in Fig. 13 are actually an average over the colonies that survive (i.e., colonies that have at least one fertile molecule) at least $n = 100$ cycles. The argument is that the extinct colonies cannot be observed experimentally. If the extinct colonies are included in the average, the expected size of the colony is further reduced. Another phenomenon associated with the detachment of molecules is that as x increases, there is a possibility that a colony actually splits into two (or more) distinct parts making the results harder to interpret. Note that the actual value of x^* is expected to correspond to the case where the probability of detachment in one cycle is equal to the net duplicating probability for that cycle ($(1 - x)p$). The value of x^* is thus independent of the lattice type, but depends on the value of p. For $p = 0.40$, we have $0.4\ (1 - x^*) = x^*$ leading to $x^* = 0.2857$, which is consistent with our results.

The colony density profile

One drawback to using a lattice to model SPA is that the lattice rigidly fixes the maximum density of molecules (e.g., to one per lattice site). Although a uniform density seems to be a fairly good approximation, one should expect the density at the center of the colony to be somewhat higher than at the fringe. Indeed, while it is very difficult for a molecule surrounded by others to bend so that its end can find a matching primer, it is not completely impossible. This section explores three alternatives to model this phenomenon.

One simple way to model a greater density at the center of the colony is to allow a molecule to make copies of itself on interstitial lattice sites. In practice, the algorithm is modified in the following way: at each cycle, a molecule that is completely surrounded (all its nearest east-west-north-south neighbors are occupied) tries to find a primer in one of the four interstitial sites (chosen randomly) situated in between these neighbors (see Fig. 14). If that site is empty, the molecule has a probability $d < p$ of making a copy.

Here, the average size of the colonies will be studied as a function of the number of cycles for various values of d assuming $p = 0.4$, $s = r = x = 0$, and $n = 100$. Fig. 15 shows these results, averaged over 100,000 colonies. As expected, the average population size of a colony increases with d. This increase is far from being linear, though. After a fast increase when d is varied from 1% to 5%, a further

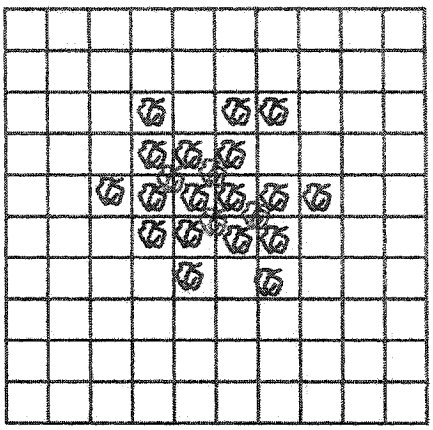

FIGURE 14 An example of a lattice with a smaller effective mesh size. At each cycle a *main* molecule (in *black*) that is completely surrounded (all its nearest neighbors are occupied) tries to find a primer in one of the four interstitial sites (chosen randomly). If that site is empty, the molecule has a probability d of making a copy (in *gray*).

increase of d causes little change to the average colony size. The reason is that the maximum density is limited, therefore a larger d simply results in a faster increase, but not in a higher density. This is an important finding because it means that the probability that a molecule produces a new copy in a dense environment cannot be neglected even if it is very small.

An alternative way to model a continuous growth at the center of the colony is to let more than one molecule occupy each site in our lattice model. In practice, the algorithm is modified in the following way: at each cycle, a molecule that is completely surrounded tries to duplicate onto its own

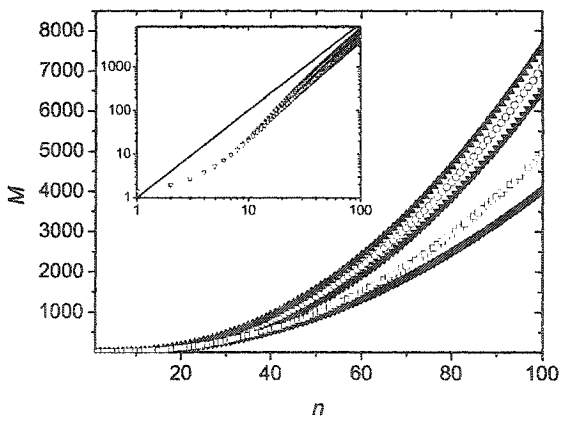

FIGURE 15 Average size M of the colony as a function of the number n of cycles for $d = 0\%$, 1%, 5%, 10%, and 20%, where d is the probability that a molecule makes a copy on an interstitial site. For each set of data the results were averaged over 100,000 colonies and $p = 0.4$ was used. *Inset*: Same data on a log-log graph. All curves are now almost undistinguishable. The *solid line* corresponds to a geometrical growth and has a slope of 2.

lattice site. The probability for the duplication to be successful ($p_d(N)$) depends on the number N of molecules on the site like, e.g.,

$$p_d(N) = e^{-AN}, \tag{9}$$

where A is a parameter regulating the strength of the local (on-site) steric interactions. When $A \to \infty$, the system is reduced to the ordinary SPA thermocycled algorithm presented in The Basic System, and colonies grow in a geometrical manner. On the other hand, when $A \to 0$, the system behaves like a perfect solution PCR (with no steric interaction) and the size of the colony grows exponentially. For intermediate values of A, the growth becomes geometric after a transition regime whose duration (number of cycles) depends upon the value of A (a large value of A leads to a short transition period). This transition regime can be observed in Fig. 16, where the average colony size is plotted as a function of the number n of thermal cycles for a value of $A = 0.5$. The inset of Fig. 16 shows a typical density profile obtained with the algorithm. The density profile of the colony is not flat, unlike the colonies generated in the previous sections.

In fact, we can also propose a deterministic analytical model for the growth behavior of such a colony, using a continuous time approximation. In dimensionless units, the model is defined by the differential equation:

$$\dot{\rho}(r,t) = H(vt - r)f(\rho), \tag{10}$$

where $\rho(r,t)$ is the local density of the colony at time t, H is the Heaviside (or step) function, v is the radial speed at which the colony grows (one could take this to be roughly given by p since this is the probability for the perimeter to grow out by one more lattice site), and $f(\rho)$ is a function describing the steric influence of the current density on the local growth. Here, r is the distance from the center of the colony (we assume a polar symmetry). Following Eq. 9, we can use, for example, the exponential constraint

$$f(\rho) = e^{-\rho(r,t)}. \tag{11}$$

With the blank initial condition $\rho(r,0) = 0$, we obtain

$$\rho(r,t) = \ln\left[\left(\frac{vt - r}{v}\right)H\left(\frac{vt - r}{v}\right) + 1\right]. \tag{12}$$

The solution can be integrated to obtain the total intensity of the colony as

$$I = \int_0^{vt} r\rho(r,t)dr \to t^2\ln(t). \tag{13}$$

The results confirm that the growth is always geometric after a transient regime, and that the density profile of the colony is peaked. Therefore, geometric growth and nonflat profiles are not contradictory. Note that we also tried other $f(\rho)$ functions (e.g., the simple ceiling equation $f(\rho) \sim (\rho_{max} - \rho)^n$), and obtained qualitatively similar results.

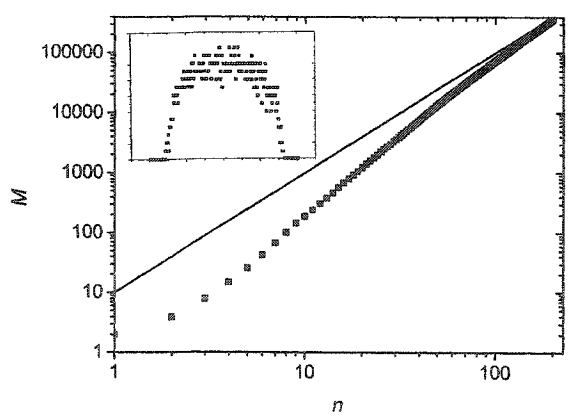

FIGURE 16 Average size M of the colony as a function of the number n of thermal cycles for the case where more than one molecule can occupy the same site (see Eq. 9, with $A = 0.50$). After a fairly long transition time, the colony grows in a geometrical manner. The simulations were performed for up to 200 thermal cycles and were averaged over 200 colonies. *Inset*: Example of a density profile.

DISCUSSION

The simple lattice model of solid phase DNA amplification (SPA) presented in this article predicts major qualitative differences between solution PCR and SPA. First, we find that SPA cannot be characterized by an exponential growth because of the phenomenon of molecular crowding (a chain has less chance to produce an offspring when surrounded by other chains). Therefore, the molecules at the center of the colony slow, or even stop, their duplication and only the perimeter molecules can reproduce freely. The colonies thus grow outwards, i.e., from their perimeter in a geometric manner. An exponential phase can nevertheless be observed in the first few thermal cycles, when the duplication probability of all molecules is little affected by the presence of the others. Another difference between solution PCR and SPA is the probability distribution function for the population of offspring. Because SPA is less sensitive to failures in the first few thermal cycles, the distribution for the population of offspring is much sharper than the one obtained for solution PCR.

SPA characteristics (geometrical growth and sharper size distribution) are unaffected by the addition of sterile molecules or random detachment of molecules if the related probabilities do not reach critical values where they completely stop the growth of the colony. Furthermore, nonflat density profiles, obtain when the molecules at the center of the colony do not completely stop duplicating, still lead to geometrical growth and sharper size distributions than solution PCR.

The present algorithm is based on many educated assumptions currently lacking solid foundations. To test those as-

sumptions and obtain realistic values for the parameters, a combination of precise experimental data and microscopic simulations in which the polymeric nature of the chain is explicitly taken into account, should be used. Among the possible aspects that a microscopic model could address are the time required for the free end to touch the surface and the average spatial distribution of those contacts as a function of the chain density. These simulations would provide some answers to many interrogations. For example, they would give a clear indication on the lattice best suited to model thermocycled SPA and provide a realistic description of the dependence of the probability of making a copy (p) upon the local density. Comparison with experimental data is also undoubtedly required. Growth curves, size distributions, and density profiles should be compared to experimental data to identify the relevant minimal set of parameters and to estimate their numerical values.

A reliable and quantitative model of SPA would help not only to explain experimental data, but also to optimize the experimental procedures. Also, it could be used to model more global phenomena than the growth of single isolated colonies. For example it could easily be used to model the interaction between two (or more) colonies with different characteristics.

The authors thank F. Deguerry and I. Lawrence for useful discussions.

This work was supported by a Research Grant from the Natural Science and Engineering Research Council of Canada to G.W.S. and by scholarships from Ontario Graduate Scholarship, Ontario Graduate Scholarship in Science and Technology, Fonds pour la Formation des Chercheurs et l'Aide à la Recherche (Québec), Manteia, and the University of Ottawa to J.F.M.

REFERENCES

Adessi, C., G. Matton, G. Ayala, G. Turcatti, J.-J. Mermod, P. Mayer, and E. Kawashima. 2000. Solid phase amplification: characterisation of primer attachment and amplification mechanisms. *Nucleic Acids Res.* 28:e87.

Bailey, N. T. J. 1963. The Element of Stochastic Processes. Wiley Classics Library, Oxford, UK.

Bing, D. H., C. Boles, F. N. Rehman, M. Audeh, M. Belmarsh, B. Kelley, and C. P. Adams. 1996. Bridge amplification: a solid phase PCR system for the amplification and detection of allelic differences in single copy genes. *In* Genetic Identity Conference Proceedings, Seventh International Symposium on Human Identification, http://www.promega.com/geneticidproc/ussymp7proc/0726.html.

Boom, R., C. Sol, Y. Gerrits, M. D. Boer, and P. W. van Dillen. 2002. Highly sensitive assay for detection and quantitation of human cytomegalovirus DNA in serum and plasma by PCR and electrochemiluminescence. *J. Clin. Microbiol.* 37:1489–1497.

Brownie, J., S. Shawcross, J. Theaker, D. Whitcombe, R. Ferrie, C. Newton, and S. Little. 1997. The elimination of primer-dimer accumulation in PCR. *Nucleic Acids Res.* 25:3235–3241.

Currie, E. P. K., G. J. Fleer, M. A. C. Stuart, and O. V. Borisov. 2000. Grafted polymers with annealed excluded volume: a model for surfactant association in brushes. *Eur. Phys. J. E.* 1:27–40.

Eden, M. 1961. A two-dimensional growth process. *In* Proceedings of the 4th Berkeley Symposium on Mathematical Statistics and Probability. University of California Press, Berkeley, CA. pp.223–239.

Feller, W. 1968. An Introduction to Probability Theory and its Applications, vol. 1. John Wiley and Sons, New York.

Halford, W. P., V. C. Falco, B. M. Gebhardt, and D. J. J. Carr. 1999. The inherent quantitative capacity of the reverse transcription polymerase chain reaction. *Anal. Biochem.* 266:181–191.

He, Q. A., J. Wang, M. Osato, and L. B. Lachman. 2002. Real-time quantitative PCR for detection of *Helicobacter pylori*. *J. Clin. Microbiol.* 40:3720–3728.

Hogdall, E., K. Boye, and J. Vuust. 1999. Simple preparation method of PCR fragments for automated DNA sequencing. *J. Cell. Biochem.* 73: 433–436.

Markoulatos, P., N. Siafakas, and M. Moncany. 2002. Multiplex polymerase chain reaction: a practical approach. *J. Clin. Lab. Anal.* 16:47–51.

Meinhardt, H. 1982. Models of Biological Pattern Formation. Academic Press, London.

Nazarenko, I., B. A. Lowe, M. Darfler, P. Ikonomi, D. Schuster, and A. Rashtchian. 2002. Multiplex quantitative PCR using self-quenched primers labeled with a single fluorophore. *Nucleic Acids Res.* 30:e37.

Netz, R. R., and M. Schick. 1998. Polymer brushes: from self-consistent field theory to classical theory. *Macromolecules.* 31:5105–5140.

Pang, Y. S., H. Wang, T. Girshick, Z. X. Xie, and M. I. Khan. 2002. Development and application of a multiplex polymerase chain reaction for avian respiratory agents. *Avian Dis.* 43:691–699.

Peccoud, J., and C. Jacob. 1996. Theoretical uncertainty of measurements using quantitative polymerase chain reaction. *Biophys. J.* 71:101–118.

Sams, T., K. Sneppen, M. H. Jensen, C. Ellegaard, B. E. Christensen, and U. Thrane. 1997. Morphological instabilities in a growing yeast colony: experiment and theory. *Phys. Rev. Lett.* 79:313–316.

Skvortsov, A. M., A. A. Gorbunov, and F. A. M. L. G. J. Fleer. 1999. Long minority chains in a polymer brush: a first-order adsorption transition. *Macromolecules.* 32:2004–2015.

Stauffrer, D., and A. Aharony. 1992. Introduction to Percolation Theory. Taylor and Francis, London, UK.

Stevens, S. J. C., I. Pronk, and J. M. Middeldorp. 2002. Toward standardization of Epstein-Barr virus DNA load monitoring: unfractionated whole blood as preferred clinical specimen. *J. Clin. Microbiol.* 39:1211–1216.

Wabuyele, M. B., and S. A. Soper. 2001. PCR amplification and sequencing of single copy DNA molecules. *Single Mol.* 2:13–21.

Wagner, G., R. Halvorsrud, and P. Meakin. 1999. Extended Eden model reproduces growth of an acellular slime mold. *Phys. Rev. E.* 60:5879–5887.

Williams, T., and R. Bjerknes. 1972. Stochastic model for abnormal clone spread through epithelial basal layer. *Nature.* 236:19–21.

Ziqin, W., and L. Boquan. 1995. Random successive growth model for pattern formation. *Phys. Rev. E.* 51:R16–R19.

ARTICLE V

J. F. Mercier and G. W. Slater.

Solid phase DNA amplification: A Brownian Dynamics study.

Submitted to *Biophysical Journal.*

Solid Phase DNA Amplification: A Brownian Dynamics study.

Jean-François Mercier* and Gary W. Slater†

Department of Physics, 150 Louis-Pasteur, University of Ottawa, Ottawa, Ontario K1N 6N5, Canada

(Dated: October 18, 2004)

Solid phase amplification (SPA), a new method to amplify DNA, is characterized by the use of surface-bound primers. This limits the amplification to two-dimensional surfaces and therefore allows the easy parallelization of DNA amplification in a single system. SPA leads to the formation of small but dense DNA brushes, called DNA colonies. For a molecule to sucessfully duplicate itself, it needs to bend so that its free end can find a matching primer, located on the surface. We used Brownian Dynamics simulations (with a united atom model) to model the kinetics of a SPA experiment. The simulations mimic the temperature cycles and the molecule duplication process found in SPA; in particular, each molecule whose free end comes very close to the surface during a given cycle will duplicate at the location of the contact. Our results indicate that the finite size of the molecular colonies is an important factor because the molecules on the perimeter of the brush tend to lean outward. Furthermore, the growth of the colony as a function of the number of thermal cycles is found to be similar to the one obtained with a simple Monte Carlo simulation.

I. INTRODUCTION

Solid phase amplification (SPA) is a new type of DNA amplification that has recently been introduced by two different groups: Adessi *et al.* (2000) and Bing *et al.* (1996). The central idea of this novel method is to attach the primers (via their 5' end) to a solid surface (silica, polystyrene beads, ...). Using a chemical mixture (containing the nucleotides and the polymerase) and temperature cycles similar to the ones used in polymerase chain reaction (PCR), it is possible to amplify the DNA template using these primers. Contrary to PCR however, the copy is grafted to the 2D surface and is always in the immediate vicinity of the original molecule (see figure 1). When used in an iterative manner, the amplification leads to the growth of a very dense but rather small DNA brush, a "DNA colony". A detailed explanation of the SPA process and its differences with solution PCR can be found in (Mercier *et al.*, 2003).

Polymer brushes have been extensively studied using theoretical approaches (Alexander, 1977; Binder, 2002; Degennes, 1980; Kuznetsov and Chen, 1998), scaling concepts (Baranowski and Whitmore, 1995, 1998; Binder, 2002; Laradji *et al.*, 1994; Milner *et al.*, 1988; Naji *et al.*, 2003; Netz and Schick, 1997, 1998; Pepin and Whitmore, 1999, 2001; Whitmore and Noolandi, 1990), computer models (Chakrabarti and Toral, 1990; Grest, 1994; Grest and Murat, 1993; Gurler *et al.*, 1983; Hilhorst and Deutch, 1975; Lai and Binder, 1991; Murat and Grest, 1989; Pepin and Whitmore, 1999, 2001; Seidel, 2003; Seidel and Csajka, 2000; Seidel and Netz, 2000; Vongoeler and Muthukumar, 1995; Wijmans *et al.*, 1992) and experiments (Auroy *et al.*, 1991; Cosgrove *et al.*, 1991; Currie *et al.*, 2000; Field *et al.*, 1992; Kent *et al.*, 1995, 1992, 1998; Koutsos *et al.*, 1999). However, most of those studies examined essentially infinite brushes (e.g., simulations use periodic boundary conditions, experiments use macroscopically large brushes, etc ...) and they focused almost exclusively on obtaining quantities such as the layer thickness and the density profile of the monomers. In the SPA context, the most relevant feature is the dynamics of the free end of the DNA molecule. Indeed, since the density of primers is extremely high, the density of the brush is self-limiting and the amplification will stop when a DNA molecule can no longer bend so that its free end can find a matching primer before the next thermal

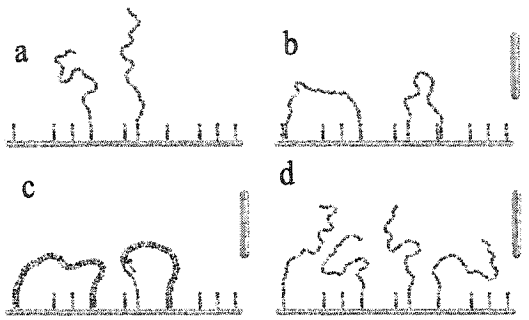

FIG. 1 Representation of one cycle of the solid phase amplification process. The solution is first heated to break the molecule into its two complementary fragments (a). The solution is then cooled down to allow the template to bind to the complementary grafted primers (b). Finally the solution is reheated to allow the polymerase to add nucleotides at the end of the primers and eventually make a complete complementary copy of the template (c). The solution is then reheated and a new thermal cycle is started (d). Those three steps are respectively called: denaturation, annealing and extension. SPA results in a spatially located ssDNA colony. Note that since a molecule always generates its complementary sequence in a thermal cycle, the two complementary branches will be present in the colony and two different types of primers have to be attached to the surface.

*Electronic address: jmercier@physics.uottawa.ca
†Electronic address: gslater@science.uottawa.ca

cycle. Note however that the amplification rate can also be limited by other effects such as the local concentration of polymerase and nucleotides. The most complete study of polymer free ends in a brush was made by Netz and Seidel (Netz and Schick, 1997; Seidel, 2003; Seidel and Csajka, 2000; Seidel and Netz, 2000), who used both molecular dynamics simulations and self-consistent field analysis. Not surprisingly, their study showed that the free end of a polymer in a brush is less likely to come close to the surface when the polymer surface concentration (often referred to as σ) is high (Netz and Schick, 1997; Seidel, 2003; Seidel and Csajka, 2000; Seidel and Netz, 2000).

Another important aspect of SPA is that the fringing molecules (i.e. the molecules on the perimeter) of the colony play a crucial role, because most of the growth of the brush occurs at its perimeter (the molecules at the center of the brush are less likely to bend). Few studies (Raphael and Degennes, 1992; Vilgis *et al.*, 1999; Xi and Milner, 1996) have examined the dynamics of the molecules on the perimeter of a brush. Vilgis *et al.* (1999) studied the edge effect in grafted polymer layers under compression using a Flory type approach (this problem is reminiscent of the end-tethered polymer compressed by an obstacle sush as an AFM tip (Ennis *et al.*, 1999; Milchev *et al.*, 1999; Sevick, 2000)). They found that the length of the outward splay and the penetration depth of the edge effects are of a characteristic length scale ξ. For an uncompressed semi-infinite brush, ξ is found to be roughly the height of the brush. For smaller brushes of diameter $\lesssim \xi$, the splay is found to be weaker, while the edge effects were felt over the whole brush. Similar results are expected for the DNA colony found in SPA. However, SPA is a dynamical process where both the density and the size of the brush constantly change. Furthermore, the density of grafted molecules can be highly inhomogeneous (the center of the colony will tend to be denser than the perimeter). Note that in this article, the small brushes found in SPA will be called DNA colonies and a brush will always refer to a large brush, with a constant density over large distances.

Our first effort to model SPA consisted in a simple lattice Monte Carlo (MC) system, where a given lattice site can be either occupied by one DNA molecule or left empty (we later refined our model to let many particles occupy the same site) (Mercier *et al.*, 2003). Using this model, we studied the growth, stability and morphology of isolated DNA colonies under various conditions (including non-ideal effects such as the presence of sterile molecules and the random detachment of molecules). Our results indicated that, in most cases, SPA is characterized by a geometric growth and a rather sharp size distribution (in comparison with an exponential growth, and a very broad distribution for solution PCR). Our MC algorithm was based on many educated assumptions lacking a solid foundation. The present article aims at testing some of those assumptions and at estimating realistic values for the parameters. To do so we use the following strategies. In section III we successively study the dynamics of a single polymer and of small symmetric colonies using the algorithm presented in section II. We look at the average time that molecules spend close to the surface (when they are assumed to make "contact" with primers), and the average spatial distribution of those contacts, as a function of the chain density and distribution. In section IV, we look at the growth process of both DNA colonies and brushes (to model the uniform density over large distances, we use periodic boundary conditions). We find that the dynamics of molecules in a colony significantly differs from that found in brushes. Furthermore we find that the early growth of a colony cannot be described by either an exponential (like in solution PCR) or a geometrical growth (predicted by most of our MC models). In section V we use our results to optimize our previous Monte Carlo model and find very good agreement between the two models.

Note that SPA could also be compared to the clever "polony" technique developed by Mintra and Church (Mitra *et al.*, 2003a; Mitra and Church, 1999; Mitra *et al.*, 2003b; Zhu *et al.*, 2003). In this technique, one of the two primers is grafted to the fibers of a polyacrylamide gel film. The solution thus contains both free and grafted DNA templates and primers. However, because of the gel matrix, the diffusion of the free templates is very small, so the amplification remains spatially localized. After the amplification, typically consisting of 40 PCR cycles (Mitra and Church, 1999), each initial template is amplified to form a localized "polony" of up to 10^8 identical molecules (Mitra and Church, 1999). Like SPA, the "polony" technique leads to spatially located DNA amplification. However the amplification mechanisms are different for the two techniques because of the $3D$ and "diffusive" nature of the "polony" growth (i.e. a molecule does not have to bend to duplicate). When "polony" growth (number of molecules in a "polony" as a function of the number of PCR cycles) was modelled, an exponential growth for early amplification cycles, followed by a polynomial growth once most of the primers at the center of the "polony" were extended (neither the grafted nor the diffusing molecules can then reach the primers on the perimeter of the "polony"), was found (Mitra and Church, 1999). In SPA, the exponential growth phase is expected to be a lot shorter because of the strong steric interactions between neighbouring molecules (Mercier *et al.*, 2003).

II. METHOD: BROWNIAN DYNAMICS SIMULATIONS

Our Brownian Dynamics (BD) model is based on a bead-spring representation of a ssDNA molecule (see figure 2). This is a coarse-grained approach where the short-time dynamical effects, such as the vibrations of the C-H bonds, are neglected and where the effect of the solvent is modelled by a stochastic force $f_{sto}(t)$ and a friction coefficient ξ for each bead. The electrostatic and hydrody-

namic interactions are also neglected. In this model, the equation of motion for a bead is reduced to the Langevin equation of motion:

$$m\frac{\partial^2 \vec{r}(t)}{\partial t^2} = -\frac{\partial U(\vec{r})}{\partial \vec{r}} - \xi\frac{\partial \vec{r}}{\partial t} + \vec{f}_{sto}(t), \qquad (1)$$

where ξ is the friction coefficient and U the potential energy. Of course, this equation must reproduce the fluctuation-dissipation law $D\xi = k_BT$ (D is the diffusion constant and k_BT the thermal energy); therefore the stochastic and frictional terms cannot be independent. Since we are interested in the long-time behaviour, we can further simplify the model by working in the overdamped limit (accelerations are neglected). Equation 1 is thus reduced to:

$$\xi\frac{\partial \vec{r}}{\partial t} = -\frac{\partial U(\vec{r})}{\partial \vec{r}} + \vec{f}_{sto}(t). \qquad (2)$$

For a finite (but small) time step δt, equation 2 can be rewritten as:

$$\vec{r}(t+\delta t) = \vec{r}(t) + \frac{1}{\xi}\vec{f}(t)\delta t + \delta\vec{r}^{G}, \qquad (3)$$

where $\vec{f} = -\partial U(\vec{r})/\partial\vec{r}$ is the force applied on the bead and $\delta\vec{r}^{G}$ a random displacement due to collisions with the solvent molecules. Each component of $\delta\vec{r}^{G}$ is chosen independently from a Gaussian distribution of mean 0 and variance $< (r_\alpha^G)^2 >= 2D\delta t$, where $\alpha = \{x, y, z\}$.

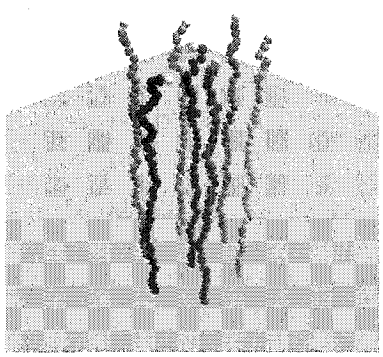

FIG. 2 Example of the system studied using our BD algorithm. The molecule is made of a series of beads (the monomers), linked with a FENE potential and interacting with a truncated Lennard-Jones potential. Each bead interacts with the grafting impenetrable wall (here in light blue) via the truncated Lennard-Jones. Here the system is a small regular brush made of a central molecule, surrounded by six others, regularly placed around the central one at a distance $R = 7\sigma$.

To treat the polymer itself, we use a variation of the united atom model developed by Grest and Kremer (1986), where a group of atoms is regrouped and replaced by a bead. A polymer is thus reduced to a series of beads linked to each other by springs (we use the finitely extensible nonlinear elastic (FENE) springs) and interacting via a truncated (we keep only the repulsive part) Lennard-Jones potential (Grest and Kremer, 1986). The FENE potential energy for a spring connecting two consecutive beads reads:

$$H_F(l_i) = \begin{cases} -0.5\,k_F\,{L_M}^2\,ln\left[1-\left(\frac{l_i}{L_M}\right)^2\right] & ,l_i < L_M \\ \infty & ,l_i > L_M \end{cases} \qquad (4)$$

where L_M is the maximum extension for the spring and k_F the spring constant. For the Lennard-Jones potential, all beads interact with each other via the potential:

$$H_{LJ}(r) = 4\epsilon\left[\left(\frac{\sigma}{r}\right)^{12} - \left(\frac{\sigma}{r}\right)^{6} - \left(\frac{\sigma}{r_c}\right)^{12} + \left(\frac{\sigma}{r_c}\right)^{6}\right] \qquad (5)$$

when $r < r_c$ and 0 otherwise. Choosing $r_c = 2^{1/6}\sigma$, the Lennard-Jones potential becomes purely repulsive (Grest and Kremer, 1986). Furthermore, choosing $L_M = 1.5\sigma$ and $k_F = 30\epsilon/\sigma^2$ ensures that bond crossing is prevented (Grest and Kremer, 1986).

In order to perform dimensionless simulations, we use the fundamental units:

$$\begin{aligned} \text{Length } & \sigma \\ \text{Energy } & \epsilon \\ \text{Time } & \tau = \frac{\xi\sigma^2}{2k_BT}. \end{aligned} \qquad (6)$$

All other necessary parameters are scaled and expressed in terms of the fundamental units described above.

III. SINGLE GRAFTED MOLECULES AND SMALL REGULAR COLONIES

In this section we study an isolated grafted molecule and small regular colonies using the algorithm described in section II. Each DNA molecule is reduced to a polymer of $Z = 39$ beads (or monomers) and we use a time step of 0.0001 τ and $k_BT = \epsilon$. Since there is no explicit bending energy in our system, the persistence length is reduced to (approximately) the size of a single bead σ. As a result, our molecule roughly corresponds to a ssDNA molecule of size $\sim$ 400 base pairs or $\sim$ 160 nm (the persistent length of single stranded DNA is $\sim$ 10 bases or $\sim$ 4 nm), which is similar to the DNA template used in a SPA experiment (Adessi *et al.*, 2000).

The simulation itself starts with the molecule in a selected initial conformation (usually straight up). The first monomer of the molecule is grafted to an impenetrable surface. Each monomer interacts with the flat grafting surface (at $z = 0$) via the same truncated Lennard-Jones potential (Eq. 5). The simulation then follows

Eq. 3 and the molecule relaxes. After a warmup time of $T_{WU} = 1000\tau > t_{relax} \approx 140\tau$), whenever the free end of the molecule is close enough to the surface to touch a primer (i.e., if $z < z_{min} = 2\sigma$, roughly the size of a primer with ~ 20 bases (Adessi *et al.*, 2000)) the position of the last bead is recorded.

Using this algorithm, we study four different configurations. The first one is a single isolated molecule. Figures 3a and 4a show a density plot and the corresponding distribution function for the end-to-end distances of the contacts (defined as the distance h (in the grafting plane) between the free end and the grafted monomer of a molecule: $h = \sqrt{(x_{free-end} - x_{grafted})^2 + (y_{free-end} - y_{grafted})^2}$, when $z_{free-end} < z_{min} = 2$). The average end-to-end distance of these contacts is $\langle h \rangle = 8.2(1)$. The free end of the molecule spends about 3.35(5)% of its time in contact with the primers.

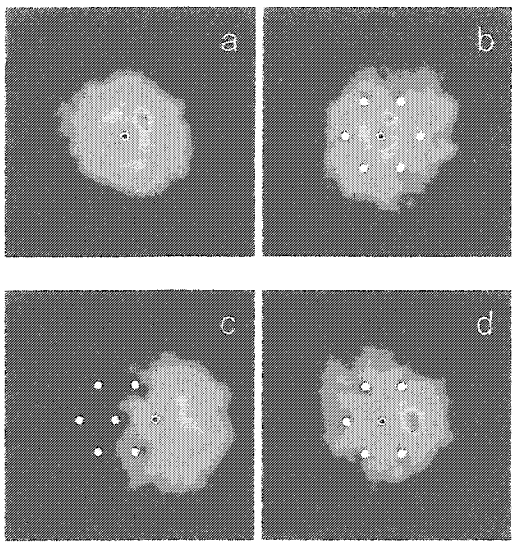

FIG. 3 Density plot of the end-to-end distance (h) of the contacts of the free end of the molecules with the grafted primers for various configurations. The red and white dot represents the molecule being followed, while the white dots represent other grafted molecules. In (a), a single molecule is considered. As expected the distribution is symmetric around the grafted monomer. In (b) and (c), the central molecule and one of the molecules on the perimeter of the small symmetric brush (see figure 2) are considered. The effect of the other molecules can clearly be seen. In the case of the molecules on the perimeter, their free ends are pushed outwards, away from the others molecules. In (d), the central molecule of a small brush missing one perimeter molecule is considered. The free end of the central molecule tends to occupy the space left empty by the missing molecule.

The second configuration considered is a small regular brush. In this system, a central molecule is surrounded by six others, regularly placed around it at a distance $R = 7\sigma$ (see figure 2). Figures 3b and 4b show the corresponding density plot and distribution function of the contacts for the central molecule. On both of these graphs, the effect of the surrounding molecules can clearly be seen. The free end of the central molecule avoids the location of its six neighbours. This leads to a decreased probability of contact at the radius where the neighbouring molecules are grafted (see figure 4b). Note that the average end-to-end distance of the contact is not much affected by the presence of the neighbours ($\langle h \rangle = 8.4(2)$) but the free end spends significantly less time, 2.5(2)%, in contact with the primers. As expected, the six molecules on the perimeter behave differently. As can be seen in figures 3c and 4c, the colony tends to push a perimeter molecule outwards. This is also obvious in figure 5a where the distribution of the x-component of the end-to-end distance of contact ($x = x_{free-end} - x_{grafted}$) is plotted for one molecule of the perimeter. There is an obvious bias in the direction away from the center of the colony (located at $x = -7\sigma$ in this case). The free end of a molecule on the perimeter of the colony spends less time, 3.0(1)%, in contact with the primers than an isolated molecule, but more than a molecule at the center of a colony.

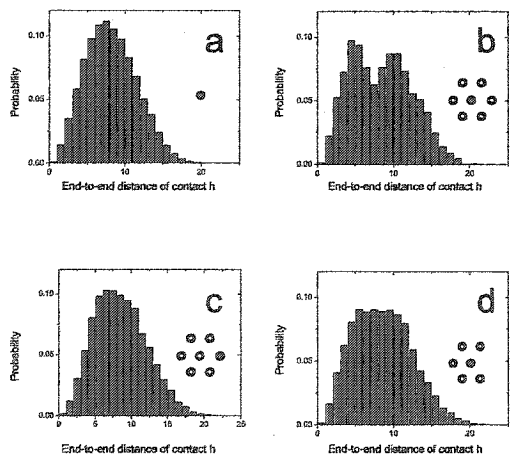

FIG. 4 Probability distribution function for the end-to-end distance of contacts (h), for the molecules shown in figure 3, and has solid circles in the insets. (a) A single isolated molecule. (b) The center molecule of a small symmetric colony shows a dip at the radius corresponding to the other molecules. The distributions for both a molecule from the perimeter of a small symmetric colony (c) and the central molecule of a small symmetric colony missing one molecule (d) are flatten in comparison with the distribution found for an isolated molecule. The average contact distance is similar for all configurations: (a) $\langle h \rangle = 8.2(1)$, (b) $\langle h \rangle = 8.4(2)$, (c) $\langle h \rangle = 8.5(2)$ and (d) $\langle h \rangle = 8.5(1)$

We now look at a slight variation of the system de-

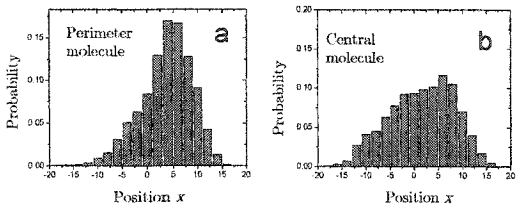

FIG. 5 Probability distribution function for the $x = x_{free-end} - x_{grafted}$ component of the end-to-end distance of contacts, for the two anisotropic cases (c and d) shown in figure 3. (a) A molecule on the perimeter gets pushed outwards (the center molecule is at $x = -7\sigma$). (b) The molecule at the center ($x = 0$) of an incomplete colony tends to occupy the space left by the missing molecule (at $x = 7\sigma$ here).

scribed in the previous paragraph: one of the perimeter molecules is removed, while all the others are kept at the same positions. There is no significant difference in the behavior of the molecules on the perimeter of the two systems. However, the molecule at the center of the colony tends to fill the void left by the missing molecule. This can clearly be seen in figures 3d and 5b. Furthermore, the free end of the molecule at the center of the colony spends significantly less time, 2.5(1)%, in contact with the primers than a free isolated molecule. Note that the average contact distances are similar for all configurations (see figure 4).

Finally, we look at a large colony where one outer layer of molecules is added to the small colony previously considered. The colony is thus made of 13 molecules (see figure 6), and the distance between two adjacent molecules remains 7σ. There are three types of molecule in the colony: the center one (#1 in figure 6), the "core" molecules (# 2, 3, 4, 5, 6 and 7) and the molecules on the perimeter (# 8, 9, 10, 11, 12 and 13). The behavior of the different molecules are consistent with the previous results: molecules at the perimeter are pushed outwards and "core" molecules tend to occupy the empty spots. Furthermore, the molecule at the center of the colony spend significantly less time in contact with the primers (1.6(2)%) than the "core" molecules (2.5(2)%) or the molecules on the perimeter (3.4(2)%). The average contact distances for perimeter ($\langle h \rangle$=8.5(2)) and "core" ($\langle h \rangle$=8.5(2)) molecules are similar and a little larger than the value found previously for a isolated molecule. However, the average contact distance for the center molecule, $\langle h \rangle = 7.3(2)$, is now significantly less, indicating that the molecule at the center of the colony tends to bend closer to its grafting point. Clearly, the probability of duplication during a thermal cycle is going to be inhomogeneous in a dense colony.

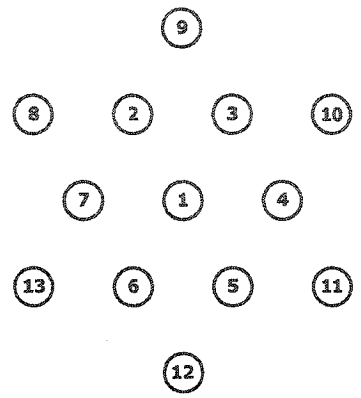

FIG. 6 Configuration of a small regular brush made of 13 molecules. The distance between two adjacent molecules is 7σ (i.e. position of #1 = $(0,0)$, #2 = $(-3.5\sigma, 6.056\sigma)$, #10 = $(10.5\sigma, 6.056\sigma)$, etc). The time spent in contact with the primers is 1.6(2)% for the molecule at the center of the colony, 2.5(2)% for the "core" molecules (# 2, 3, 4, 5, 6 and 7) and 3.4(2)% for the molecules on the perimeter (# 8, 9, 10, 11, 12 and 13). The average contact distances are $\langle h \rangle = 7.3(2)$ for the central molecule, $\langle h \rangle$=8.5(2) for the "core" molecules and $\langle h \rangle$=8.5(2) for the molecules on the perimeter.

IV. SPA MODELLING

In this section we use our Brownian Dynamics algorithm to model the kinetics of a SPA experiment. To do so some fairly drastic assumptions have to be made: 1. We neglect both hydrodynamic and electrostatic interactions. 2. The number of primers is assumed to be infinite, which is of course untrue (although the grafting density of primers is extremely high), so that as soon as a molecule come close enough to the surface, it is assumed to have found a primer. 3. Each molecule that finds the surface is assumed to successfully duplicate (make a copy), i.e., there is no shortage of polymerase or nucleotides and the new thermal cycle does not start before the copy process is finished. Also, the polymerase, which is a fairly large enzyme (comparable to the persistence length of ssDNA), is able to operate even in a very dense environment, such as the center of the colony. With those assumptions it is possible to model SPA using our simple algorithm.

As for the previous section, the DNA molecules are reduced to chains of $Z = 39$ beads (or monomers) and we use a time step of 0.0001 τ and $k_BT = \epsilon$. The simulation starts with a single molecule; its first monomer is grafted to an impenetrable surface. The simulation then follows Eq. 3 for one thermal cycle ($T_{tc} = 1000\tau$). If at any time during the cycle, the free end of the molecule comes close enough to the surface to touch a primer ($z_{free-end} < z_{min} = 2\sigma$), it is assumed to have found a matching primer, and the free end stops moving for the rest of the thermal cycle (but the rest of the molecule is

still free to move). At the end of the thermal cycle, a new molecule is placed at the location of the contact between the free end and the primers (there is no distinction between the two complementary strands). This process is repeated in an iterative manner for n temperature cycles and leads to a growing random DNA colony. To avoid any configurational (overlap) problem, all molecules are placed straight up at the beginning of each thermal cycle. The cycle time is much larger than the characteristic relaxation time of a strait molecule ($t_{relax} \approx 140\tau$). Note that we did not include any warmup time at the beginning of each cycle. The reason is that the free end of the molecules will be far away from the surface during essentially the whole relaxation process (less then 1% of the molecules will touch the surface in the first 140τ).

Simulations were performed for up to 8 thermal cycles and were averaged over 54 colonies. Figure 7 shows the average size of a colony as a function of the number of cycles n. Our results indicate that at this early stage ($n \leq 8$), the growth cannot be described by either an exponential (like in solution PCR (Peccoud and Jacob, 1996)) or a geometrical growth (predicted by a simple MC model (Mercier *et al.*, 2003)).

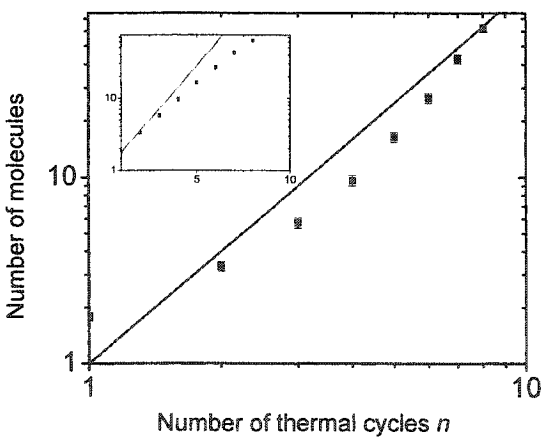

FIG. 7 Average number of molecules in a colony as a function of the number of thermal cycles n for our BD simulations presented in log-log and semi-log (inset) formats. At this early stage, the growth cannot be described by an exponential growth (solid line, inset), as found in solution PCR; it cannot be described by a geometrical growth either (solid line, main graph), as predicted by a simple MC model.

We then look at the probability (p_t) that the free end of a molecule touches the grafting surface during these thermal cycles (of duration 1000τ each). For a single isolated molecule, we find $p_t = 0.77(1)$. Figure 8 shows p_t as a function of the number of close neighbours (defined as the number of molecules grafted within the average radius of contact $\langle h \rangle = 8.2\sigma$; see section III). The data represent an average over all 8 thermal cycles and 54 different simulations. For comparison, we also show the results obtained with a traditional brush. To mimic an infinite brush, we used the same growth algorithm but we used periodic boundary conditions with a square surface of size $L = 20\sigma$ (this is the minimum length that can ensure that a molecule does not interact with itself; see figure 4). Both the brush and the colony show a decrease of p_t with the number of close neighbours, consistent with an exponential decay. Our results agree qualitatively with those reported by Seidel and Csajka (2000), where a smaller probability for the free end to be close to the surfacte in a dense brush was observed for larger grafting densities. The crowding effect is less important for a colony than for a brush. This can be explained using the results of section III. In a colony, the local anisotropy plays a major role. The molecules on the perimeter tend to be pushed outward, where there is no molecule (hence, no steric constraint). This results in a large probability for the free end of the perimeter molecules to make contact in a cycle even when these molecules have a large number of neighbours. Furthermore, since the perimeter molecules are pushed outward, the molecule at the center of the colony has slightly more space to bend. In a brush, the density is uniform and no such effects are present.

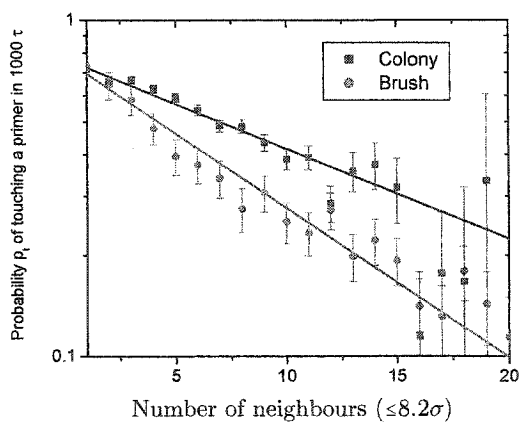

FIG. 8 Probability p_t that the free end of a molecule touches the grafting surface ($z_{free-end} < z_{min} = 2$) during one thermal cycle ($t = 1000\tau$) as a function of the number of close neighbours N_{neib} (defined as the number of molecules grafted with the average distance of contact: $\langle h \rangle = 8.2\sigma$) for both a colony and a brush. Both simulations used the algorithm described in sections II and IV and were left to evolve for $n = 8$ thermal cycles. The difference comes from the periodic boundary conditions ($L = 20$) used to model the brush. In the case of the colony, an infinite plane was used. Both cases are well described by an exponential decay function. For a brush we find the best fit to be $p_t = 0.77e^{-N_{neib}/9.64}$, and for a colony, we find $P_t = 0.77e^{-N_{neib}/16.2}$.

V. MONTE CARLO VS BROWNIAN DYNAMICS

In this section we use our previously developed lattice Monte Carlo (MC) model (Mercier *et al.*, 2003) and optimize its parameters to match the results obtained in the current study using our BD model. In our MC model, the system is reduced to a lattice where a given site can be either occupied by one (or many) ssDNA molecules or left empty. Monte Carlo techniques are then used to simulate the amplification process, i.e. the growth of the colony. The main assumptions of this model are that the duplicated molecules are always roughly at the same distance from the original molecule and that once a molecule is surrounded, its free end mostly remains away from the surface so that it cannot duplicate anymore (or does so more slowly). The model also assumes that molecules prefer empty space, i.e., if a molecule is surrounded by some empty neighbouring lattice sites, it will fill one of them. Some of these assumptions were confirmed in this study (see section III).

The MC simulation algorithm goes as follows. A molecule is first positioned at the center of a square lattice. At each cycle, each molecule, chosen in a random order, makes one attempt to copy itself into one of its empty nearest neighbour sites (if any). If more than one such site is available to a molecule, one of them is chosen randomly, but the molecule still has only one chance (per cycle) to make a copy. Each attempt has a probability $p_t = 0.77$ of being successful (this value comes from the probability for an isolated molecule to make contact with the grafted primers in our BD simulations; see section III). When a molecule is completely surrounded by copies (i.e. when all of its nearest neighbour sites are occupied), it tries to duplicate onto its own lattice site. The probability for the duplication of the molecule located at site (i,j) to be successful ($p_d(N_t)$) depends on the total number $N_t(i,j)$ of molecules on the site and on its nearest neighbour sites:

$$p_d(N) = p_t e^{-N_t/N_0} \tag{7}$$

where $N(i,j)$,

$$\begin{aligned} N_t(i,j) &= N(i,j) + N(i+1,j) + N(i-1,j) \\ &+ N(i,j-1) + N(i,j+1) \end{aligned} \tag{8}$$

is the number of molecules on a given site and N_0 regulates the strength of the local steric interactions. Since the geometry of the lattice is only a rough estimate of the real problem, we choose to let N_0 be a free parameter. We found that a value of $N_0 = 7.1$ provides the best agrement between the growth results of the two models. This value is close to the exponential decay coefficient for a brush (see figure 8). Simulations were performed using the MC algorithm for up to 200 thermal cycles and the results were averaged over 1000 colonies. Figure 9 shows the average size of a colony as a function of the number of cycles n, for both our MC and BD models. For the available common data (the first 8 cycles), the two models are in excellent agreement. In the case of the Monte Carlo model, which is far less computer intensive, we eventually reach, after a very long transition time, a geometric growth ($\propto n^2$). The transition occurs when the sites at the center of the colony are completely saturated ($N_t \gg N_0$). At this point, the growth can only take place from the perimeter. Since the radius of the colony can only increase by 1 unit every cycle, it follows that the number of molecules in the colony, which is proportional to the colony surface area, increases like n^2.

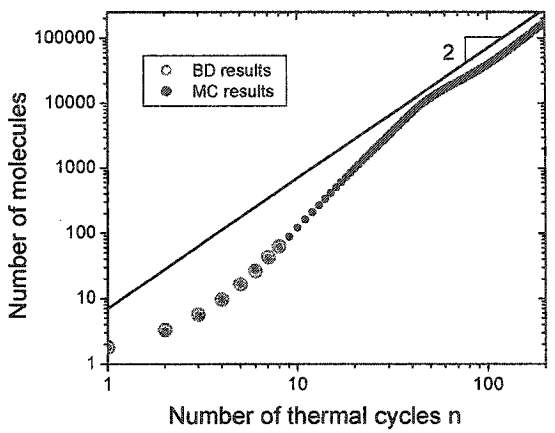

FIG. 9 Average number of molecules in a colony as a function of the number of thermal cycles n, for both BD (large open circles) and MC (small solid circles) simulations. The uncertainty is smaller than the size of the circles. In the case of the MC simulations, after a very long transition time, the growth becomes geometric. The solid line has a slope of 2. The MC simulations used a duplication probability of $p_t = 0.77$ per cycle, a steric interaction strength parameter of $N_0 = 7.1$ (see Eq.7) and the results were averaged over 1000 colonies

VI. CONCLUSIONS

In this article we used Brownian Dynamics simulations to model the growth kinetics of the DNA colonies (small inhomogeneous brushes) found in a SPA experiment. We first considered simple systems such as an isolated molecule and a small symmetric brush. We found that the mean distance (between a chain free end and its grafted monomer) of contact with the primers remains similar for all systems studied. This finding suggests that a lattice model of SPA might be able to capture the main features of the kinetics of growth. Our results also indicate that molecules tend to be "pushed" towards empty space, i.e. molecules from the perimeter and central molecules with an empty "neighbour" will tend to duplicate into the empty space. Furthermore,

surrounded molecules tend to duplicate less (their free end spend less time touching the grafting surface) and the probability of contact decreases exponentially with the local density of molecules.

Those results, obtained with a BD model, are consistent with the assumptions made previously to develop our simple Monte Carlo model of SPA colonies (Mercier *et al.*, 2003). We thus used our BD results to find the values of the MC parameters and to discriminate between many variations of our MC model. When the size of a SPA colony was calculated as a function of the number of cycles, the two models agreed nicely (see figure 9). Since our Brownian Dynamics simulations are very computer intensive, we were only able to model the first few (8) cycles of a SPA experiment. At that very early stage, the growth cannot be described by either an exponential ($\propto 2^n$) or a geometrical ($\propto n^2$) growth. Our MC model predicts that the growth will eventually become geometric, but the transition time is so large for these parameters ($\sim$ 90 thermal cycles) that this regime is possibly beyond what is possible experimentally.

Our results also indicate that the probability of duplication in a given cycle decreases exponentially with the density of grafted chains. Nevertheless, if only steric forces were involved, SPA experiments would lead to very high grafting densities (see figure 7). For example, a molecule surrounded by 10 neighbours within a radius of 8.2σ, still has a 18% probability of duplication per cycle. When the density of grafted chains increases, other effects, not considered in this study, can play an important role. Among those effects are: 1. *Electrostatic forces.* Single stranded DNA has a large electric charge per unit length. At low density, counter ions shield most of the electrostatic interactions, but when the grafting density is very high, electrostatic interactions could increase the repulsion between molecules, and stretch the molecules upward (Seidel, 2003) preventing the free end from reaching the surface. 2. *The finite number of primers.* In this study, we assumed that as soon as a molecule comes close enough to the grafting surface to touch a primer, it duplicates. In reality, the density of primers is $\sim 10^{11}$ primers per mm^2 (Adessi *et al.*, 2000), which corresponds to a mean distance of the order of $\sim 5 - 10$ nm ($\sim 2\sigma$) between primers. This is a very high concentration which corresponds to $\sim$ 30 primers for an 8.2σ radius (in our model, a molecule still has a 1% chance to duplicate when its has 30 neighbours). Once all the primers have been used, no molecule can duplicate. 3. *Polymerase and nucleotide availability.* In SPA, finding a matching primer is only the first step of the duplication process. Polymerase then needs to add the nucleotides and complete the double stranded DNA molecule. Polymerase and nucleotide shortage could play a role. Also, polymerase is a fairly large enzyme (comparable to the persistence length of ssDNA). How such a big, charged molecule will behave in a dense brush is unclear. 4. *Sterile molecules.* If a thermal cycle finishes before the polymerase has completely copied the complementary DNA strand, the resulting molecule is sterile. Such a molecule is unable to produce new copies because the DNA sequence at its free end does not correspond to the primer sequences on the surface. However, a sterile molecule still occupies space; therefore, it does impose steric constraints to its neighbours. We previously showed that, unless the concentration of those molecules reaches a critical threshold, they do not qualitatively affect the long term colony growth (but it can slow it down considerably) (Mercier *et al.*, 2003). 5. *DNA stiffness.* A double-stranded DNA is approximately 10 times stiffer than a single-stranded one. Therefore, when the polymerase completes the double-stranded molecule, the molecule becomes a lot stiffer. How this added stiffness will affect the duplication probability in such a dense environment is unclear.

All these effects will play a role in the SPA growth process and should be considered for a complete understanding of SPA. However, any molecular model, like the one presented in this paper, is likely to remain too computer intensive to track more than the first few thermal cycles. The good news is that the BD study presented in this paper has clearly demonstrated that a simple MC lattice model can capture the essential features of the kinetics of an SPA process. Such a model thus presents the best hope to understand the various effects, neglected in the BD study.

Acknowledgments

The authors would like to thank Pascal Mayer for useful discussions and the High Performance Computing Virtual Laboratory (HPCVL) consortium for computing resources. This work was supported by a Discovery Grant from the Natural Science and Engineering Research Council (NSERC) of Canada to GWS and by scholarships from the Ontario Graduate Scholarship in Science and Technology (OGSST) Program, Fonds pour la formation des chercheurs et l'aide à la recherche (FCAR, Québec), the University of Ottawa and Manteia Predictive Medicine S.A. to JFM.

References

Adessi, C., G. Matton, G. Ayala, G. Turcatti, J.-J. Mermod, P. Mayer, and E. Kawashima. 2000. Solid phase amplification: characterisation of primer attachment and amplification mechanisms. *Nucleic Acids Res.* 28:e87–e87.

Alexander, S. 1977. Adsorption of chain molecules with a polar head a-scaling description. *Journal De Physique* 38:983–987.

Auroy, P., L. Auvray, and L. Leger. 1991. Characterization of the brush regime for grafted polymer layers at the solid-liquid interface. *Phys. Rev. Lett.* 66:719–722.

Baranowski, R., and M. D. Whitmore. 1995. Theory of the structure of adsorbed block-copolymers - detailed comparison with experiment. *J. Chem. Phys.* 103:2343–2353.

Baranowski, R., and M. D. Whitmore. 1998. Numerical self-consistent field study of tethered chains in theta solvent. *J. Chem. Phys.* 108:9885–9892.

Binder, K. 2002. Scaling concepts for polymer brushes and their test with computer simulation. *Eur. Phys. J. E* 9:293–298.

Bing, D. H., C. Boles, F. N. Rehman, M. Audeh, M. Belmarsh, B. Kelley, and C. P. Adams. 1996. in *Genetic Identity Conference Proceedings, Seventh International Symposium on Human Identification.* http://www.promega.com/geneticidproc/ussymp7proc/0726.html.

Chakrabarti, A., and R. Toral. 1990. Density profile of terminally anchored polymer-chains - a monte-carlo study. *Macromolecules* 23:2016–2021.

Cosgrove, T., T. G. Heath, J. S. Phipps, and R. M. Richardson. 1991. Neutron reflectivity studies of polymers adsorbed on mica from solution. *Macromolecules* 24:94–98.

Currie, E. P. K., M. Wagemaker, M. A. C. Stuart, and A. A. van Well. 2000. Structure of grafted polymers, investigated with neutron reflectometry. *Physica B* 283:17–21.

Degennes, P. G. 1980. Conformations of polymers attached to an interface. *Macromolecules* 13:1069–1075.

Ennis, J., E. M. Sevick, and D. R. M. Williams. 1999. Compression of a polymer chain by a small obstacle: The effect of fluctuations on the escape transition. *Phys. Rev. E* 60:6906–6918.

Field, J. B., C. Toprakcioglu, R. C. Ball, H. B. Stanley, L. Dai, W. Barford, J. Penfold, G. Smith, and W. Hamilton. 1992. Determination of end-adsorbed polymer density profiles by neutron reflectometry. *Macromolecules* 25:434–439.

Grest, G. S. 1994. Grafted polymer brushes - a constant surface pressure molecular-dynamics simulation. *Macromolecules* 27:418–426.

Grest, G. S., and K. Kremer, 1986. Molecular dynamics simulation for polymers in the presence of a heat bath. *Phys. Rev. A* 33:3628–3631.

Grest, G. S., and M. Murat. 1993. Structure of grafted polymeric brushes in solvents of varying quality - a molecular-dynamics study. *Macromolecules* 26: 3108–3117.

Gurler, M. T., C. C. Crabb, D. M. Dahlin, and J. Kovac. 1983. Effect of bead movement rules on the relaxation of cubic lattice models of polymer-chains. *Macromolecules* 16:398–403.

Hilhorst, H. J., and J. M. Deutch. 1975. Analysis of monte-carlo results on kinetics of lattice polymer-chains with excluded volume. *J. Chem. Phys.* 63:5153–5161.

Kent, M. S., L. T. Lee, B. J. Factor, F. Rondelez, and G. S. Smith. 1995. Tethered chains in good solvent conditions - an experimental-study involving langmuir diblock copolymer monolayers. *J. Chem. Phys.* 103:2320–2342.

Kent, M. S., L. T. Lee, B. Farnoux, and F. Rondelez. 1992. Characterization of diblock copolymer monolayers at the liquid air interface by neutron reflectivity and surface-tension measurements. *Macromolecules* 25:6240–6247.

Kent, M. S., J. Majewski, G. S. Smith, L. T. Lee, and S. Satija. 1998. Tethered chains in theta solvent conditions: An experimental study involving langmuir diblock copolymer monolayers. *J. Chem. Phys.* 108:5635–5645.

Koutsos, V., E. W. van der Vegte, and G. Hadziioannou. 1999. Direct view of structural regimes of end-grafted polymer monolayers: A scanning force microscopy study. *Macromolecules* 32:1233–1236.

Kuznetsov, D. V., and Z. Y. Chen. 1998. Semiflexible polymer brushes: A scaling theory. *J. Of Chem. Phys.* 109:7017–7027.

Lai, P. Y., and K. Binder. 1991. Structure and dynamics of grafted polymer layers - a monte-carlo simulation. *J. Chem. Phys.* 95:9288–9299.

Laradji, M., H. Guo, and M. J. Zuckermann. 1994. Off-lattice monte-carlo simulation of polymer brushes in good solvents. *Phys. Rev. E* 49:3199–3206.

Mercier, J. F., G. W. Slater, and P. Mayer. 2003. Solid phase dna amplification: a simple monte carlo lattice model.. *Biophys. J.* 85:2075–2086.

Milchev, A., V. Yamakov, and K. Binder. 1999. Escape transition of a compressed polymer mushroom under good solvent conditions. *Europhys. Lett.* 47:675–680.

Milner, S. T., T. A. Witten, and M. E. Cates. 1988. Theory of the grafted polymer brush. *Macromolecules* 21:2610–2619.

Mitra, R. D., V. L. Butty, J. Shendure, B. R. Williams, D. E. Housman, and G. M. Church. 2003a. Digital genotyping and haplotyping with polymerase colonies. *P. Nat. Aca. Sci. USA* 100:5926–5931.

Mitra, R. D., and G. M. Church. 1999. In situ localized amplification and contact replication of many individual dna molecules. *Nucleic Acids Res.* 27,: e34.

Mitra, R. D., J. Shendure, J. Olejnik, u. n. k. n. o. w. n. Edyta-Krzymanska-Olejnik, and G. M. Church. 2003b. Fluorescent in situ sequencing on polymerase colonies. *Anal. Biochem.* 320:55–65.

Murat, M., and G. S. Grest. 1989. Structure of a grafted polymer brush - a molecular-dynamics simulation. *Macromolecules* 22:4054–4059.

Naji, A., R. R. Netz, and C. Seidel. 2003. Non-linear osmotic brush regime: Simulations and mean-field theory. *Euro. Phys. J. E* 12:223–237.

Netz, R. R., and M. Schick. 1997. Classical theory of polymer brushes. *Euro. Lett.* 38:37–42.

Netz, R. R., and M. Schick. 1998. Polymer brushes: From self-consistent field theory to classical theory. *Macromolecules* 31:5105–5122.

Peccoud, J., and C. Jacob. 1996. Theoretical uncertainty of measurements using quantitative polymerase chain reaction. *Biophys. J.* 71:101–118.

Pepin, M. P., and M. D. Whitmore. 1999. Monte carlo and numerical self-consistent field study of end-tethered polymers in good solvent. *J. Chem. Phys.* 111:10381–10388.

Pepin, M. P., and M. D. Whitmore. 2001. Monte carlo and numerical self-consistent field study of systems with end-grafted and free polymers in good solvent. *J. Chem. Phys.* 114:8181–8195.

Raphael, E., and P. G. Degennes. 1992. Aggregation of flexible-rigid-flexible triblock copolymers. *Makromolekulare Chemie-Macromolecular Symposia* 62:1–17.

Seidel, C. 2003. Strongly stretched polyelectrolyte brushes. *Macromolecules* 36:2536–2543.

Seidel, C., and F. S. Csajka. 2000. Strongly charged polyelectrolyte brushes: A molecular dynamics study. *Macromolecules* 33:2728–2739.

Seidel, C., and R. R. Netz. 2000. Individual polymer paths and end-point stretching in polymer brushes. *Macromolecules* 33:634–640.

Sevick, E. M. 2000. Compression and escape of a star polymer. *Macromolecules* 33:5743–5746.

Vilgis, T. A., A. Johner, and J. F. Joanny. 1999. Compression of finite size polymer brushes. *Phys. Chem. Chem. Phys.* 1:2077–2081.

Vongoeler, F., and M. Muthukumar. 1995. Polyelectrolyte brush density profiles. *Macromolecules* 28:6608–6617.

Whitmore, M. D., and J. Noolandi. 1990. Theory of adsorbed block copolymers. *Macromolecules* 23:3321–3339.

Wijmans, C. M., J. M. H. M. Scheutjens, and E. B. Zhulina. 1992. Self-consistent field-theories for polymer brushes - lattice calculations and an asymptotic analytical description. *Macromolecules* 25 :2657–2665.

Xi, H. W., and S. T. Milner. 1996. Surface waves on polymer brushes. *Macromolecules* 29:4772–4776.

Zhu, J., J. Shendure, R. D. Mitra, and G. M. Church. 2003. Single molecule profiling of alternative pre-mrna splicing. *Science* 301:836–838.

Conclusion

In this thesis, new modelling tools related to the human genome project are developed. The thesis is based on five distinct papers (four published articles and one submitted manuscript) and could be separated in two distinct projects: 1. A study of the Ogston regime for small analytes and 2. Models for solid phase DNA amplification. The five papers, and the two projects, all aimed at providing a better understanding of current bioanalytical chemistry methods.

6.1 A Study of the Ogston Regime for Small Analytes

We first showed how to use lattice results to rapidly reach the continuum limit [I]. In this limit the size of the lattice mesh is infinitely small in comparison with the size of both the analyte and the obstacles. The results are thus independent of the lattice type and are identical to the ones obtained with off-lattice simulations. To test the method, we showed how such a procedure can be applied efficiently to the simple case of periodic spherical obstacles to generate extremely accurate results. We found a general relation between the diffusion coefficient D, the total obstructed volume $\phi(C)$ and the dimensionality d of the problem. Our results are in perfect agreement with previous off-lattice work, in both the low and highly obstructed limit cases. This technique is a powerful alternative to the off-lattice simulations which have been used to study a wide range of problems.

We then used this continuum limit modelling technique to re-examine the theoretical foundation of the OMRC model. First, we tested the main assumption of the OMRC model ($\mu^* = f(C) = 1 - \phi(C)$) for both periodic and random three-dimensional gels in the continuum limit [II]. When the mobility was expressed as a polynomial form $\mu^* = a_1\phi + a_2\phi^2 + a_2\phi^3...$, we found the first coefficient to be identical $a_1 = \frac{2}{3}$ for all three-dimensional gels considered. However, we found higher coefficients not to be equal to 0 in general and to be strongly affected by the specific gel geometry. For example, changing a simple periodic gel to a random one changes the sign of the second coefficient (a_2). This is in agreement with our previous results [25–27, 24], and proved that the latter were not non-physical lattice aberrations. Nevertheless, since the first coefficient (a_1) is identical for all the gels studied, we concluded that a modified relation $\mu^* \simeq 1 - \frac{2}{3}\phi(C) = \frac{1}{3} + \frac{2}{3}f(C)$ seems to be a good approximation for the low concentration limit of three-dimensional gels made of long stiff fibers.

To respond to a very critical letter by Locke and Trinh [28], who argued that the assumption of

uniform field lines was the reason why our results disagreed with the OMRC hypothesis, we extended our model to take into account the curvature of the field lines around non-conducting gel fibers [III]. Our continuum limit results showed that, contrary to Locke and Trinh's claim, the dependence of the mobility of a point-like particle upon the concentration of the gel is not affected by the field line distortions in the low-field limit. These results indirectly proved that the Nernst-Einstein relation, which says that in the zero-field limit the mobility of a migrating analyte is directly related to the scaled diffusion coefficient, is valid for both straight and curved field lines.

The next logical step to our re-examination of the OMRC model was to go beyond the low-field limit. This is particulary important because most of the sequencing is now made by capillary electrophoresis, for which the low-field limit is usually not a good approximation. Note that we already know that, in this limit, the ORMC model is inadequate to describe the mobility dependence of a molecule since the field intensity does not enter the model. We also expect the Nernst-Einstein relation to be invalid for non-vanishing fields. The generalization to higher electric fields is not trivial because, contrary to the low-field case, the transition rate (the mean time required to make a lattice "jump") is not uniform and is a function of the intensity of the field. However, Michel Gauthier has recently found a clever mathematical method to expand our approach to treat high electric fields [35, 36]. The idea is to adapt the transition probability to take into account the different transition rates (which are a function of the field) [35]. Note that this generalization gives the exact mobility for any value of the field but not the diffusion coefficient (since the Nernst-Einstein relation is not valid for high field intensities). This issue was recently resolved by introducing a probability of not moving during the Monte Carlo step [36].

6.2 Models for Solid Phase DNA Amplification

In our study of Solid Phase DNA Amplification (SPA), we first used a simple lattice Monte Carlo (MC) technique to model the growth of a typical SPA colony [IV]. In this model, a given lattice site can be either occupied by one DNA molecule or left empty. We examined non-ideal effects, such as the effect of sterile molecules and molecules that detach themselves from the surface. We demonstrated that, except for extreme cases, SPA colonies show a geometrical growth and a rather sharp size distribution (in comparison with an exponential growth and a very broad distribution for solution PCR colonies). We also refined our model to let many particles occupy the same site. This led to a non-flat molecular density profile across the colony. Even in this case, sharp size distributions and, after a long transition time, geometrical growth are obtained.

The sharp colony size distribution predicted by our model means that all the DNA colonies have roughly the same number of molecules after many thermal cycles. This is a very important and positive finding for the "sequencing" SPA technique. Recall that a surface covered with SPA colonies is then exposed to successive solutions containing one of the four nucleotides, part of them being fluorescent, allowing the DNA sequences to be read by analyzing which of the colonies turn bright. When the fluorescent nucleotides are incorporated to the SPA DNA colonies, it is essential to be able to distinguish colonies that have just integrated one, two or even more bases. For example, if a given colony is twice as bright as one of its neighbours (after one fluorescent base has been introduced), it could mean that its sequence is made of two successive identical nucleotides (e.g. AATCG with a A nucleotide incorporated), or that the colony has simply twice as many molecules. Sharp size distributions remove that ambiguity and greatly simplify the image interpretation step.

Although we were confident that our rather macroscopic MC model captured the essential features of SPA colony growth, we recognized that the macroscopic model was based on many educated assumptions lacking solid foundations. To test those assumptions, experimental data where the size of the colonies of a SPA experiment would be recorded as a function of the number of thermal cycles would be ideal. For that purpose, I spent part of the summer of 2002 at the Manteia Predictive Medicine facilities. I performed several SPA-related experiments. Unfortunately, technical problems (beyond my control) and some legal aspects, have prevented us to use any of these results for publication or for this thesis. Many of the technical problems encountered in the summer 2002 visit were solved in the following months by the Manteia researchers and another visit was scheduled for the summer of 2003. Unfortunately at that time, the company encountered financial problems (which ultimately led to the closing of the company) and the visit was cancelled.

Since experimental data could not be obtained (at least until now), the next best thing to test the assumptions of our MC model was to build a more microscopic model. We thus developed a molecular approach to model the kinetics of a SPA experiment [V]. To do so we used Brownian Dynamics simulations with a united atom model. In this model, each ssDNA molecule is reduced to a series of beads linked with springs and interacting through a Lennard-Jones potential. We first considered a simple geometry, similar to the one assumed in the MC lattice model, and looked at the average time the free end of each molecule spends close to the grafting surface, and at the spatial distribution of the "contacts". We found a clear confirmation for the assumptions we made for the MC model. In particular, the bending probability is strongly affected by the chain density and the molecules on the perimeter tend to lean outward. Also, the average distance of "contact" of the free end and the average

time that the free end of a molecule spends close to the surface are similar for isolated molecules and molecules on the perimeter. We also modelled directly the SPA kinetics. The simulations mimic the temperature cycles and the molecule duplication process found in SPA; in particular, each molecule whose free end comes very close to the surface during a given cycle duplicates at the location of the contact. We looked at the duplication (bending) probability as a function of the local chain density and found that it was consistent with an exponential decay. Since the algorithm is extremely computer intensive, we were only able to model the first few (8) cycles of a SPA experiment. At that very early stage, the growth cannot be described by either an exponential ($\propto 2^n$) or a geometrical ($\propto n^2$) growth.

We finally optimized the parameters of our macroscopic MC model to match the results, including the growth, obtained in the microscopic (BD) study. In particular, we added a duplicating probability for a completely surrounded molecule which decreases exponentially with the number of neighbours of the molecule. Using these improvements, we found that the growth of the colony as a function of the number of thermal cycles of our macroscopic MC model agrees nicely with the one obtained with the microscopic BD model, for the available common data. This indicates that the simple MC lattice model can capture the essential features of the kinetics of a SPA process.

6.3 Final Thoughts

The BD algorithm used to simulate SPA could easily be adapted to include other effects, such as sterile molecules or molecules that detach themselves from the grafting surface. With more effort other less obvious interactions, such as electrostatic and hydrodynamic forces could also be included. However, I believe that our model captures the essential features of SPA colony growth1 and that any more attempts to model SPA, even with the simple MC model, would be highly speculative without proper experimental data to compare with. On the other hand, more work can definitely be done on the most fundamental aspects of finite polymer brushes. This problem has rarely been studied and deserves more attention. In particular, a full and systematic investigation using a microscopic model, such as our BD model, has, to our knowledge, never been undertaken.

For the other project of modelling the Ogston regime, I think that our study of realistic three-dimensional gels in the continuum limit and our generalization to curved field lines, put the final nail in the coffin of the OMRC model. We hope that this work will lead people to look at the OMRC model as what it really is: a semi-empirical mean field theory, which should only be used as a rough approximation. Nevertheless, the calculation techniques developed in this thesis could be used to go

beyond the OMRC model. The first major steps in that direction have already been made when a member of our group extended the model to non-vanishing electric fields [35, 36]. The computational technique could also be used to study various diffusion and mobility problems. For example, the case of drug delivery system based on polymer hydrogels will soon be undertaken by a new member of our group.

I believe that the new modelling tools developed in this thesis offer meaningful physical insights for both a very old and basic separation technique, gel electrophoresis, and a very new DNA amplification (and possibly sequencing) method, solid phase DNA amplification. I hope that this study will help better understand and perhaps help the development of these two bioanalytical chemistry methods.

Appendix A

J. F. Mercier, G. W. Slater and Hong L. Guo.

Numerically exact diffusion coefficients for lattice systems with periodic boundary conditions. I. Theory.

Journal of Chemical Physics, 110: 6050–6056, 1999.

Note

This paper was published during my master's thesis, and is included as supplementary information only. It explains in detail the numerical approach we used to obtain exact mobilities (section III) and compares this approach with a more complex one based on first passage times (section II).

JOURNAL OF CHEMICAL PHYSICS VOLUME 110, NUMBER 12 22 MARCH 1999

Numerically exact diffusion coefficients for lattice systems with periodic boundary conditions. I. Theory

Jean-François Mercier, Gary W. Slater,[a] and Hong L. Guo
Department of Physics, University of Ottawa, 150 Louis-Pasteur, Ottawa, Ontario K1N 6N5, Canada

(Received 29 May 1998; accepted 28 December 1998)

The standard method to study the diffusion of a particle in a system with immobile obstacles is to use Monte Carlo simulations on finite-size lattices with periodic boundary conditions. For example, the diffusion of proteins on the surface of biomembranes in the presence of fractal and random aggregates of obstacles has been studied extensively by M. J. Saxton. In this article, we derive two algebraically exact methods to calculate the diffusion coefficient D for such systems. The first method reduces the problem to that of a first passage problem. The second one uses the Nernst–Einstein relation to transform the problem into a field-driven drift problem where D is related to the zero-field mobility. Systems with closed volumes and multiple independent pathways are discussed. In the second part [Mercier and Slater, J. Chem. Phys. **110**, 6057 (1999), following paper], a numerical implementation will be described and tested, and several examples of applications will be given. © *1999 American Institute of Physics.* [S0021-9606(99)51812-6]

I. INTRODUCTION

Many biological, chemical, and physical problems can be reduced to that of the diffusion of a particle in a quenched system of obstacles. For example, Saxton has modeled the diffusion of proteins in a two-dimensional ($d=2$) plane of a biomembrane by a lattice random-walk model with fixed impenetrable obstacles.[1–6] The diffusion of particles in polymer solutions[7,8] and the migration of analytes in gel electrophoresis[9–11] represent two other typical problems studied using similar mathematical and numerical models.

Lattice Monte Carlo (LMC) computer simulations are frequently used for such problems. The approach is quite simple and, with modern computers, allows one to follow the diffusion of millions of independent (or even interacting) particles over macroscopic distances. Essentially, the simulation reduces to randomly moving a particle by one lattice site in one of z directions, where $z \geqslant 2$ is the number of nearest-neighbor lattice sites connected to a given site, subjected to the constraint that jumps towards occupied sites are rejected. Periodic boundary conditions (PBC) are usually necessary for LMC simulations. The effects of the PBCs on LMC results can be estimated, and diffusion coefficients D, defined by

$$D=\lim_{t\to\infty}\frac{\langle x^2\rangle}{2dt}, \tag{1}$$

can be obtained with error bars as small as 0.1%.[2] LMC simulations can also provide information about the short time dynamics of the particles.[3–6]

In LMC simulations, the effects of the environment is modeled by jump rejections. Therefore, the structure of the medium, the lattice parameter z (hence the dimensionality d of the space), and the size of the migrating particle all affect the diffusion coefficient D of the system.

In this article, we present two different approaches that can be used to calculate the EXACT diffusion coefficient D for a LMC, one-particle quenched system with PBCs. These approaches do not allow the study of the short-time dynamics of the migrating particle, but provide exact values for D, which is useful to test theoretical models and understand subtle geometrical effects. The general idea is quite simple. A LMC simulation can be seen as a Markov chain for which one can write coupled linear master equations, one per available lattice site. These equations can be solved exactly for systems that are not too large, and the diffusion coefficient D can be obtained from the resulting probability distribution functions. Since our most efficient approach can provide exact D values for two-dimensional systems of size larger than 256×256 (which is the typical size used for LMC simulation) in a few minutes of CPU on a standard workstation, we believe that our method offers a most powerful alternative to LMC simulations.

The first method that we present transforms the diffusion problem into a one-dimensional first-passage problem, a standard procedure. However, we show that such a transformation is not straightforward and that one in fact must calculate both first-passage times and probability distribution functions in order to obtain the exact diffusion coefficient D for one of the $d>1$ spatial directions. The second method exploits the Nernst–Einstein[12] relation

$$D=\frac{kT}{e}\mu, \tag{2}$$

where k is the Boltzmann factor, T the temperature, and e the charge of the particle. This relation between the mobility μ and the diffusion D must be satisfied in the presence of a

[a]Author to whom correspondence should be addressed. Electronic mail: gary@physics.uottawa.ca

J. Chem. Phys., Vol. 110, No. 12, 22 March 1999

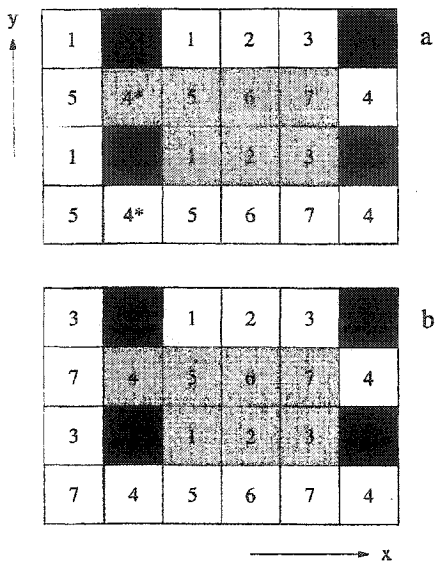

FIG. 1. The model system used in Sec. II–III D. The periodic cell is of size 4×2 (in gray). (a) The labeling scheme used when D^* is calculated directly (Sec. II). (b) The labeling scheme for the calculation of the mobility μ (Sec. III C and III D).

vanishingly small external field ϵ. Instead of calculating D directly, we thus calculate the mobility $\mu(\epsilon)$ and subsequently calculate the zero-field diffusion coefficient D using the simple relation

$$\frac{D}{D_0}=\lim_{\epsilon\to0}\frac{\mu(\epsilon)}{\mu_0}, \tag{3}$$

where D_0 and μ_0 are the diffusion coefficient and mobility in absence of obstacles. In the following, we will use the standard notation $D^*=D/D_0$ and $\mu^*=\mu/\mu_0$ for the scaled diffusion coefficient and mobility, respectively. In order to obtain the mobility, we simply calculate the probability of presence of the particle on each lattice site in the steady-state, and multiply these probabilities by the local mobilities. This procedure is much simpler than the first-passage method and can be generalized to much more complicated situations (e.g., to random fields). Note that this procedure actually gives the diffusion coefficient in the direction of the applied field ϵ.

Calculating the exact diffusion coefficient D in the presence of closed volumes and/or multiple unconnected channels is a further challenge, even when using computer simulations. Such cases will be discussed after some simpler examples are treated.

To better illustrate the two methods briefly described in the introduction, we calculate in the following two sections the diffusion coefficient D^* of one 1×1 particle in the system shown in Fig. 1, using both methods. This will demonstrate very clearly that the method based on the Nernst–Einstein relation is much more powerful than the one based on first-passage problem theories, although both methods agree.

II. D^* via FIRST PASSAGE TIMES

Consider a particle (a 1×1 lattice plaquette) which undergoes unbiased, free (no obstacles) random jumps on a two-dimensional square lattice. Its continuous diffusion process is thus modeled by random Brownian jumps of fixed length $a=1$ (the lattice parameter in scaled units) and mean duration $\tau_B=1$ (also in scaled units). The free diffusion coefficient is then given by $D_0=2D_{0x}=2D_{0y}=a^2/2\tau_B=\frac{1}{2}$. At each step, the particle is simply jumping to one of the four adjacent sites (noted $+x$, $-x$, $+y$, and $-y$). In the presence of obstacles, we have an additional rule: If a move leads to a particle overlapping with an obstacle, the move is rejected and the particle returns to its previous position. However, the time step counts regardless of the acceptance of such moves. These hard-core interactions between the particle and the obstacles will obviously reduce the scaled diffusion coefficient D^* of the particle.

A. Diffusion in the x direction

In this case, we can reduce the problem to that of the first passage problem between the columns containing site #4 [see Fig. 1(a)]. Let us first calculate the mean first passage time $t(4)$ for a random walk starting from a specific column marked 4*. In other words, $t(4)$ is the time it takes for this particle to get absorbed by the next column of sites marked 4 (in either direction) if, at each time step, the particle has a equal probability of jumping towards one of the 4 adjacent sites. The seven different times $t(i)$ are obviously coupled because of the diffusion dynamics. For example, the equation for site #4 is (note the right–left symmetry for sites #5)

$$t(4)=1+\frac{t(4)}{2}+\frac{t(5)}{2}, \tag{4}$$

where the $\frac{1}{2}t(4)$ term comes from move rejections due to the obstacles. For this situation, the particle leaves the cell through site #7 and the boundary condition is

$$t(7)=1+\frac{t(6)}{4}+\frac{t(3)}{2}. \tag{5}$$

The complete set of equations for the first-passage times $|t\rangle$ is given by (we use the Dirac notation where $|t\rangle$ and $\langle t|$ represent column and row vectors, respectively, while matrices are denoted by capital letters and scalars by lower case letters)

$$|t\rangle=A|1\rangle, \tag{6}$$

where

$$A=\frac{1}{4}\begin{pmatrix}3&-1&0&0&-2&0&0\\-1&4&-1&0&0&-2&0\\0&-1&3&0&0&0&-2\\0&0&0&2&-2&0&0\\-2&0&0&-1&4&-1&0\\0&-2&0&0&-1&4&-1\\0&0&-2&0&0&-1&4\end{pmatrix},$$

6052 J. Chem. Phys., Vol. 110, No. 12, 22 March 1999 Mercier, Slater, and Guo

$$|t\rangle=\begin{pmatrix} t(1)\\ t(2)\\ t(3)\\ t(4)\\ t(5)\\ t(6)\\ t(7)\end{pmatrix}, \quad \text{and} \quad |1\rangle=\begin{pmatrix} 1\\ 1\\ 1\\ 1\\ 1\\ 1\\ 1\end{pmatrix}. \tag{7}$$

The solution of these equations is $|t\rangle=\{1490,1334,1098,1568,1498,1304,910\}/35$. During a mean-time duration $t(4)=1568/35$, the particle migrates over a distance $\Delta x=\pm 4$. Therefore,

$$D_x=\frac{\Delta x^2}{2t(4)}=\frac{5}{28}. \tag{8}$$

Since the free diffusion coefficient $D_{0x}=\frac{1}{4}$, we obtain $D_x^*=D_x/D_{0x}=\frac{5}{7}$. This method is quite simple but its usefulness is restricted. For the y direction, the calculation becomes more involved because the selected absorption row contains more than one open site.

B. Diffusion in the y direction

The equations for mean first passage times of the particle between the 1–2–3 rows are

$$\frac{1}{4}\begin{pmatrix} 3 & -1 & 0 & 0 & -2 & 0 & 0\\ -1 & 4 & -1 & 0 & 0 & -2 & 0\\ 0 & -1 & 3 & 0 & 0 & 0 & -2\\ 0 & 0 & 0 & 2 & -1 & 0 & -1\\ -1 & 0 & 0 & -1 & 4 & -1 & 0\\ 0 & -1 & 0 & 0 & -1 & 4 & -1\\ 0 & 0 & -1 & -1 & 0 & -1 & 4\end{pmatrix}\begin{pmatrix} t(1)\\ t(2)\\ t(3)\\ t(4)\\ t(5)\\ t(6)\\ t(7)\end{pmatrix}=\begin{pmatrix} 1\\ 1\\ 1\\ 1\\ 1\\ 1\\ 1\end{pmatrix}. \tag{9}$$

The solution here is given by $|t\rangle=\{216,212,216,218,172,162,172\}/23$. Since $t(1)=t(3)\neq t(2)$, it is not clear what the actual mean first passage time is. Choosing the 4–7 rows instead would make things even more complicated. Therefore, we must calculate the relative weights of the first passage times $t(1)$, $t(2)$, and $t(3)$ in order to compute the proper (weighted) mean first passage time. As we will show below this new step may be quite subtle.

First, we must calculate the probabilities p_{ij} that a particle starting at site i will reach the next 1–2–3 row at site j. The different p_{ij} also satisfy linear equations; for example, we have

$$\begin{aligned} p_{11}&=\tfrac{1}{4}p_{11}+\tfrac{1}{4}p_{21}+\tfrac{1}{2}p_{51},\\ p_{51}&=\tfrac{1}{4}+\tfrac{1}{4}p_{11}+\tfrac{1}{4}p_{41}+\tfrac{1}{4}p_{61}. \end{aligned} \tag{10}$$

The complete set of equations governing the probabilities that a particle reaches the next 1–2–3 rows at site 1 is given by

$$\frac{1}{4}\begin{pmatrix} 3 & -1 & 0 & 0 & -2 & 0 & 0\\ -1 & 4 & -1 & 0 & 0 & -2 & 0\\ 0 & -1 & 3 & 0 & 0 & 0 & -2\\ 0 & 0 & 0 & 2 & -1 & 0 & -1\\ -1 & 0 & 0 & -1 & 4 & -1 & 0\\ 0 & -1 & 0 & 0 & -1 & 4 & -1\\ 0 & 0 & -1 & -1 & 0 & -1 & 4\end{pmatrix}\begin{pmatrix} p_{11}\\ p_{21}\\ p_{31}\\ p_{41}\\ p_{51}\\ p_{61}\\ p_{71}\end{pmatrix}=\begin{pmatrix} 0\\ 0\\ 0\\ 0\\ \frac{1}{4}\\ 0\\ 0\end{pmatrix}. \tag{11}$$

Solving the three set of equations (one set for each of the possible finishing sites; 1, 2, and 3) gives $p_{11}=p_{33}=\frac{103}{230}$, $p_{22}=\frac{9}{23}$, $p_{23}=p_{21}=p_{12}=p_{32}=\frac{7}{23}$, and $p_{13}=p_{31}=\frac{57}{230}$. Given these probabilities, we may now calculate the probability $q(i)$ that the journey of the particle between a given 1–2–3 row and the next one will actually start at site i (with $i=1,2,3$). These probabilities are given by the solution of the following set of equations:

$$\begin{pmatrix} q(1)\\ q(2)\\ q(3)\end{pmatrix}=\begin{pmatrix} p_{11} & p_{12} & p_{13}\\ p_{21} & p_{22} & p_{32}\\ p_{31} & p_{32} & p_{33}\end{pmatrix}\begin{pmatrix} q(1)\\ q(2)\\ q(3)\end{pmatrix}. \tag{12}$$

Here, the normalized solution is $q(1)=q(2)=q(3)=\frac{1}{3}$ [note that in general, the $q(i)$'s are not equal.] Therefore, the mean transit time between consecutive 1–2–3 rows is $\langle t\rangle=q(1)t(1)+q(2)t(2)+t(3)q(3)=\frac{28}{3}$, and the scaled diffusion coefficient is

$$D_y^*=\frac{D_y}{D_{0y}}=\frac{\Delta y^2/2\langle t\rangle}{1/4}=\frac{6}{7}, \tag{13}$$

where $\Delta y^2=4$ in this case.

As we can see, the calculation of the exact diffusion coefficient may become quite complicated here because one needs to evaluate conditional first passage times as well as their relative weights. The method presented next greatly simplifies the calculation of the diffusion coefficient(s).

III. D^* via THE ZERO-FIELD MOBILITY μ

Instead of directly calculating the diffusion coefficient D, we can make use of the relative Nernst–Einstein relationship between the mobility μ and the diffusion coefficient D given by Eq. (3). In order to do that, we first apply a small external (dimensionless) field ϵ to bias the random-walk migration of the particle. We then calculate the mean velocity $V(\epsilon)$ and the mobility $\mu(\epsilon)=V(\epsilon)/\epsilon$. The zero-field diffu-

J. Chem. Phys., Vol. 110, No. 12, 22 March 1999 Mercier, Slater, and Guo 6053

sion coefficient is then given by Eq. (3). It turns out that calculating the mobility $\mu(\epsilon)$ is a lot simpler than calculating the diffusion coefficient D using the approach described in Sec. II. In fact, calculating D using the mobility has other advantages. For instance, it is easy to treat cases where there are many independent pathways (such cases lead to multiple values of μ). Moreover, the mobility can be calculated numerically, with arbitrary precision, or even algebraically (for small enough systems). This section is divided as follows: We introduce the biased random-walk model in Secs. III A and III B, and we solve the two cases described in Sec. II using this approach in Secs. III C and III D (comparison of the results validates our method). Systems with multiple independent zones are discussed in Sec. III E, while powerful algebraic simplifications are presented in Sec. III F.

A. The biased random walk

Consider again a two-dimensional square lattice. At each step, the particle is simply jumping to one of the four adjacent sites (noted $+x$, $-x$, $+y$, and $-y$). With a field $\epsilon = \epsilon\hat{x}$, the mean (scaled) time duration $\tau(\epsilon)$ of a $\pm x$ jump is given by[13]

$$\tau(\epsilon)=\frac{\tanh(\epsilon)}{\epsilon}\approx 1-\frac{\epsilon^2}{3}+O(\epsilon^4). \tag{14}$$

Note that the series expansion does not have a first-order term (ϵ^1). In other words, the time durations of the $\pm x$ and $\pm y$ jumps are not perturbed, to first order in ϵ, by the external field. This greatly simplifies the problem since it means that the jumps are evenly distributed, in time, between the two spatial directions. This is the reason why it will be easy to write and solve the master equations for this process. Because we are only interested in the $\epsilon\to 0$ limit, we will carry all our algebraic calculations only to first order in ϵ.

With this field direction ($+\hat{x}$) (our systems are nondispersive), the probability for the next jump to be in the $\pm y$ direction is

$$p_{\pm y}=\tfrac{1}{4}, \tag{15}$$

while the probability for the next jump to be in the $\pm x$ direction is:[13]

$$p_{\pm x}=\frac{1/2}{1+e^{\mp 2\epsilon}}\approx\frac{1\pm\epsilon}{4}+\cdots. \tag{16}$$

Note that $p_{+y}+p_{-y}=p_{+x}+p_{-x}=\frac{1}{2}$, as it should. These probabilities do depend on the field intensity ϵ to the first power; this is indeed why the mobility is finite in the zero-field limit. In absence of obstacles, the mean velocity is given by $V_0=(p_{+x}-p_{-x})=\epsilon/2$, and the free-solution mobility by

$$\mu_0\equiv V_0/\epsilon=\tfrac{1}{2}. \tag{17}$$

The obstacles will lead to jump rejections and smaller mobilities (and diffusion coefficients).

B. General description of the method

The method presented here also requires one to use a finite-size lattice with PBCs. Let the system size be L^d, where d is the dimensionality and L is the linear size of the box, and let N be the number of sites occupied by obstacles. Briefly, the method is as follows. We first calculate the steady-state probability of presence of the particle on each of the L^d-N vacant sites of the lattice, using PBC's. This probability is not uniform if $\epsilon\neq 0$. Once this is done, we calculate the mean (global) velocity by multiplying the probability of presence on each site by the local mean velocity. Finally, the mobility is calculated and, from Eq. (3), the diffusion coefficient is obtained.

C. Diffusion in the *x* direction

Let us solve again the problem treated in Sec. II A. Figure 1(b) shows the new site labeling scheme (the left–right symmetry does not exist in the presence of a field). The probability $n(i,t+1)$ for the particle to be on site i ($i=1,2,3,4,5,6,7$) at time $t+1$ can easily be computed from the probabilities $n(i,t)$ and the jumping probabilities given by Eqs. (15) and (16). Indeed, $n(i,t+1)$ is related to the flow from adjacent sites towards site i (the particle moves once per unit time). For example, the one-step rate equation for site #3 reads

$$n(3,t+1)=p_{+x}n(3,t)+\tfrac{1}{2}n(7,t)+p_{+x}n(2,t). \tag{18}$$

The first term on the right-hand-side (r.h.s.) of Eq. (18) is due to the reflection on the obstacle in front of site #3, while the next two calculate the probability for the particles on the adjacent sites (#7 and #2) to jump onto site #3. In the steady state, we have $|n(t+1)\rangle=|n(t)\rangle=|n(t\to\infty)\rangle\equiv|n\rangle$. We must, therefore, solve the following system of equations:

$$T|n\rangle=|n\rangle, \tag{19}$$

where

$$T\equiv\frac{1}{4}\begin{pmatrix} 1-\epsilon & 1-\epsilon & 0 & 0 & 2 & 0 & 0\\ 1+\epsilon & 0 & 1-\epsilon & 0 & 0 & 2 & 0\\ 0 & 1+\epsilon & 1+\epsilon & 0 & 0 & 0 & 2\\ 0 & 0 & 0 & 2 & 1-\epsilon & 0 & 1+\epsilon\\ 2 & 0 & 0 & 1+\epsilon & 0 & 1-\epsilon & 0\\ 0 & 2 & 0 & 0 & 1+\epsilon & 0 & 1-\epsilon\\ 0 & 0 & 2 & 1-\epsilon & 0 & 1+\epsilon & 0 \end{pmatrix}$$

$$\text{and } |n\rangle\equiv\begin{pmatrix} n(1)\\ n(2)\\ n(3)\\ n(4)\\ n(5)\\ n(6)\\ n(7)\end{pmatrix}. \tag{20}$$

Only 6 of the 7 equations are independent. Besides these rate equations, we also have the normalization condition

$$\sum_{i=1}^{7} n(i)=1. \tag{21}$$

This system of linear equations (which can be seen as an eigenvector problem $T|n\rangle=\lambda|n\rangle$ with an eigenvalue $\lambda=1$)

6054 J. Chem. Phys., Vol. 110, No. 12, 22 March 1999 Mercier, Slater, and Guo

can be solved either symbolically or numerically. To first order in ϵ, we find that the normalized probability vector $|n\rangle$ is given by

$$|n\rangle \equiv \begin{pmatrix} n(1) \\ n(2) \\ n(3) \\ n(4) \\ n(5) \\ n(6) \\ n(7) \end{pmatrix} = \frac{1}{7}\begin{pmatrix} 1 \\ 1 \\ 1 \\ 1 \\ 1 \\ 1 \\ 1 \end{pmatrix} + \frac{\epsilon}{14}\begin{pmatrix} -2 \\ 0 \\ 2 \\ 0 \\ -1 \\ 0 \\ 1 \end{pmatrix}. \tag{22}$$

The mean velocity on each site is $v(i)=p_{+x}L_+(i)-p_{-x}L_-(i)$, where the displacements $L_\pm=1$ if there is no obstacle in the given direction, and zero otherwise. Here, we thus find

$$|v\rangle \equiv \begin{pmatrix} v(1) \\ v(2) \\ v(3) \\ v(4) \\ v(5) \\ v(6) \\ v(7) \end{pmatrix} = \frac{1}{4}\begin{pmatrix} 1+\epsilon \\ 2\epsilon \\ -1+\epsilon \\ 2\epsilon \\ 2\epsilon \\ 2\epsilon \\ 2\epsilon \end{pmatrix}. \tag{23}$$

The mean (global) velocity v is given by the scalar product of the probability vector $|n\rangle$ with the velocity vector $|v\rangle$. To first order of ϵ, we find

$$v \equiv \langle v|n\rangle = \tfrac{5}{14}\epsilon. \tag{24}$$

Therefore, the reduced diffusion coefficient is given by $D_x^* = \mu^* = \mu/\mu_0 = (v/\epsilon)/(\frac{1}{2}) = \frac{5}{7}$ consistent with the scaled diffusion coefficient D_x^* obtained in Sec. II A. Note that since the system is symmetric, taking the field in the opposite direction $(-\hat{x})$, will lead to the same diffusion coefficient.

D. Diffusion in the y direction

A similar approach for a field pointing in the y direction gives

$$|n\rangle \equiv \begin{pmatrix} n(1) \\ n(2) \\ n(3) \\ n(4) \\ n(5) \\ n(6) \\ n(7) \end{pmatrix} = \frac{1}{7}\begin{pmatrix} 1 \\ 1 \\ 1 \\ 1 \\ 1 \\ 1 \\ 1 \end{pmatrix} \quad \text{and} \quad |v\rangle = \frac{\epsilon}{2}\begin{pmatrix} 1 \\ 1 \\ 1 \\ 0 \\ 1 \\ 1 \\ 1 \end{pmatrix}, \tag{25}$$

for all values of ϵ. We thus obtain $v=\langle v|n\rangle = 3\epsilon/7$ and $D_y^* = \mu^* = \mu/\mu_0 = \frac{6}{7}$ in agreement with the much more complicated calculation presented in Sec. II C. As we can see, the present approach is much easier.

This method reduces the problem to solving a system of J linear equations with J unknowns, where $J \leq L^d - N$ is the number of unique empty sites on the lattice of linear size L (we can sometimes use the symmetries of the lattice to minimize J). Solving such systems of equations using a direct technique takes a time $T \sim J^3$. Therefore, the CPU time increases like $T \sim L^{3d}$ for a system of linear size L with PBCs; this represents the most important limitation of this approach, especially if large precision (or an exact value) is seeked. More efficient iterative methods will be discussed in Part II of this series.[14]

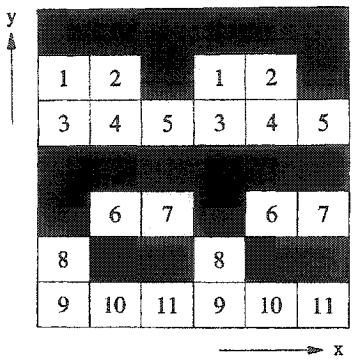

FIG. 2. The periodic cell of a simple system with periodicities $L_x=3$ and $L_y=6$. Sites #6 and #7 form a closed lake. Sites #1–5 form an independent channel, as do sites #8–11. We thus have three unconnected zones.

E. Closed volumes and multiple independent pathways

When the obstacles are placed randomly, the system can contain closed volumes (lakes) or multiple independent pathways (channels). Figure 2 shows a simple example of a 3×7 system containing a closed lake and two unconnected channels (the field is assumed to point in the $+x$ direction). Of course, it would be unrealistic to simply reject these cases in the calculation of the mean diffusion coefficient. Therefore, we must be able to treat such cases in a systematic way. Note that $D_y^*=0$ for this example.

The sites of a lake or a secondary channel are not related, via the probability or rate equations, to the sites of the main channel. In other words, each lake or channel results in an independent set of probability equations (the transition matrix is block-diagonal). Therefore, we must treat each lake or channel as an independent "system" or "zone;" for instance, we must normalize each set of solutions independently. This will lead to a different diffusion coefficient for each independent zone. How these different diffusion coefficients are used to obtain an average value depends on the problem that is being modeled, as will be discussed later.

Our example (Fig. 2) has one lake (zone b, formed by sites #6 and #7) and two channels (zone a, formed by sites #1 to #5, and zone c, formed by sites #8 to #11), i.e., three independent zones. If we follow the method described in Sec. III C, the probability matrix T is block-diagonal. These blocks can be solved (and normalized) separately in order to determine the relative probability for the particle to be on each site if it diffuses in the given zone. The first order of ϵ, the normalized solutions are given by

J. Chem. Phys., Vol. 110, No. 12, 22 March 1999 Mercier, Slater, and Guo 6055

$$|n_a\rangle=\begin{pmatrix} n(1)\\ n(2)\\ n(3)\\ n(4)\\ n(5)\end{pmatrix}=\frac{1}{5}\begin{pmatrix} 1-\frac{8}{11}\epsilon\\ 1+\frac{8}{11}\epsilon\\ 1-\frac{2}{11}\epsilon\\ 1+\frac{2}{11}\epsilon\\ 1\end{pmatrix},$$

$$|n_b\rangle=\begin{pmatrix} n(6)\\ n(7)\end{pmatrix}=\frac{1}{2}\begin{pmatrix} 1-\epsilon\\ 1+\epsilon\end{pmatrix}, \tag{26}$$

$$|n_c\rangle=\begin{pmatrix} n(8)\\ n(9)\\ n(10)\\ n(11)\end{pmatrix}=\frac{1}{4}\begin{pmatrix} 1\\ 1\\ 1\\ 1\end{pmatrix}.$$

The mean velocity on each site is

$$|v_a\rangle=\begin{pmatrix} v(1)\\ v(2)\\ v(3)\\ v(4)\\ v(5)\end{pmatrix}=\frac{1}{4}\begin{pmatrix} 1+\epsilon\\ -1+\epsilon\\ 2\epsilon\\ 2\epsilon\\ 2\epsilon\end{pmatrix},$$

$$|v_b\rangle=\begin{pmatrix} v(6)\\ v(7)\end{pmatrix}=\frac{1}{4}\begin{pmatrix} 1+\epsilon\\ -1+\epsilon\end{pmatrix}, \tag{27}$$

$$|v_c\rangle=\begin{pmatrix} v(8)\\ v(9)\\ v(10)\\ v(11)\end{pmatrix}=\frac{1}{4}\begin{pmatrix} 0\\ 2\epsilon\\ 2\epsilon\\ 2\epsilon\end{pmatrix}.$$

Finally, the three different diffusion coefficients can be calculated

$$D_a^*=\lim_{\epsilon\to 0}\frac{\langle v_a|n_a\rangle}{\mu_0\epsilon}=\frac{36}{55},$$

$$D_b^*=\lim_{\epsilon\to 0}\frac{\langle v_b|n_b\rangle}{\mu_0\epsilon}=0, \tag{28}$$

$$D_c^*=\lim_{\epsilon\to 0}\frac{\langle v_c|n_c\rangle}{\mu_0\epsilon}=\frac{3}{4}.$$

Note that the diffusion coefficient [as defined by Eq. (1)] in the closed lake is zero, as it should, since a particle trapped in a lake cannot move over macroscopic distances. One can thus save time by attributing, e.g., an *a priori* zero diffusion coefficient to all zones containing less sites than the length of the cell in the field direction (in this example, the lengths are: $L_x=3$ and $L_y=6$).

When the values of D^* are known for each independent zone, a global (or weighted) value of D^* can be calculated. However, this step is very problem dependent. For example, if particles are injected randomly and the measured diffusion coefficient takes all of them into account, one must weight the various values using the number of empty sites in each zone; here, this procedure would give $D^*=(5D_a^*+2D_b^*+4D_c^*)/11=\frac{69}{121}$. One could also disregard closed lakes (e.g., if it is impossible to follow these molecules), or consider only the largest zone. Clearly, this depends on the problem being studied.

F. Algebraic simplifications

In order to save one mathematical step, the normalization condition can be introduced in the matrix equation. For each separate zone, one can replace one of the equations of the matrix block (which is linearly dependent upon the others anyway) by the normalization equation $\Sigma n_i=1$. In this way, the solution is automatically normalized. In practice, we first rewrite the matrix equation $T|n\rangle=|n\rangle$ as $(T\text{-}1)|n\rangle=|0\rangle$, 1 being the unit matrix and $|0\rangle$ the zero vector. To normalize the solution we then replace the last line of the T-1 matrix and the last element of the $|0\rangle$ vector by ones. The resulting matrix equation is $A|n\rangle=|b\rangle$, where $|b\rangle=\{0,0,...,1\}$ and A is the new (i.e., modified) transition matrix.

We can further simplify the numerical problem by eliminating the need for an arbitrary (finite) value of ϵ. First, let us separate each term in the $A|n\rangle=|b\rangle$ matrix equation (and the velocity vector, $|v\rangle$) into a constant term (with a subscript I) and a ϵ^1-dependent term (with a ϵ subscript)

$$\begin{aligned}&\text{Transition matrix:}\quad A=A_I+\epsilon|A_\epsilon\rangle,\\ &\text{Probability vector:}\quad |n\rangle=|n_I\rangle+\epsilon|n_\epsilon\rangle,\\ &b\text{ vector:}\quad |b\rangle=|b_I\rangle,\\ &\text{Velocity vector:}\quad |v\rangle=|V_I\rangle+\epsilon|V_\epsilon\rangle.\end{aligned} \tag{29}$$

Note that the b-vector is always independent of ϵ. With Eq. (29), the relation $A|n\rangle=|b\rangle$ becomes

$$A_I|n_I\rangle+\epsilon(A_I|n_\epsilon\rangle+A_\epsilon|n_I\rangle)+\epsilon^2A_\epsilon|n_\epsilon\rangle=|b_I\rangle. \tag{30}$$

To first order in ϵ, this relation can be satisfied for an arbitrary field intensity ϵ only if

$$A_I|n_I\rangle=|b_I\rangle\quad\text{and}\quad A_I|n_\epsilon\rangle=-A_\epsilon|n_I\rangle. \tag{31}$$

The first relation corresponds to the field-free case and leads to the trivial solution $n_I(i)=1/J$ (where J is the number of connected sites in the given zone). It is in fact the second relation that contains the nontrivial effects of the fixed obstacles on the diffusion coefficient (or mobility).

Once the total probability vector n is calculated, the mean velocity v is given by

$$\begin{aligned}v=\langle v|n\rangle&=(\langle v_I|+\epsilon\langle v_\epsilon|)\cdot(|n_I\rangle+\epsilon|n_\epsilon\rangle)\\ &=\langle v_I|n_I\rangle+\epsilon(\langle v_I|n_\epsilon\rangle+\langle v_\epsilon|n_I\rangle).\end{aligned} \tag{32}$$

The term $\langle v_I|n_I\rangle=0$ since it gives the velocity when $\epsilon=0$. The reduced diffusion coefficient is thus given by

$$D^*=\frac{\langle v_\epsilon|n_I\rangle+\langle v_I|n_\epsilon\rangle}{D_0}. \tag{33}$$

This approach does not require us to use any specific value for the arbitrary field intensity ϵ. The only step here is the evaluation of the field-dependent correction term $|n_\epsilon\rangle=-(A_I)^{-1}A_\epsilon|n_I\rangle$ of the total probability density vector $|n\rangle=|n_I\rangle+\epsilon|n_\epsilon\rangle$.

6056 J. Chem. Phys., Vol. 110, No. 12, 22 March 1999 Mercier, Slater, and Guo

IV. CONCLUSION

We have presented two algebraically exact methods to calculate the diffusion coefficient D of a particle in a system with immobile obstacles and periodic boundary conditions. The first one reduces the problem to that of a traditional first passage problem, while the second one uses the Nernst–Einstein relation to transform the problem into a field-driven drift problem where D is related to the zero-field mobility. As an example, we calculated the diffusion coefficients of a simple anisotropic system using both methods; this example clearly demonstrated that, while results were identical, the second method was preferable. In fact, the most efficient approach reduces the diffusion problem to the solution of a (large) system of linear equations.

When the obstacles are placed randomly, a system can contain closed volumes (lakes) and/or multiple independent pathways (channels). We have shown how one can treat these cases in a systematic way.

Our method can easily be adapted to any type of lattice of dimensionality $d>1$. It is also possible to have nonsimilar bonds, local binding energies, etc. Moreover, the diffusing particle does not have to be a simple square; indeed, it can take various sizes and shapes (rigid rods, crosses, etc.), and may even be a flexible dimer or trimer. Finally, finite concentrations can also be studied (many simultaneous diffusing particles).

Our numerical method does not allow the study of the short-time dynamics of the migrating particle (exact enumeration[15,16] or eigenvalue[17–19] methods could be used for such studies). Also, like all methods using periodic boundary conditions, it formally excludes anomalous cases. In the second Part of this series,[14] a powerful numerical implementation will be described and tested and several applications will be given.

ACKNOWLEDGMENTS

The authors would like to thank George Weiss and Michael J. Saxton for useful suggestions. This work was supported by a Research Grant from the National Science and Engineering Research Council of Canada to G.W.S., and by a scholarship from the Fond pour la Formation de Chercheurs et l'Aide à la Recherche (Québec) to J.F.M.

[1] M. J. Saxton, Biophys. J. **64**, 1053 (1993).
[2] M. J. Saxton, Biophys. J. **64**, 1766 (1993).
[3] M. J. Saxton, Biophys. J. **66**, 394 (1994).
[4] M. J. Saxton, Biophys. J. **69**, 389 (1995).
[5] M. J. Saxton, Biophys. J. **70**, 1250 (1996).
[6] M. J. Saxton, Biophys. J. **72**, 1744 (1997).
[7] G. D. J. Phillies and A. Quinlan, Macromolecules **25**, 3110 (1992).
[8] L. Johansson and C. Elvingson, Macromolecules **24**, 6024 (1991).
[9] G. W. Slater and H. L. Guo, Electrophoresis **17**, 977 (1996).
[10] G. W. Slater, and H. L. Guo, Electrophoresis **17**, 1407 (1996).
[11] G. W. Slater and J. R. Treurniet, J. Chromatogr., A **772**, 39 (1997).
[12] R. K. Pathria, *Statistical Mechanics*, 2nd ed. (Butterworth Heinemann, Oxford, 1996), p. 465, Eq. (13).
[13] G. W. Slater, Electrophoresis **14**, 1 (1993).
[14] J. F. Mercier and G. W. Slater, J. Chem. Phys. **110**, 6057 (1999), following paper.
[15] S. Havlin and D. Ben-Avraham, Adv. Phys. **36**, 695 (1987).
[16] S. Havlin, G. H. Weiss, J. E. Kiefer, and M. J. Dishon, J. Phys. A **17**, L347 (1984).
[17] D. J. Jacobs and H. Nakanishi, Phys. Rev. A **14**, 706 (1990).
[18] N. H. Fuchs and H. Nakanishi, Phys. Rev. A **43**, 1721 (1991).
[19] H. Nakanishi, S. Mukherjee, and N. H. Fuchs, Phys. Rev. E **47**, R1463 (1993).

Glossary

ϵ	Lennard-Jones energy scale in the Brownian Dynamics simulations (in article [V])
ϵ	Scaled electric field (in article [I] and [II])
ε	Scaled electric field
ϕ	Excluded volume (volume fractions)
σ	Lennard-Jones length scale in the Brownian Dynamics simulations (in article [V])
τ	Lennard-Jones time scale in the Brownian Dynamics simulations (in article [V])
μ	Electrophoretic mobility
μ_0	Free solution (no obstacle) electrophoretic mobility
μ^*	Scaled electrophoretic mobility
ξ	Friction coefficient
a	Mean gel pore size
A	Adenine (nucleotide)
BD	Brownian Dynamics
C	Cytosine (nucleotide)
C	Obstacle concentration (volume fractions)
D	Diffusion coefficient
D_0	Free solution (no obstacle) diffusion coefficient
D^*	Scaled diffusion coefficient
DNA	Deoxyribonucleic acid
dsDNA	Double stranded deoxyribonucleic acid

f	Free available volume
f	Excluded volume (in article [I])
G	Guanine (nucleotide)
K	Retardation coefficient
k_BT	Thermal energy
M	Average size of a SPA colony
MC	Monte Carlo
n	Number of thermal cycles
OMRC	Ogston-Morris-Rodbard-Chrambach
p	Probability of duplication per thermal cycle
PCR	Polymerase chain reaction
r	Radius of the gel fiber
R	Radius of the analyte
s	Probability that a duplication results in a sterile molecule
SNP	Single nucleotide polymorphism
SPA	Solid Phase DNA amplification
ssDNA	Single stranded deoxyribonucleic acid
T	Thymine (nucleotide)
x	Probability of a molecule detachment per thermal cycle

Bibliography

[1] D. Baltimore and *al.* The human genome project. *Nature*, 409:813–958, 2001.

[2] S. Pääbo and *al.* The human genome project. *Science*, 291:1145–1434, 2001.

[3] J. Bednar, P. Furrer, V. Katritch, A. Z. Stasiak, J. Dubochet, and A. Stasiak. Determination of DNA persistence length by cryoelectron microscopy - separation of the static and dynamic contributions to the apparent persistence length of DNA. *J. Mol. Biol.*, 254:579–591, 1995.

[4] Tinland B., Pluen A., Sturm J., and Weill G. Persistence length of single-stranded dna. *Macromolecules*, 30:5763–5765, 1997.

[5] B. Alberts, D. Bray, J. Lewis, M. Raff, K. Roberts, and J. D. Watson. *Molecular biology of the cell.* Garland, New York, 1997.

[6] G. W. Slater, M. G. Gauthier, M. Kenward, and L. C. McCormick. The theory of DNA separation by capillary electrophoresis. *Curr. Opin. Biotechnol.*, 14:58–64, 2003.

[7] A. G. Ogston. The space in a uniform random suspension of fibers. *Trans. Faraday Soc.*, 54:1754–1756, 1958.

[8] K. A. Ferguson. Starch-gel electrophoresis–application to the classification of pituitary proteins and polypeptides. *Metabolism*, 13:985–1002, 1964.

[9] C. J. O. R. Morris. *Protides of the Biological Fluids, 14th Colloquium.* Elsevier, New York, 1967.

[10] D. Rodbard and A. Chrambach. Unified theory for gel electrophoresis and gel filtration. *Proc Nat Acad Sci, USA*, 65:970–977, 1970.

[11] J. C. Giddings and J. R. Boyack. Mechanism of electrophoretic migration in paper. *Anal. Chem.*, 7:1229–1234, 1964.

[12] T. L. Faley and W. Strieder. Knudsen-flow through a random bed of unidirectional fibers. *J. App. Phys.*, 62:4394–4397, 1987.

[13] T. L. Faley and W. Strieder. The effect of random fiber orientation on knudsen permeabilities. *J. Of Chem. Phys.*, 89:6936–6940, 1988.

[14] H. C. Chang. Multi-scale analysis of effective transport in periodic heterogeneous media. *Chem. Eng. Com.*, 15:83–91, 1982.

[15] Anderson T. B. and Jackson R. A fluid mechanical description of fluidized beds. *Ind. Eng. Chem. Fundam.*, 527-533:81–133, 1967.

[16] Whitaker S. Diffusion and dispersion in porus media. *AIChE J.*, 34:420–427, 1967.

[17] Whitaker S. Advances in theory of fluid motion in porus media. *I.E.C. Res.*, 61:297–303, 1969.

[18] Locke B. R. Electroiphoretic transport in porus merdia: A volum-averaging approach. *Ind. Eng. Chem. Res.*, 37:615–625, 1998.

[19] H. Brenner. Dispersion resulting from flow through spatially periodic porous-media. *Philosophical Transactions Of The Royal Society Of London Series A-Mathematical Physical And Engineering Sciences*, 297:81–133, 1980.

[20] D. A. Edwards, M. Shapiro, H. Brenner, and M. Shapira. Dispersion of inert solutes in spatially periodic, 2-dimensional model porous-media. *Trans. Por. Med.*, 6:337–358, 1991.

[21] G. W. Slater and H. L. Guo. An exactly solvable Ogston model of gel electrophoresis: I. the role of the symmetry and randomness of the gel structure. *Electrophoresis*, 17:977–988, 1996.

[22] G. W. Slater and H. L. Guo. An exactly solvable Ogston model of gel electrophoresis: Ii. sieving through periodic gels. *Electrophoresis*, 17:1407–1415, 1996.

[23] G. W. Slater and J. R. Treurniet. An exactly solvable Ogston model of gel electrophoresis: Iii. percolation and sieving through two-dimensional gels. *J. Chromat. A*, 772:41–48, 1997.

[24] J. F. Mercier. Calculating the diffusion coefficient of a random walker among immobile obstacles: New numerically exact theory and applications. Master's thesis, University of Ottawa, 1999.

[25] J. F. Mercier, G. W. Slater, and H. L. Guo. Numerically exact diffusion coefficients for lattice systems with periodic boundary conditions. i. theory. *J. Chem. Phys.*, 110:6050–6056, 1999.

[26] J. F. Mercier, G. W. Slater, and H. L. Guo. Numerically exact diffusion coefficients for lattice systems with periodic boundary conditions. ii. numerical approach and applications. *J. Chem. Phys.*, 110:6057–6065, 1999.

[27] J. F. Mercier and G. W. Slater. An exactly solvable ogston model of gel electrophoresis 4: Sieving through periodic three-dimensional gels. *Electrophoresis*, 19:1560–1565, 1998.

[28] D. R. Locke and S. H. Trinh. When can the Ogston-Morris-Rodbard-Chrambach model be applied to gel electrophoresis? *Electrophoresis*, 20:3331–3334, 1999.

[29] Locke B. R. The effect of obstacle conductivity and electric field on effective mobility and dispersion in electrophoretic transport: A volume averaging approach. *Electrophoresis*, 23:2745–2754, 1998.

[30] J. F. Mercier, F. Tessier, and G. W. Slater. An exactly solvable Ogston model of gel electrophoresis: Viii. nonconducting gel fibers, curved field lines, and the nernst-einstein relation. *Electrophoresis*, 22:2631–2638, 2001.

[31] K. D. Dorfman. Exact computation of the mean velocity, molecular diffusivity, and dispersivity of a particle moving on a periodic lattice. *J. Chem. Phys.*, 118:8428–8436, 2003.

[32] K. D. Dorfman, G. W. Slater, and M. G. Gauthier. Generalized taylor-aris dispersion analysis of spatially periodic lattice monte carlo models: Effect of discrete time. *J. Chem. Phys*, 119:6979–6980, 2003.

[33] J. Labrie, J. F. Mercier, and G. W. Slater. An exactly solvable Ogston model of gel electrophoresis 5. attractive gel-analyte interactions and their effects on the ferguson plot. *Electrophoresis*, 21:823–833, 2000.

[34] J. Boileau and G. W. Slater. An exactly solvable Ogston model of gel electrophoresis - 6. towards a theory for macromolecules. *Electrophoresis*, 22:673–683, 2001.

[35] M. G. Gauthier and G. W. Slater. Exactly solvable Ogston model of gel electrophoresis. ix. generalizing the lattice model to treat high field intensities. *J. Chem. Phys.*, 117:6745–6756, 2002.

[36] M. G. Gauthier and G. W. Slater. An exactly solvable Ogston model of gel electrophoresis: X. application to high-field separation techniques. *Electrophoresis*, 24:441–451, 2003.

[37] M. M. Tomadakis and S. V. Sotirchos. Transport-properties of random arrays of freely overlapping cylinders with various orientation distributions. *J. Chem. Phys.*, 98:616–626, 1993.

[38] M. J. Saxton. Lateral diffusion in an archipelago - single-particle diffusion. *Biophys. J.*, 64:1766–1780, 1993.

[39] B. P. Boudreau. *Diagenetic models and their imprementation.* Springer-Verlag, Berlin, 1997.

[40] B. Amsden. Solute diffusion within hydrogels. mechanisms and models. *Macromolecules*, 31:8382–8395, 1998.

[41] G. K. Batchelor. Transport properties of 2-phase materials with random structure. *Annu. Rev. Fluid Mech.*, 6:227–255, 1974.

[42] D. J. Jeffrey and A. Acrivos. Rheological properties of suspensions of rigid particles. *AIChE J.*, 22:417–432, 1976.

[43] D. K. Hale. Physical-properties of composite-materials. *J. Mater. Sci.*, 11:2105–2141, 1976.

[44] P. G. Klemens. Thermal-conductivity of composites. *Int. J. Thermophys.*, 11:971–976, 1990.

[45] J. T. Mottram and R. Taylor. Thermal-conductivity of fiber phenolic resin composites .2. numerical evaluation. *Compos. Sci. Technol.*, 29:211–232, 1987.

[46] L. E. Nielsen. Thermal and electrical-conductivity of 2-phase systems. *Ind. Eng. Chem. Fundam*, 13:17–20, 1974.

[47] W. E. A. Davies. Dielectric-constant of fiber composites. *J. Phys. D*, 7:120–130, 1974.

[48] B. Abeles and J. I. Gittleman. Composite-material films - optical-properties and applications. *Appl. Optics*, 15:2328–2332, 1976.

[49] J. G. Berryman. Effective conductivity by fluid analogy for a porous insulator filled with a conductor. *Phys. Rev. B*, 27:7789–7792, 1983.

[50] D. Abukay, K. V. Rao, S. Arajs, and Y. D. Yao. Electrical-resistivity of aluminium-boron composites between 78k and 400k. *Fibre Science & Technology*, 10:313–318, 1977.

[51] L. Rayleig. On the influance of obstacles arranged in rectangular order upon the properties of a medium. *Philos. Mag.*, 34:481–489, 1892.

[52] H. G. Craighead. Nanostructure science and technology: Impact and prospects for biology. *J. Vac. Sci. Technol. & Technology A*, 21:S216–S221, 2003.

[53] J. Kameoka and H. G. Craighead. Fabrication of oriented polymeric nanofibers on planar surfaces by electrospinning. *Appl. Phys. Lett.*, 83:371–373, 2003.

[54] H. Cao, Z. N. Yu, J. Wang, J. O. Tegenfeldt, R. H. Austin, E. Chen, W. Wu, and S. Y. Chou. Fabrication of 10 nm enclosed nanofluidic channels. *Appl. Phys. Lett.*, 81:174–176, 2002.

[55] P. S. Doyle, J. Bibette, A. Bancaud, and J. L. Viovy. Self-assembled magnetic matrices for DNA separation chips. *Science*, 295:2237–2237, 2002.

[56] M. Akeson, D. Branton, J. J. Kasianowicz, E. Brandin, and D. W. Deamer. Microsecond time-scale discrimination among polycytidylic acid, polyadenylic acid, and polyuridylic acid as homopolymers or as segments within single RNA molecules. *Biophys. J.*, 77:3227–3233, 1999.

[57] J. J. Kasianowicz, E. Brandin, D. Branton, and D. W. Deamer. Characterization of individual polynucleotide molecules using a membrane channel. *Proc Nat Acad Sci, USA*, 93:13770–13773, 1996.

[58] A. Bensimon, A. Simon, A. Chiffaudel, V. Croquette, F. Heslot, and D. Bensimon. Alignment and sensitive detection of DNA by a moving interface. *Science*, 265:2096–2098, 1994.

[59] C. Adessi, G. Matton, G. Ayala, G. Turcatti, J.-J. Mermod, P. Mayer, and E. Kawashima. Solid phase amplification: characterisation of primer attachment and amplification mechanisms. *Nucleic Acids Res.*, 28:e87–e87, 2000.